THE UNIVERSITY OF CALGARY

EPR SPECTROMETER SENSITIVITY STUDIES I

An Investigation of the Application of Digital Fourier Analysers to Optimize the Performance of EPR Spectrometer Systems

by

S. COHN-SFETCU

A THESIS

SUBMITTED TO THE FACULTY OF GRADUATE

STUDIES IN PARTIAL FULFILLMENT OF THE REQUIREMENTS

FOR THE DEGREE OF MASTER OF SCIENCE

DEPARTMENT OF PHYSICS

CALGARY, ALBERTA

April, 1973

THE UNIVERSITY OF CALGARY

FACULTY OF GRADUATE STUDIES

The undersigned certify that they have read and recommend to the Faculty of Graduate Studies for acceptance, a thesis entitled: "EPR Spectrometer Sensitivity Studies I," submitted by S. Cohn-Sfetcu in partial fulfillment of the requirements for the degree of Master of Science in Physics.

H.A. Buckmaster (Supervisor)
Department of Physics

D.J.I. Fry
Department of Physics

S.T. Nichols
Dept. of Electrical Engineering

R.B. Streets, Jr.
Dept. of Electrical Engineering

Date: April 23, 1973

ABSTRACT

This thesis investigates the utility of a digital Fourier analyser in improving the performance of electron paramagnetic resonance (EPR) spectrometers.

A brief introduction to the concepts of experiment performance and EPR spectroscopy is given, followed by four major sections:

1. A general introduction to EPR and a description of the basic configuration of EPR spectrometers.

2. An introduction to random data analysis and the discrete finite Fourier transform (DFT).

3. A systematic analysis of optimum configurations for reducing the system noise and improving its sensitivity. This analysis is supported by experimental data concerning noise spectral measurements in reflection-cavity EPR spectrometers obtained using a digital Fourier analyser. A new method for an *in situ* determination of microwave detector performance is described.

4. A description of EPR signal processing techniques and their DFT implementation using a digital Fourier analyser.

ACKNOWLEDGEMENTS

The author wishes to thank all members of the EPR group, led by Dr. H.A. Buckmaster, who have contributed in so many ways to the completion of this work. In particular, the author wishes to thank:

Dr. H.A. Buckmaster, for his supervision of the entire work and valuable help in the writing and presentation of this thesis;

Dr. S.T. Nichols and Dr. R.B. Street, Jr., for the high standard courses they have presented and helpful discussions and suggestions;

Dr. D.J.I. Fry, Dr. R. Chatterjee, Dr. M. Smith, Dr. Y.H. Shing and Mr. C. Hansen, for informal discussions and suggestions;

Mrs. B. Delay, for her cheerful encouragement and help during the years spent in the EPR group;

Mrs. V. Matwick and Mrs. J. Fountain, in their typing of the bulk of this thesis;

The Physics Department of The University of Calgary for a Graduate Teaching Assistantship during the 1970-1973 academic years;

The University of Calgary for an Intersession Bursary during the summer of 1971 and for a University of Calgary Bursary during the 1972-1973 academic year.

To my parents,

Debora and Haim Cohn

of Bucharest, Romania

"Coping with spectrometer noise is an art within which highly successful practitioners can find large areas of controversy or disagreement."

G.E. Pake

Blois, M.S., Brown, H.W., Lemmon, R.M., Lindblom, R.O. and Weissbluth, M., Eds., 1961, Free Radicals in Biological Systems, (Academic Press, New York).

TABLE OF CONTENTS

CHAPTER PAGE

CHAPTER PAGE

CHAPTER PAGE

CHAPTER PAGE

LIST OF FIGURES

LIST OF SYMBOLS

Oscillator of frequency ν

Variable attenuator

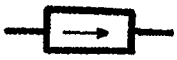

Isolator

Variable phase shifter

Directional coupler

Resonant Cavity

Amplifier

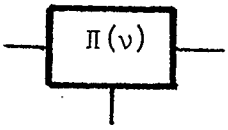

Synchronous demodulator of frequency ν

Magic tee

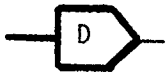

Microwave detector

Microwave diode detector

Microwave short circuit

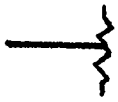

Microwave matched termination

CHAPTER I

INTRODUCTION

All experiments are performed under non-ideal conditions. The results are not exact since the measurements provide information only in a finite probabilistic sense. Instrumentation can be improved until inherent microscopic fluctuations in the system are the limiting factor. The sensitivity is a measure of the capability of an experiment or apparatus to extract information about a phenomenon in the presence of sources of error, i.e. noise. This definition of sensitivity encompasses two parameters describing the information extraction process in a restrictive sense. One of these parameters, which is also called sensitivity, is a measure of the minimum phenomenon "intensity" for which information can be extracted with a non-zero probability. The other is the resolution, which is a measure of the ability to distinguish "adjacent" phenomena. There are situations when the sensitivity in the limited sense can be improved only at the expense of the resolution and vice versa. The economic cost of extracting information is another very important parameter characterizing an experiment. Usually, a compromise must be made between sensitivity and cost. The history of any experimental technique is a record of the continuous struggle to improve the sensitivity while minimizing the cost. This thesis reports an investigation of the application of digital Fourier analysers to improve the performance of electron paramagnetic resonance (EPR) experiments.

EPR is one branch of magnetic resonance spectroscopy. It studies transitions between electronic energy levels whose energy separation is a function of an external magnetic field. Substances containing permanent

electronic magnetic moments are called paramagnetic. The microscopic electronic magnetic dipoles are oriented randomly due to thermal motion and no net magnetic moment is detectable on a macroscopic scale in the absence of an external magnetic field. Such a field produces a macroscopic magnetic moment proportional to its intensity. Chapter II is a succint review of those theories which describe resonance phenomena in paramagnetic substances immersed in electromagnetic fields. EPR spectroscopy has developed enormously since its "discovery" by Zavoiski in 1945. It has been applied to an ever widening range of problems of both a fundamental and an applied nature. EPR is a highly selective technique since it is relevant only for unpaired electrons. At the same time, EPR is very sensitive to phenomena originating in the environment of the paramagnetic dipole because it deals with low-energy transitions.

EPR, in common with other types of spectroscopy, provides information about the location, amplitude and shape of the absorption bands. The photon energies involved are 10^{-27} - 10^{-21}J. The frequency depends on the value of the external magnetic field. Experimentally, EPR uses frequencies in the microwave region. The intensity of the resonance phenomenon is a measure of the number of magnetic dipoles in the sample. The minimum number of spins that an EPR spectrometer can detect is $\sim 10^{11}$. The line shape and the fine, hyperfine and superhyperfine structure components give information concerning the environment of the electronic dipole. The number of structure components may vary from one in a simple environment to hundreds in some organic radicals. The commonest lineshapes are described mathematically by Lorentzian or Gaussian functions although intermediate shapes also occur. The wealth of information that can be extracted using EPR explains the extensive use of this

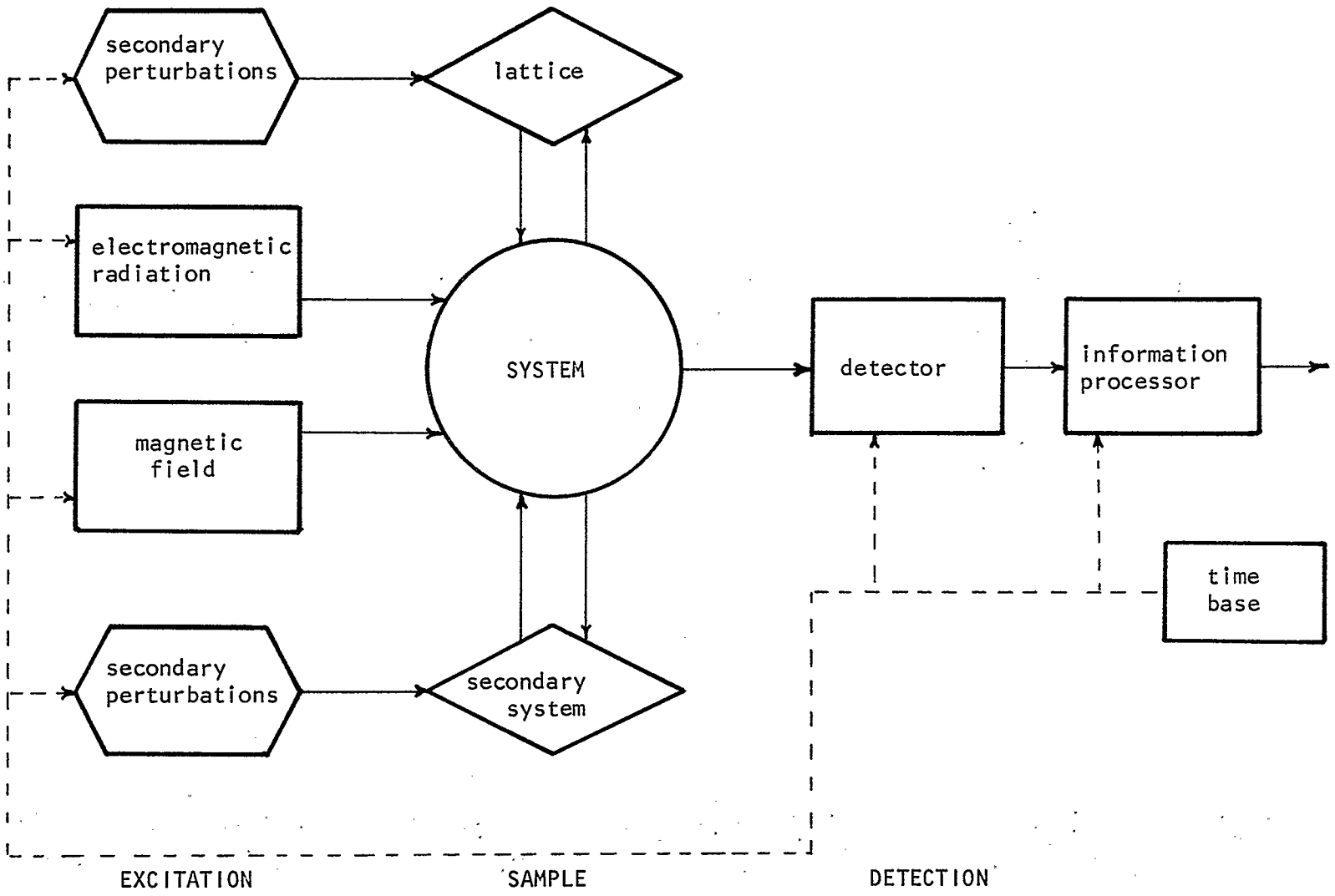

FIGURE 1.1 Block diagram of an EPR experiment

technique as a research tool in many areas of investigation (Alger, 1968; Ursu, 1971).

EPR is an extremely valuable tool in the study of well-ordered systems such as single crystals of metals, dielectrics and semiconductors. Special attention has been extended to trapped electrons or defect centers which are responsible for some important processes occurring in solids. Great advances have been made in investigating the colour, luminescence, charge carrier mobility, etc. using EPR. EPR studies of paramagnetic ions of transition elements in a variety of host crystals played and continue to play an important role in developing lasers and masers. EPR studies have been instrumental in understanding free radicals. Organic free radicals are especially important in polymer chemistry, pyrolysis, radiochemistry, photochemistry, electrochemistry, etc. Ions, triplet state molecules and solvated electrons can be also studied. Many reactions can be studied dynamically without interference using EPR. Consequently, EPR is used in closed-loop controls of various chemical processes. EPR studies have led to the development of many new catalysts. Recently, EPR studies have been extended to biological research since the radicals can be monitored in various biological processes. Magnetic resonance studies have been performed even on animals *in vivo*.

An EPR experiment involves three basic units: 1) the system to be investigated; 2) the electromagnetic excitation and 3) the detection system. These elements are common to all forms of electromagnetic spectroscopy. A block diagram of an EPR experiment is given in Fig. 1.1. The investigated system is usually complex. The electronic magnetic dipoles whose behaviour in an electromagnetic field is studied by EPR are embedded in a lattice which influences their response to excitation.

In addition, the magnetic dipole system may not be homogeneous or it may interact with other quantum mechanical systems so that secondary perturbations occur. The magnetic resonance condition implies that a relationship exists between a steady magnetic field and the frequency of the electromagnetic radiation field. These fields are provided by the excitation system. The resonance phenomenon may be influenced by secondary perturbations acting upon either the lattice or other quantum mechanical systems interacting with the magnetic dipoles to be studied. These secondary perturbations may introduce experimental difficulties but they may also be used to enhance the information extracted. The detection system consists of a detector for the resonance phenomenon, an information processor and a time base. The latter is used to obtain information dynamically and display its time dependence graphically, but it is not an essential part of the detection system. The time base usually controls the amplitude of the steady magnetic field in EPR experiments. The complexity of EPR experiments can be seen by considering the ranges of the parameters usually involved: steady magnetic field 0-3T; electromagnetic radiation frequency 10^6-10^{11}Hz; electromagnetic excitation field power 10^{-12}-10W; temperature 1-1000K; pressure 0-10^5 atm; magnetic field modulation frequency 10-10^6Hz. The samples studied range from metals, semiconductors, dielectrics, gases, liquids and solids to complex biologic compounds.

It is a formidable task to determine the experimental configuration yielding maximum of information with maximum probability. An analytical expression containing all the parameters that can be optimized cannot be derived. The sensitivity is a function of the signal strength and the noise level. The experimental sensitivity can be enhanced by

a) increasing the signal strength, b) decreasing the noise level and c) separating the signal from the noise. The signal strength can be increased by increasing the static or transverse magnetization or by improving the instrumentation. The static magnetization can be increased by using a large sample, a high magnetic field, double resonance decoupling, indirect detection of resonance or by cooling the lattice or the spin system. The transverse magnetization can be increased by shortening the longitudinal relaxation time, using flowing sample and fast passage techniques. Alternatively, multichannel, pulse or Fourier transform spectroscopic techniques can be employed. The noise level can be decreased by optimizing the detector input circuit, the excitation source and the experiment environment. The signal can be separated from noise by using field and time sharing modulation, time averaging methods and spectrum processing. It is usually necessary to use some combination of these methods.

This thesis is concerned with a critical study of methods for reducing the noise and separating the signal from the noise. The use of a digital Fourier analyser in connection with these methods is investigated as a practical application. Chapter III reviews several basic concepts of noise theory, namely the mathematical description of random processes and their properties under various linear transformations. Chapter IV describes the basic configuration of an EPR experiment with particular reference to the "noise properties" of the radiation source, the sample cell and the microwave detector. A brief analysis of the influence of their operating parameters on the signal strength and hence on the sensitivity is given. Methods for decreasing the noise level are discussed in Chapter V, where the most important noise sources are identified and

the possibilities of improving their "noise performance" are then reviewed. An analysis of noise propagation in an EPR spectrometer is presented in order to draw conclusions regarding the optimum configuration design. Magnetic field modulation techniques, although identified as methods to separate the signal from noise, are discussed in this chapter to give a unified picture of the technical problems encountered in the design of an EPR spectrometer. The other methods used to separate the signal from noise are discussed in Chapter VI. Time sharing modulation techniques which apply primarily to pulsed experiments are not discussed in this thesis. Special attention is given to spectrum processing techniques. They can be used to improve either the sensitivity or the resolution and occasionally both. The last section of this chapter reviews the digital implementation of these techniques.

The remainder of this thesis is concerned with the implementation of sensitivity enhancement methods using a digital Fourier analyzer. A digital Fourier analyzer is a twofold valuable tool since on one hand it enables the measurement of noise spectra in the low frequency region and, on the other hand, it can simulate linear systems. Chapter VII presents the fundamentals of the Discrete Fourier transform and its implementation on digital computers using the Fast Fourier Transform algorithm. The use of the digital Fourier analyser as a noise measurement device in an EPR spectrometer is described in Chapter VIII. Such measurements provide a necessary basis for a comprehensive discussion of methods for decreasing the noise level since an <u>in situ</u> assesment of the relative importance of noise sources in different frequency regions is possible. Conclusions regarding an optimum design of an EPR spectrometer are given. In addition, methods of noise measurement in microwave devices

are discussed critically and constructively. A new method of measuring the performance of a microwave detector is described in Sec. 8.6. Chapter IX analyses the use of a digital Fourier analyser in processing EPR spectra for both sensitivity and resolution enhancement. Section 9.3 discusses the implementation of the Hilbert transform and its use in calculating the Kramers-Krönig relation.

A digital Fourier analyser is also an indispensable component of random and/or Fourier transform spectrometers. The application of random and Fourier transform spectroscopy in NMR has been described by Ernst (1971) and Ernst and Anderson (1966) respectively. They have not been applied in electron paramagnetic resonance spectroscopy and consequently will not be discussed in this thesis although they are expected to play a role in the future.

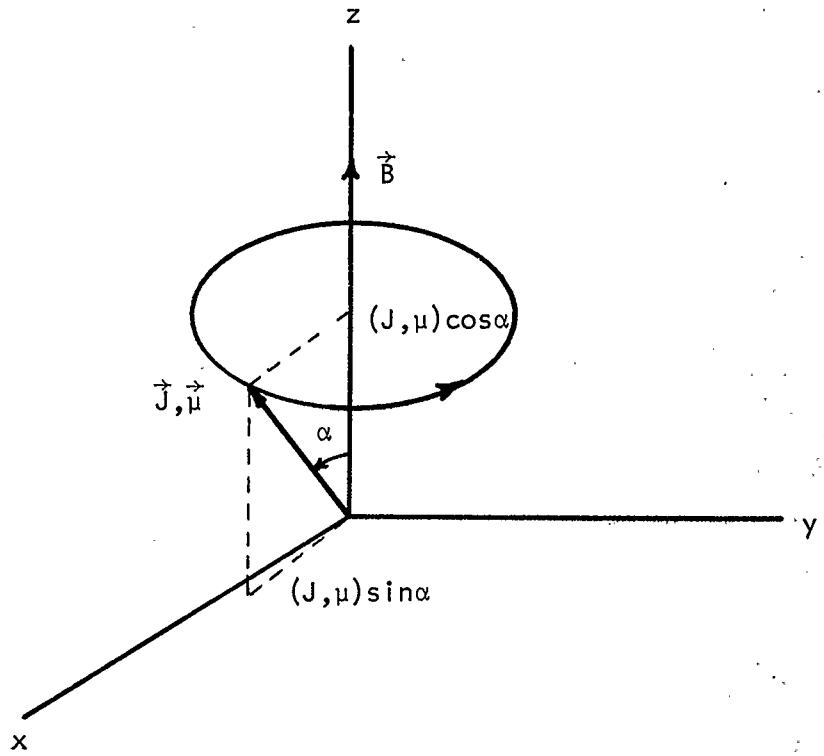

FIGURE 2.1 Diagram illustrating the precession of a magnetic dipole μ with angular momentum J around an applied magnetic field B.

CHAPTER II

ELEMENTARY THEORY OF EPR

2.1 The Resonance Phenomenon

Permanent magnetic dipoles exist in atoms and molecules whenever there is a resultant angular momentum $\vec{J}$. The angular momentum and the magnetic moment $\vec{\mu}$ are related by

$$\vec{\mu} = \gamma\hbar\vec{J} \tag{2.1.1}$$

where $\hbar$ is Planck's constant divided by 2π and γ is the gyromagnetic ratio. These magnetic dipoles are oriented randomly in the absence of an external magnetic field. The equation of motion of a magnetic dipole in an external magnetic field is

$$\hbar\frac{d\vec{J}}{dt} = \vec{\mu}\times\vec{B} = \gamma\hbar(\vec{J}\times\vec{B}) \tag{2.1.2}$$

where $\vec{B}$ is the magnetic flux density.

The solution of Eq. 2.1.1 shows that the angular momentum $\vec{J}$ precesses around the direction of the magnetic field $\vec{B}$ with an angular velocity

$$\vec{\omega}_L = -\gamma\vec{B}. \tag{2.1.3}$$

Figure 2.1 is a diagram of this effect. The sense of the precession is governed by the sign of γ. This sign is rarely of interest in EPR; however Koepp (1969) has designed a spectrometer with which this sign determination can be made.

The Zeeman energy W, the energy of a magnetic dipole in an external magnetic field, is a constant of the motion since the component

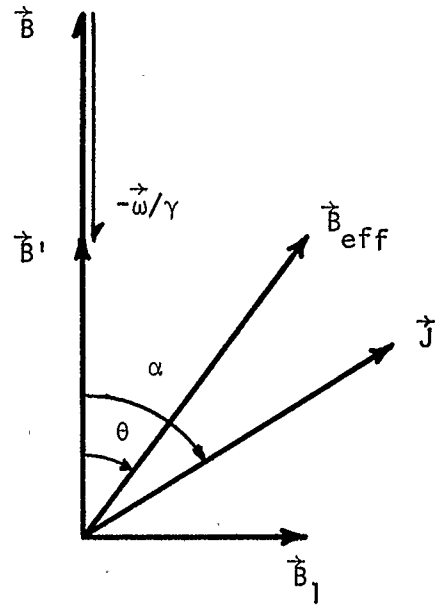

FIGURE 2.2 Diagram showing the effective fields in the rotating coordinate system.

of the angular momentum parallel to the direction of the magnetic field has constant magnitude.

$$W = -\vec{\mu}\cdot\vec{B} = -\gamma\hbar|\vec{J}||\vec{B}|\cos\alpha \tag{2.1.4}$$

The oscillatory motion of the x- and y-components of the angular momentum permits them to interact with a rotating magnetic field $\vec{B}_1$ which is not parallel to the constant external magnetic field $\vec{B}$.

The equations of motion are easier to solve in a coordinate system which rotates around $\vec{B}$ with the same angular velocity $\vec{\omega}$ as the rotating magnetic field $\vec{B}_1$. The time derivative of a vector in the rotating system is

$$\frac{\delta\vec{A}}{\delta t} = \frac{d\vec{A}}{dt} - \vec{\omega} \times \vec{A} \tag{2.1.5}$$

Substituting Eq. 2.1.5 into Eq. 2.1.2 yields

$$\frac{\delta\vec{J}}{\delta t} = \gamma\hbar\vec{J} \times (\vec{B} + \vec{\omega}/\gamma) = \gamma\hbar\vec{J} \times \vec{B}' \tag{2.1.6}$$

where $\vec{B}'$ is the effective external magnetic field in the rotating system. The angular momentum $\vec{J}$ and the magnetic dipole moment $\vec{\mu}$ precess about $\vec{B}'$ with an angular velocity $\vec{\omega}'$ where

$$\vec{\omega}' = -\gamma\vec{B}' = \vec{\omega}_L - \vec{\omega} . \tag{2.1.7}$$

When a rotating field $\vec{B}_1$ is also applied, the effective magnetic field becomes

$$\vec{B}_{eff} = \vec{B}' + \vec{B}_1 \tag{2.1.8}$$

and the precession occurs around the direction of $\vec{B}_{eff}$. This situation is illustrated in Fig.2.2.

The angle α in Eq.2.1.4. is of interest. If $\alpha = 0$ at time $t = 0$, then

$$\cos\alpha = 1 - 2\sin^2\theta \sin\left((1/2)[(\omega-\omega_L)^2 + (\gamma B_1)^2]^{1/2}t\right) \qquad (2.1.9)$$

Resonance occurs when $\omega=\omega_L$ because $\theta=\pi/2$ and $\vec{J}(\vec{\mu})$ precesses around $\vec{B}_1$ in a plane normal to its direction. $\vec{J}(\vec{\mu})$ is alternatively parallel and anti-parallel to the external magnetic field $\vec{B}$. This implies that the energy of the magnetic dipole alternates in sign. This resonance phenomenon can be observed in various ways. This thesis will be concerned mainly with the steady-state methods, in which a net absorption of energy from the rotating field is detected.

The discussion has been based on purely classical arguments, however Pake (1962) has shown that a quantum mechanical approach leads to identical conclusions. Quantum mechanics allows only integral or half integral values of J and limits the projections of $\vec{J}$ on the direction of the external magnetic field to discrete values

$$|\vec{J}| \cos\alpha = M, M-1, \ldots, -M \qquad (2.1.10)$$

where M is the magnetic quantum number ($M = |J|$). Rabi (1937) has shown for $J = 1/2$ that the probability of finding the system in the state $|-1/2\rangle$ at time t if it was in the state $|+1/2\rangle$ at $t = 0$ is

$$P\{|-1/2\rangle\} = \frac{\gamma B_1^2}{[(\gamma B+\omega)^2 + (\gamma B_1)^2]^{1/2}} \sin^2\left((1/2)[(\gamma B+\omega)^2 + (\gamma B_1)^2]^{1/2}t\right) \qquad (2.1.11)$$

The similarity of Eq.2.1.11 with Eq.2.1.9 is evident. This probability will be significant only if $(\gamma B+\omega)$ approximates to zero, which implies that $\omega\approx\omega_L$. In this case the atom will alternate between the two states even

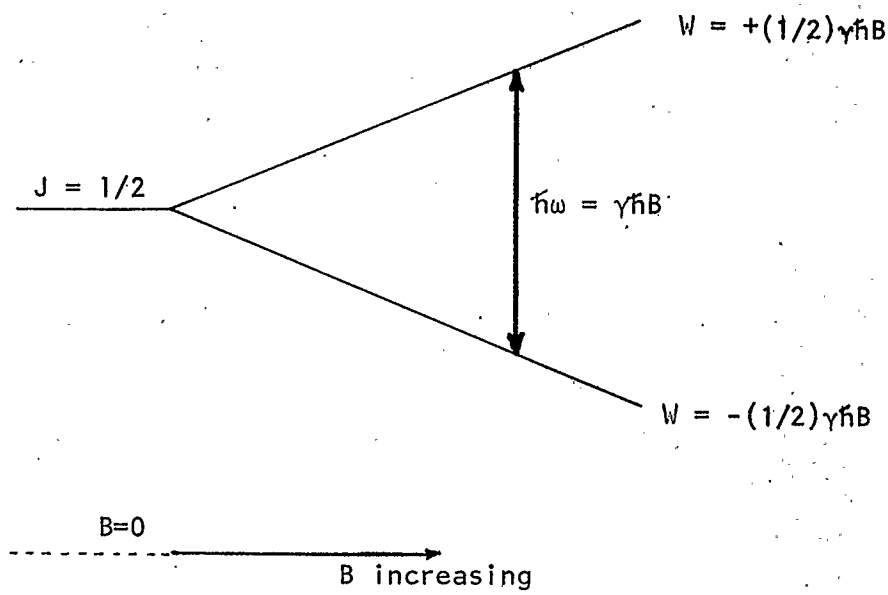

FIGURE 2.3 Energy levels diagram for J = 1/2 in an applied field B, showing Zeeman transitions.

if the field $\vec{B}_1$ is very small. The magnitude of $\vec{B}_1$ determines the rate of change between the two states. This transition corresponds to the selection rule $\Delta M=\pm 1$. The resonance condition

$$\hbar\omega = W_M - W_{M-1} = \gamma\hbar B \tag{2.1.12}$$

corresponds to the resonance condition obtained using the classical approach.

It can be shown that the classical equation of motion itself is quantum mechanically valid. The time derivative of an operator is proportional to the commutator of the same operator with the system Hamiltonian

$$-j\hbar \frac{d\vec{J}}{dt} = \left[H\cdot\vec{J} - \vec{J}\cdot H\right] \tag{2.1.13}$$

For the system under discussion

$$H = -\vec{\mu}\cdot\vec{B} = -\gamma\hbar\vec{J}\cdot\vec{B} \tag{2.1.14}$$

It can be shown that Eq.2.1.13 reduces to Eq.2.1.2 if account is taken of relations between the components of $\vec{J}$. The subsequent discussion will employ the classical approach since it is more intuitive.

The previous discussion has assumed that the system consists of a single, free particle. Aggregate systems consisting of a number of particles have complex Hamiltonians and the classical approach breaks down. There are cases when this approach remains approximately valid. The analysis of such systems focuses on $\vec{M}$, the magnetic moment of the system, which is the vectorial sum of the individual magnetic moments. The equation of motion is

$$\frac{d\vec{M}}{dt} = \gamma\vec{M} \times \vec{B} \tag{2.1.15}$$

if the particles have identical values of γ. The analysis is then similar to that for a single particle.

The resonance phenomenon involves an alternate absorption and emission of energy. The particles jump between energy levels emitting or absorbing quanta of energy. The populations of the two levels will become equal and there will be no further interaction with the external field unless the population of the upper energy level decreases due to nonradiative processes. These processes are discussed in Sec. 2.2.

2.2 The Relaxation Phenomena

There are three types of transition involving the interaction of electromagnetic radiation with an atomic system. Stimulated absorption and emission are coherent (in phase and frequency) interactions with the radiation field in which the number of transitions is proportional to the energy density of this field at the transition frequency. The third process is spontaneous emission in which the emission of photons by the system is independent of the radiation field. This process can be neglected since the Einstein coefficient for spontaneous emission is negligible compared with that for stimulated emission at the frequencies involved in magnetic resonance. The coefficients for stimulated emission and absorption are then effectively equal. Consequently, absorption or emission of energy can be detected in magnetic resonance only if the populations of the two energy levels are unequal.

Boltzmann statistics are valid for states of thermodynamical equilibrium so that

$$N_b/N_a = \exp(-\hbar\omega/kT) \qquad (2.2.1$$

where N_a and N_b are the populations of the lower and upper levels, $\hbar\omega$ is the difference in energy, k is the Boltzmann's constant and $T=T_o$ is the ambient temperature. The power absorbed by the spin system immersed in a radiation field is

$$\frac{dW}{dt} = w_e(\hbar\omega)(n_a-n_b) \tag{2.2.2}$$

where w_e is the atomic rate at which transitions are induced and n_a and n_b are the instantaneous populations of the lower and upper energy states. The two instantaneous populations tend to equalize if no other process is involved. A spin temperature T_s may be defined by assuming that Eq.2.2.1. is also valid for nonequilibrium conditions.

$$T_s = (\hbar\omega/k)/\ell n(n_a/n_b) \tag{2.2.3}$$

This temperature becomes infinite if $n_a=n_b$. Then it is necessary to infer the existence of other nonradiative processes which tend to restore the population difference. These processes describe the interaction between the spin system and the thermal fluctuations of the lattice in which the spin system is embedded. It is appropriate to describe such a tendency toward equilibrium by a relaxation equation

$$\frac{d(n_a-n_b)}{dt} = (1/\tau_1)[(N_a-N_b) - (n_a-n_b)] \tag{2.2.4}$$

where τ_1 is the time constant or relaxation time of the process. In the presence of the radiation field, Eq.2.2.4. becomes

$$\frac{d(n_a-n_b)}{dt} = (1/\tau_1)(N_a-N_b) - (2w_e+1/\tau_1)(n_a-n_b) \tag{2.2.5}$$

which has the steady-state solution

$$(n_a-n_b)/(N_a-N_b) = (1+2w_e\tau_1)^{-1} . \tag{2.2.6}$$

The power absorbed from the electromagnetic radiation field is

$$\frac{dW}{dt} = w_e(\hbar\omega)(N_a - N_b)/(1+2w_e\tau_1). \tag{2.2.7}$$

Eqs.2.2.6 and 2.2.7 describe the power saturation phenomenon. The power absorbed in a strong electromagnetic field has a maximum value which is a function of τ_1. The power absorbed from the field balances the power absorbed by the thermal heat-sink via the spin-lattice relaxation mechanism.

Waller (1932) made the first analysis of the mechanisms involved in this interaction. Many quantitative formulations have been proposed to describe the temperature dependance of the relaxation time. The most notable is due to Orbach (1961). The concept of a "phonon radiation bath" describing the lattice vibrations is fundamental to all these mechanisms. A general formula for the temperature dependance of τ_1 which includes the effects of these different spin-lattice interaction processes is

$$1/\tau_1 = A\coth(\hbar\omega/2kT_0) + BT_0^n + C/[\exp(\Delta/kT_0)-1]. \tag{2.2.8}$$

The first term in Eq.2.2.8 describes the direct process which requires the interaction with coherent phonons, i.e. phonons of the same energy as the magnetic resonance quantum $\hbar\omega$. It is important only in the low temperature region ($\leq 4^oK$), since otherwise the number of phonons at resonance with the magnetic system is very small. The second term in Eq.2.2.8 describes Raman processes, in which a phonon is scattered inelastically. This is equivalent to a two-phonon process; their energy difference is the quantum necessary for the "magnetic" transition. Such processes are strongly temperature dependent. They play a major role in the high temperature region since all phonons can participate

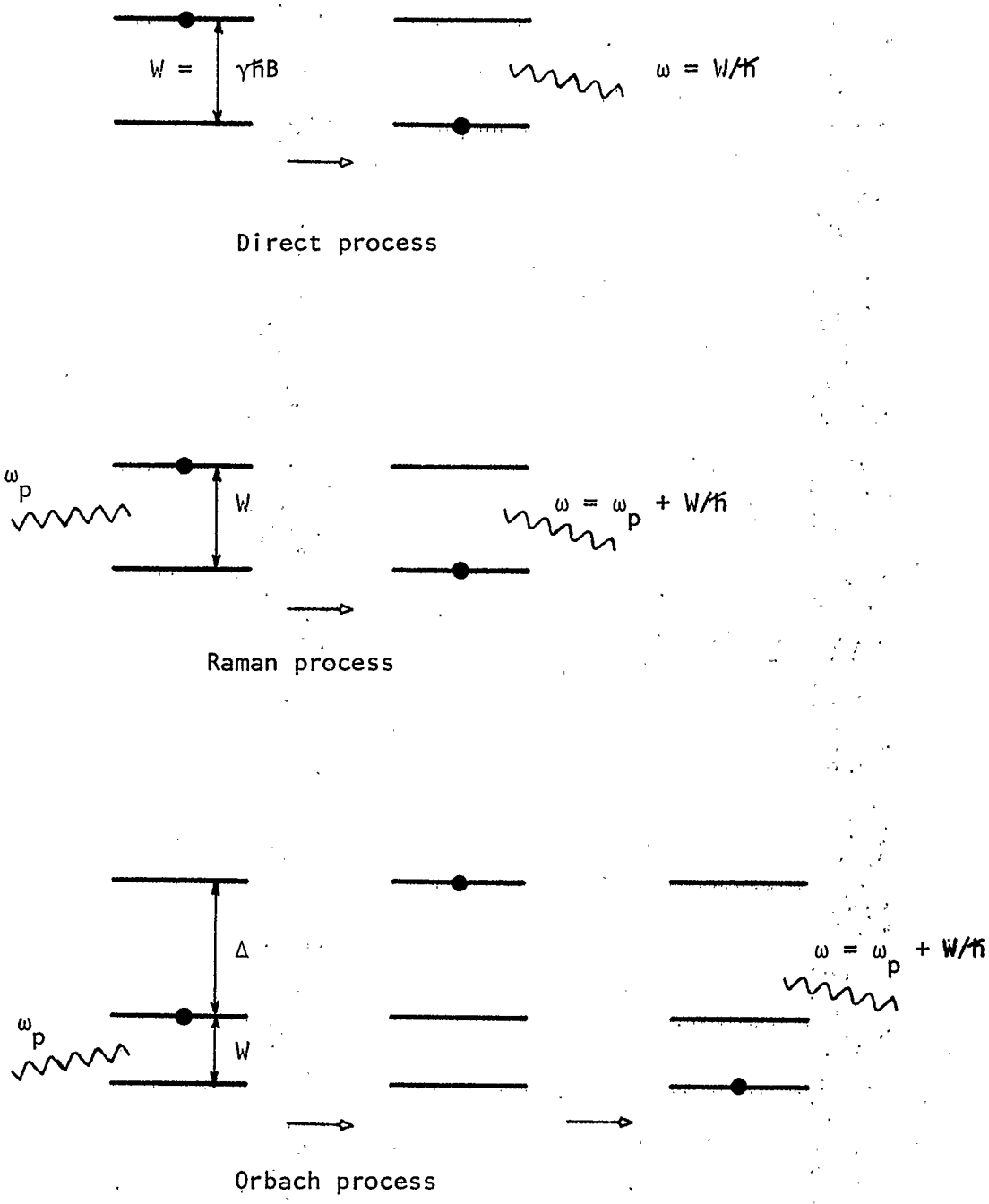

FIGURE 2.4 Diagram illustrating the various spin-lattice relaxation processes.

although they are second-order processes because of the weak coupling between the phonons and the spin system. The third term in Eq.2.2.8 describes the effect of the Orbach process, which is also a direct process but involves a third, higher energy level as well as the ground state doublet. The Orbach process is also strongly temperature dependent since it requires phonons of energy Δ in order to excite the atom to the upper level. Fig.2.4 is an energy diagram describing these three processes. This represents a simplified picture of the actual process. Mention should be made of the important mechanism of transmitting the thermal energy from the resonant phonon system to the rest of the phonons and the thermal bath. This involves such phenomena as the "phonon bottle-neck" and/or the "phonon avalanche".

The spin-spin interaction is another nonradiative process involved in the magnetic resonance phenomenon. It describes the nondissipative interaction between neighbouring paramagnetic ions. There are various ways in which such an interaction can occur and influence the response of the system to an electromagnetic field. For example, the total magnetic field, which is a vectorial composition of the external fields with the local field due to the neighbouring magnetic moments depends on the lattice. The components of the local field parallel to the external field may introduce a variation of the total field value and hence a variation of the resonant frequency from site to site. Random resonant field values have an effect similar to that due to an inhomogeneous external magnetic field and both lead to an "inhomogeneous broadening" of the resonance line.

The precessing magnetic moments also create an oscillating field at the site of the neighbouring ions enhancing the probability of magnetic

resonance transitions. This effect shortens the lifetime of an atom in the respective quantum states and leads, through the uncertainty principle, to a broadening of the energy levels. This phenomenon is characterized by a spin-spin relaxation time τ_2, which determines the linewidth of a "spin-packet", a group of spins having the same precessional frequency.

Other forms of interaction can occur due to the overlap of electronic charge clouds when the separation between neighbour ions is less than ~ 0.5 nm. This "exchange interaction" leads to a narrowing of the linewidth. The phenomenon resembles the narrowing caused by the rapid fluctuations of the atoms in a fluid. This rapid change in the orientations of the magnetic dipoles produces an oscillating local field which is less effective in broadening the resonance line.

2.3 Bloch Formalism

Bloch (1946) derived a set of equations describing the behaviour of the system magnetization $\vec{M}$ in which account was taken of both the spin-lattice and the spin-spin relaxation phenomena. The component of $\vec{M}$ parallel to the external magnetic field $\vec{B}$ is influenced only by the spin-lattice interaction since this is the mechanism causing the energy dissipation. The Zeeman energy W is

$$W = -\vec{M}\cdot\vec{B} = -M_z B, \tag{2.3.1}$$

M_z is directly proportional to the population difference of the ground doublet and tends to an equilibrium value M_o.

$$\frac{dM_z}{dt} = \dot{M}_z = -(M_z - M_o)/\tau_1 \tag{2.3.2}$$

where τ_1, the spin-lattice relaxation time, is also called the longitudinal relaxation time.

The spin-spin interaction enables the transverse oscillating fields due to the precessing magnetic moments to induce transitions. This affects only the x- and y-components of the magnetization $\vec{M}$. Block had the insight to assume that the same mathematical relationship was valid for these transverse components

$$\dot{M}_x = -M_x/\tau_2 \tag{2.3.3a}$$

$$\dot{M}_y = -M_y/\tau_2 \tag{2.3.3b}$$

The equilibrium values for these components are zero. τ_2 is known as the transverse relaxation time and can be related to the spin-spin relaxation time. These equations lead to an exponential free induction decay whose Fourier transform is the magnetic resonance line of Lorentzian lineshape. The fact that magnetic resonance lines have sometimes non-Lorentzian shapes indicate that Eqs.2.2.3 are not universally valid.

The Bloch formalism is

$$\dot{M}_x = \gamma(\vec{M}\times\vec{B})_x - M_x/\tau_2 \tag{2.3.4a}$$

$$\dot{M}_y = \gamma(\vec{M}\times\vec{B})_y - M_y/\tau_2 \tag{2.3.4b}$$

$$\dot{M}_z = \gamma(\vec{M}\times\vec{B})_z - (M_z-M_o)/\tau_1 \tag{2.3.4c}$$

The external magnetic field is a combination of the steady magnetic field parallel to the z-direction and the magnetic field $\vec{B}_1$ precessing in the xy-plane with an angular velocity ω. The magnetic field can be described in the xy-plane either by the Cartesian components

$$B_x = B_1 \cos(\omega t) \tag{2.3.5a}$$

$$B_y = B_1 \sin(\omega t) \tag{2.3.5b}$$

or by a complex quantity

$$B_+ = B_x + jB_y = B_1 \exp(j\omega t). \tag{2.3.5c}$$

Pake (1962) was the first to obtain a steady state solution of Eqs.2.3.4 ; however, the solution outlined by Abragam and Bleaney (1972) will be followed since it is simpler. If

$$M_\pm = M_x \pm jM_y \tag{2.3.6}$$

then Eqs.2.3.4. become

$$\dot{M}_+ + j\gamma BM_+ + M_+/\tau_2 = j\gamma M_z B_1 \exp(j\omega t) \tag{2.3.7a}$$

$$\dot{M}_- - j\gamma BM_- + M_-/\tau_2 = -j\gamma M_z B_1 \exp(-j\omega t) \tag{2.3.7b}$$

$$\dot{M}_z + M_z/\tau_1 = j\gamma[M_+\exp(-j\omega t) - M_- \exp(j\omega t)]B_1/2 + M_o/\tau_1. \tag{2.3.7c}$$

The experimental system discussed in this thesis employs slow passage signal processing which means that steady-state conditions always prevail. This is equivalent to looking for solutions of Eqs.2.3.7 when $\dot{M}_z=0$. The advantages of using this form of Bloch equations are now evident since the solutions are obtained easily.

$$\frac{M_z}{M_o} = \frac{1 + (\omega-\omega_L)^2\tau_2^2}{1 + (\omega-\omega_L)^2\tau_2^2 + \gamma^2 B_1^2 \tau_1\tau_2} \tag{2.3.8a}$$

$$\frac{M_\pm}{M_o} = \frac{[(\omega-\omega_L)\tau_2 \pm j]\ \gamma B_1\tau_2 \exp(\pm j\omega t)}{1 + (\omega-\omega_L)^2\tau_2^2 + \gamma^2 B_1^2\ \tau_1\tau_2} \tag{2.3.8b}$$

This solution corresponds to the magnetization vector $\vec{M}$ precessing at an angle θ around $\vec{B}$ with an angular velocity ω where

$$\tan\theta = |M_{\pm}|/M_z = \gamma B_1\tau_2\left[1 + (\omega-\omega_L)^2\tau_2^2\right]^{-1/2} \tag{2.3.9}$$

The equatorial component $M_{\pm}$ of the magnetization leads the rotating field B_1 by an angle ε where

$$\tan\varepsilon = 1/\tau_2(\omega-\omega_L). \tag{2.3.10}$$

These solutions are similar to those obtained to describe the forced resonance phenomenon in the theory of electromagnetic networks. An "impedance" concept, the complex susceptibility χ, can be introduced.

$$\vec{M} = \chi\cdot\vec{B} \tag{2.3.11a}$$

$$M_+ = \chi B_1 \exp(j\omega t) \tag{2.3.11b}$$

$$\frac{\chi}{\chi_o} = \frac{\gamma B\tau_2[(\omega-\omega_L)\tau_2 + j]}{1 + (\omega-\omega_L)^2\tau_2^2 + \gamma^2 B_1^2\tau_1\tau_2} \tag{2.3.11c}$$

Equation 2.3.11a is the most general definition of the susceptibility as a tensor. χ is considered a scalar in Eqs.2.3.11b and 2.3.11c and χ_o is the value corresponding to the equilibrium magnetization M_o. Experimentally, there is interest in detecting either the real or the imaginary part of χ.

$$\chi = \chi' - j\chi'' \tag{2.3.12a}$$

$$\frac{\chi'}{\chi_o} = \frac{\omega_L(\omega_L-\omega)\tau_2^2}{1 + (\omega_L-\omega)^2\tau_2^2 + \gamma^2 B_1^2\tau_1\tau_2} \tag{2.3.12b}$$

$$\frac{\chi''}{\chi_o} = \frac{\omega_L\tau_2}{1 + (\omega-\omega_L)^2\tau_2^2 + \gamma^2 B_1^2\tau_1\tau_2} \tag{2.3.12c}$$

A discussion of the lineshapes described by χ' (dispersion) and χ'' (absorption) is presented in the next section.

The spin system absorbs energy from the rotating field at a rate

$$\frac{dW}{dt} = B_x\dot{M}_x + B_y\dot{M}_y = \omega\chi''B_1^2 \qquad (2.3.13)$$

The phenomenon of dynamic power saturation occurs if $B_1^2 >> 1/\gamma^2\tau_1\tau_2$. The energy absorbed at resonance is then independent of B_1 and τ_2 since

$$\frac{dW}{dt} = \left(\frac{M_oB}{\tau_1}\right)\left(\frac{\gamma^2B_1^2\tau_1\tau_2}{1+\gamma^2B_1^2\tau_1\tau_2}\right) = \left(\frac{M_oB}{\tau_1}\right)\left(\frac{M_o-M_z}{M_o}\right) \qquad (2.3.14)$$

2.4 Magnetic Resonance Line Shapes

The ultimate minimum width of a magnetic resonance line is set by Heisenberg's uncertainty principle

$$\delta E\delta t \geq \hbar \qquad\qquad \delta\nu \geq 1/2\pi\delta t \qquad (2.4.1)$$

where δE, δt and $\delta\nu$ are the uncertainties in the energy level, in the time spent on that level and in the resonant frequency. δt is associated with the relaxation time concept discussed previously. This width is never observed since other interactions broaden the line by shortening the relaxation time. Homogeneous broadening is due to finite lifetimes of the states involved. Inhomogeneous broadening arises when the line is the envelope of a multitude of lines due to paramagnets precessing at different Larmor frequencies. Portis (1953) was the first to treat systematically these broadening phenomena.

Homogeneous broadening can be caused by

-dipole-dipole interactions between like spins

-spin-lattice relaxation

-interactions of spins with the radiation field

-motion of unpaired spins in the electromagnetic field

-motionally narrowed fluctuations in the local field

while inhomogeneous broadening can be caused by:

-hyperfine interactions

-anisotropic splitting of the spin levels

-dipolar interactions between spins with different Larmor frequencies (cross-relaxation).

The homogeneous broadening produces a Lorentzian lineshape, while the inhomogeneous broadening produces a Gaussian lineshape. In practice, some complicated combination of these broadening mechanisms occurs (Poole and Farach, 1971).

In addition, the experimental system also broadens the line. Spatial inhomogeneity of the external magnetic field over the sample as well as temporal instability in the frequency of the radiation field produce inhomogeneous broadening. High frequency magnetic field modulation employed to increase the detection sensitivity can also cause broadening. The radiation field strength is limited by the phenomenon of saturation which does not affect the lineshape uniformly. This effect may be used to discriminate between homogeneous and inhomogeneous broadening (Alger, 1968).

According to Bloch's simplified approach, the magnetic resonance lineshape is Lorentzian in the absence of saturation. The slowly varying parameter is the magnitude of the steady external magnetic field $\vec{B}$ and not the frequency ω since it is very difficult to vary the resonant frequency of the sample cavity in unison with the radiation field frequency. Equation 2.3.12 can be expressed in terms of B rather than ω.

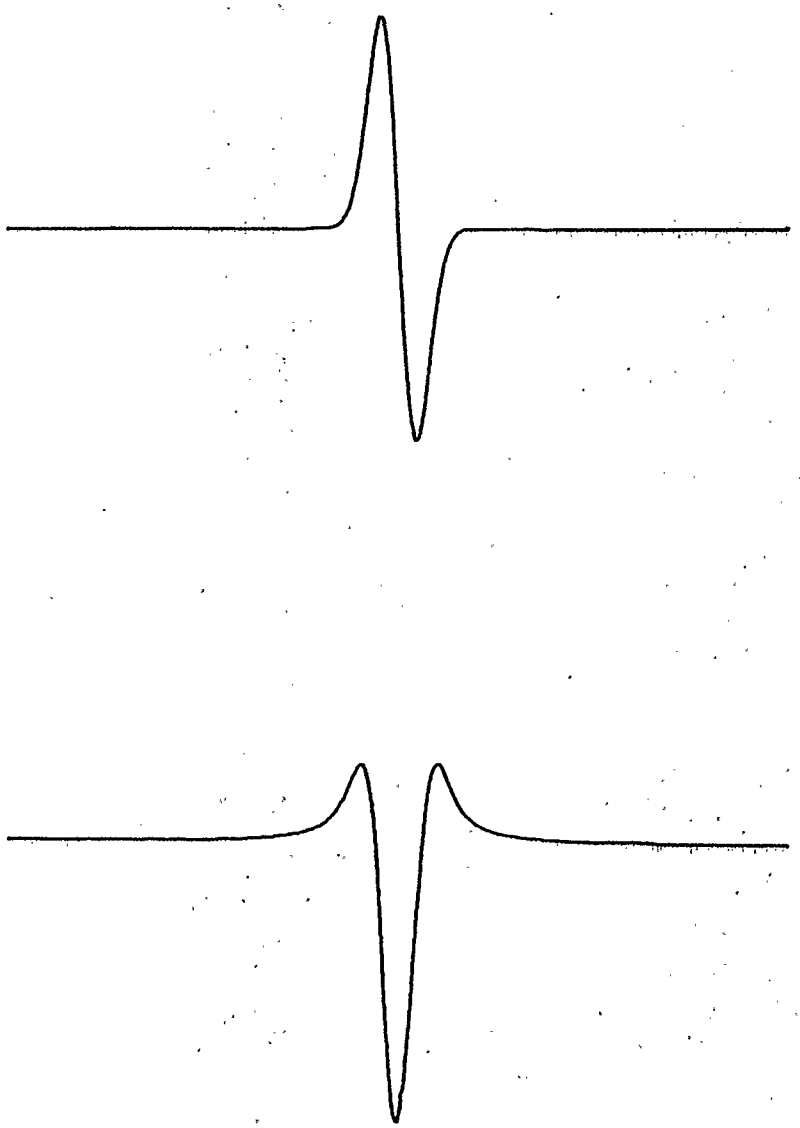

FIGURE 2.5 Diagram showing the shape of the first Fourier coefficients of the absorption and dispersion components of the magnetic susceptibility χ.

$$\chi'(B) = \frac{\chi_o B_o}{\Delta B_{1/2}} \quad \frac{2(B-B_o)/\Delta B_{1/2}}{1 + [2(B-B_o)/\Delta B_{1/2}]^2} \tag{2.4.2a}$$

$$\chi''(B) = \frac{\chi_o B_o}{\Delta B_{1/2}} \quad \frac{1}{1 + [2(B-B_o)/\Delta B_{1/2}]^2} \tag{2.4.2b}$$

where B_o is equal to ω_o/γ, ω_o is the radiation field frequency and $\Delta B_{1/2}$ is the linewidth at half-height, related to τ_2 by

$$\Delta B_{1/2} = 2/\tau_2. \tag{2.4.3}$$

Equations 2.4.2 differ from Eqs.2.3.12 by a factor of two since, experimentally, an oscillating rather than a rotating transverse field B_1 is used. This transverse field is equivalent to two fields of amplitude $B_1/2$ rotating in opposite directions. Only one of these fields is effective in producing magnetic resonances. The output of a magnetic resonance spectrometer is usually the Fourier coefficient $a_1(d_1)$, which is proportional to the first derivative of the absorption (dispersion) component described in Eqs.2.4.2 (Buckmaster, 1971). These derivatives are

$$\frac{d[\chi'(B)]}{dB} = \frac{2\chi_o B_o}{(\Delta B_{1/2})^2} \cdot \frac{1 - [2(B-B_o)/\Delta B_{1/2}]^2}{\left[1 + [2(B-B_o)/\Delta B_{1/2}]^2\right]^2} \tag{2.4.4a}$$

$$\frac{d[\chi''(B)]}{dB} = \frac{\chi_o B_o}{(\Delta B_{1/2})^2} \cdot \frac{2(B-B_o)/\Delta B_{1/2}}{\left[1 + [2(B-B_o)/\Delta B_{1/2}]^2\right]^2} \quad . \tag{2.4.4b}$$

They are shown in Fig.2.5.

There is an intrinsic relationship between χ' and χ'', the real and imaginary parts of the complex susceptibility χ. When the external fields are sufficiently weak the magnetic system is linear and its magnetization can be described by a convolution integral (Slichter, 1963).

$$M(t) = \int_{-\infty}^{+\infty} m(t-t')B(t')dt' \tag{2.4.5}$$

where m(t) is the response of the system to a δ-pulse and

$$m(t) = \int_{-\infty}^{+\infty} m(t-t')\delta(t')dt'. \tag{2.4.6}$$

Another useful definition of m(t) uses the response $M_s(t)$ of the system to a magnetic field step function,

$$m(t) = \frac{d}{dt}\left[M_s(t)\right]. \tag{2.4.7}$$

m(t) is called the "free induction decay" in magnetic resonance. The physical realizability of the magnetic system requires m(t) to satisfy the causality law, i.e. m(t)=0 for t<0, while the stability condition requires that $\int_{-\infty}^{+\infty} |m(t)|\,dt$ is finite.

Bloch's assumptions (Eqs.2.3.2 and 2.3.3) lead to an exponential form for m(t). The sample magnetization after a unit magnetic field is applied in the z-direction is

$$M_z(t) = M_o[1 - \exp(-t/\tau_1)] = M_s(t) \tag{2.4.8}$$

so that

$$m(t) = (M_o/\tau_1)\exp(-t/\tau_1). \tag{2.4.9}$$

If a transverse rotating field B_1 is applied, then

$$M_+(t) = \int_{-\infty}^{+\infty} m(t-t')B_1 \exp(-j\omega t')dt' =$$

$$= B_1\exp(j\omega t)\int_0^{\infty} m(t'')\exp(-j\omega t'')dt''. \tag{2.4.10}$$

By comparison, it is seen that the complex χ defined through Eq.2.3.11b is the Fourier transform of the function m(t).

$$\chi(\omega) = \int_{0}^{\infty} m(t)\ \exp(-j\omega t)\,dt = \mathcal{F}\{m(t)\} \tag{2.4.11a}$$

$$m(t) = (2\pi)^{-1} \int_{-\infty}^{+\infty} \chi(\omega)\ \exp(j\omega t)\,d\omega = \mathcal{F}^{-1}\{\chi(\omega)\} \tag{2.4.11b}$$

In fact these relations were implied in the definition of χ as the "impedance" or frequency transfer function of the magnetic system. Knowledge of either $\chi(\omega)$ or m(t) completely determines the other. The following relations are valid for the absorption and dispersion components

$$\chi'(\omega) = \int_{0}^{\infty} m(t)\ \cos(\omega t)\ dt \tag{2.4.12a}$$

$$\chi''(\omega) = \int_{0}^{\infty} m(t)\ \sin(\omega t)\ dt \tag{2.4.12b}$$

The real and imaginary parts of the frequency transfer function of any linear system are Hilbert transforms of each other (Guillemin, 1963). It follows that

$$\chi'(\omega) - \chi'(\infty) = (1/\pi)\ \mathcal{P} \int_{-\infty}^{+\infty} \frac{\chi''}{(\omega'-\omega)}\, d\omega' = -(1/\pi\omega) * \chi''(\omega) \tag{2.4.13a}$$

$$\chi''(\omega) = -(1/\pi)\ \mathcal{P} \int_{-\infty}^{+\infty} \frac{\chi'(\omega') - \chi'(\infty)}{(\omega'-\omega)}\, d\omega' = (1/\pi\omega) * \chi'(\omega) \tag{2.4.13}$$

where the symbol $\mathcal{P}$ stands for taking the principal part of the integral and the symbol "*" is used throughout this thesis to denote a convolution integral. Equations 2.4.13, which are known as the Kramers-Kronig

relations, demonstrate that the knowledge of one component of χ completely determines the other.

This theory is valid only if the paramagnetic system behaves linearly. Poole and Farach (1971) have surveyed theories applying to more general, nonlinear situations.

CHAPTER III

RANDOM PROCESSES AND LINEAR SYSTEMS - A REVIEW

3.1 Physical Data: Classification and Description

Mathematically, physical data can be considered as either deterministic or random. The deterministic data can be described by explicit mathematical relationships. Precise prediction can be made using such relationships. Randomness implies that only probabilistic statements can be made. This distinction is not very profound since totally random physical data are impossible. Practically, this distinction is made according to the reproducibility of the data by controlled experiments. Physical data are dependent on many variables, but the time dependence is usually of most interest in their analysis.

Deterministic data are either periodic or nonperiodic. Periodic data satisfy the relationship

$$x(t) = x(t+T), \tag{3.1.1}$$

where T is the period and $f_0 = 1/T$ is the fundamental frequency. All periodic data can be expanded into Fourier series. In general, x(t) can be assumed to be a complex function, although physical data are real valued. The Fourier expansion is defined by

$$x(t) = \sum_{n=-\infty}^{+\infty} X_n \exp(2\pi j n f_0 t) \tag{3.1.2}$$

where X_n is the nth complex Fourier coefficient

$$X_n = (1/T) \int_{-T/2}^{T/2} x(t) \exp(-2\pi j n f_0 t)\, dt. \tag{3.1.3}$$

Nonperiodic data may be either almost periodic or transient. Almost periodic data can be represented by a relation analogous to Eq. 3.1.2; however, the ratio of the discrete frequencies involved is not always a rational number

$$x(t) = \sum_{k=-\infty}^{+\infty} X_k \exp(2\pi j f_k t) \tag{3.1.4}$$

For transient data, the frequency spectrum is continuous and a Fourier integral representation is adequate.

$$x(t) = \int_{-\infty}^{+\infty} X(f) \exp(2\pi j f t)\, df \tag{3.1.5a}$$

$$X(f) = \int_{-\infty}^{+\infty} x(t) \exp(-2\pi j f t)\, dt \tag{3.1.5b}$$

Measurements of phenomena which may be considered random on a macroscopic scale will output collections of random data. These collections can be obtained either as the output in time of only one experiment (such a single time history is called a sample function) or as the output at a definite time of a large ensemble of "identical" experiments. Such a complex collection of data is called a random or stochastic process. The statistical functions used to describe random processes can be defined either in time, over a sample function, or over the ensemble of possible outputs. The behaviour in the amplitude domain is described by probability density functions, while information regarding the behaviour in the time and frequency domains is provided by correlation and spectral density functions respectively. These classes of functions are defined and analysed in the next section.

Stochastic processes are classified according to the time and ensemble dependence of these statistical functions. Random processes are either stationary or nonstationary depending on whether the correlation functions defined over the ensemble of outputs are independent of the time when they are calculated. The stationary processes having correlation functions independent of their definition either in time or over the ensemble of outputs are said to be ergodic.

3.2 Stationary Random Processes Theory Fundamentals

3.2.1 Random Variables and Probability Functions

All the possible outcomes of an experiment form a point set called a sample space. A random variable is a set function $x(k)$ defined over the sample space points k. Probability functions may be assigned to various events which are groups of points in the sample space. The probability distribution function $P(x)$

$$P(x) = \text{Prob}[x(k) \leq x] \tag{3.2.1}$$

satisfies

$$P(a) \leq P(b), \text{ if } a \leq b \tag{3.2.2a}$$

$$P(-\infty) = 0 \tag{3.2.2b}$$

and $$P(+\infty) = 1. \tag{3.2.2c}$$

The first-order probability density function is

$$p(x) = \frac{d}{dx}[P(x)] \tag{3.2.3}$$

where $$p(x) \geq 0 \tag{3.2.4a}$$

and $$\int_{-\infty}^{+\infty} p(x)\, dx = 1. \tag{3.2.4b}$$

Joint probability functions may be defined in association with subsets of points k in the sample space which satisfy simultaneously more than one type of events. For random variables $x(k)$ and $y(k)$ the joint probability distribution function is

$$P(x,y) = \text{Prob}[x(k) \leq x \text{ and } y(k) \leq y] \tag{3.2.5}$$

The joint probability density function is defined by

$$p(x,y) = \frac{\partial^2}{\partial x \partial y}[P(x,y)] \tag{3.2.6}$$

where $p(x,y) \geq 0$,

$$\int_{-\infty}^{+\infty} \int_{-\infty}^{+\infty} p(x,y)\, dx\, dy = 1 \tag{3.2.7b}$$

and $$p(x) = \int_{-\infty}^{+\infty} p(x,y)\, dy \tag{3.2.7c}$$

$$p(y) = \int_{-\infty}^{+\infty} p(x,y)\, dx. \tag{3.2.7d}$$

Two random variables are statistically independent if

$$p(x,y) = p(x) \cdot p(y). \tag{3.2.8}$$

The expected value of any real single-valued continuous function $g(x,y)$ of the two random variables $x(k)$ and $y(k)$ is defined by

$$E[g(x,y)] = \int_{-\infty}^{+\infty} \int_{-\infty}^{+\infty} g(x,y)\, p(x,y)\, dx\, dy \tag{3.2.9}$$

Similar definitions are valid for functions of one or more random variables.

The mean (average) value $\mu_x = E[x(k)]$, (3.2.10a)

the mean square value $\psi_x^2 = E[x^2(k)]$ (3.2.10b)

and the variance $\sigma_x^2 = E[(x(k) - \mu_x)^2] = \psi_x^2 - \mu_x^2$ (3.2.10c)

are some of the important expected values. The joint expected values relating two random variables are

the correlation $R_{xy} = E[x(k) \cdot y(k)]$ (3.2.11a)

and the covariance $C_{xy} = E[(x(k) - \mu_x) \cdot (y(k) - \mu_y)]$. (3.2.11b)

The correlation coefficient is defined by

$$\rho_{xy} = C_{xy} / \sigma_x \sigma_y , \quad (\rho_{xy} \leq 1) \quad . \tag{3.2.12}$$

Independent random variables are uncorrelated ($\rho_{xy} = 0$), but the reverse is not necessarily valid.

The Gaussian (normal) distribution

$$p(x) = (1/\sigma_x \pi\sqrt{2}) \exp[(x - \mu_x)^2 / 2\sigma_x^2] \tag{3.2.13}$$

plays a special role in physical problems as a consequence of the Central Limit theorem. This theorem states that under fairly general conditions the vector sum of a large number of mutually independent N-dimensional random variables approaches an N-dimensional normal distribution.

3.2.2 Stationary Random Processes

A stochastic process $\{x_k(t)\}$ is an emsemble of sample functions, which can be characterized by its probability structure. A sample space of index k which may be denumerable is a representation of the ensemble. The values of these functions at times t_i form a domain of random variables $x_k(t_i)$. The various momenta defined according to Eq. 3.2.9 are then functions of time:

Mean value $\mu_x(t) = E[x_k(t)]$, (3.2.14a)

autocorrelation function $R_x(t,\zeta) = E[x_k(t)\cdot x_k(t+\tau)]$, (3.2.14b)

autocovariance function $C_x(t,\zeta) = E[(x_k(t) - \mu_x(t))\cdot(x_k(t+\zeta) - \mu_x(t+\zeta))]$, (3.2.14c)

crosscorrelation function $R_{xy}(t,\zeta) = E[x_k(t)\cdot y_k(t+\zeta)]$, (3.2.14d)

crosscovariance function

$$C_{xy}(t,\zeta) = E[(x_k(t) - \mu_x(t))\cdot(y_k(t+\zeta) - \mu_y(t+\zeta))]. \quad (3.2.14e)$$

The random processes $\{x_k(t)\}$ and $\{y_k(t)\}$ are said to be weakly stationary or stationary in the wide sense if the functions defined by Eqs. 3.2.14 are independent of the time t. They are strongly stationary if all higher-order momenta are also time independent. The Gaussian random process is a notable exception since weak stationarity also implies strong stationarity. Weak stationary processes satisfy

$$R_x(-\tau) = R_x(\tau), \quad (3.2.15a)$$

$$R_{xy}(-\tau) = R_{yx}(\tau) \quad (3.2.15b)$$

and $$|R_{xy}(\zeta)|^2 \leq R_x(0)\cdot R_y(0). \quad (3.2.15c)$$

The normalized crosscovariance function or the correlation function coefficient

$$\rho_{xy}(\zeta) = C_{xy}(\zeta)[C_x(0)\cdot C_y(0)]^{-1/2}, \qquad |\rho_{xy}(\tau)| \leq 1 \quad (3.2.16)$$

measures the degree of linear dependence between the random processes displaced in time by ζ.

The behaviour of random processes in the frequency domain is described by spectral density functions defined as Fourier transforms of the correlation functions. A knowledge of the "frequency behaviour" may be of greater value than that of the "time behaviour," although it does not provide any additional information. Power and cross-spectral density functions can be defined in correspondence to auto- and cross-correlation functions using

$$W_{xx}(f) = \mathcal{F}\left\{R_x(\zeta)\right\} = \int_{-\infty}^{+\infty} R_x(\zeta)\ \exp(-j2\pi f\zeta)\ d\zeta \tag{3.2.17a}$$

and $$W_{xy}(f) = \mathcal{F}\left\{R_{xy}(\zeta)\right\} . \tag{3.2.17b}$$

It follows from the symmetrical properties in Eqs. 3.2.15 that

$$\mathrm{Re}[W_{xx}(-f)] = \mathrm{Re}[W_{xx}(f)] \geq 0 \tag{3.2.18a}$$

$$\mathrm{Im}[W_{xx}(-f)] = \mathrm{Im}[W_{xx}(f)] = 0 \tag{3.2.18b}$$

and $$W_{xy}(-f) = W^*_{xy}(f) = W_{yx}(f). \tag{3.2.18c}$$

If the frequency variable f is restricted to non-negative values, then one-sided spectral density functions $G_{xx}(f)$ and $G_{xy}(f)$ are defined by

$$G_{xx}(f) = \begin{cases} 2W_{xx}(f) & f > 0 \\ W_{xx}(f) & f = 0 \\ 0 & f < 0 \end{cases} \tag{3.2.19a}$$

and $$G_{xy}(f) = C_{xy}(f) - jQ_{xy}(f) = \begin{cases} 2W_{xy}(f) & f > 0 \\ W_{xy}(f) & f = 0 \\ 0 & f < 0 \end{cases} \tag{3.2.19b}$$

where $C_{xy}(f)$ is the cospectrum or coincidental spectrum density function

and $Q_{xy}(f)$ is the quad-spectrum or the quadrature spectral density function. An inequality similar to Eq. 3.2.15c holds for spectral density functions.

$$\left|W_{xy}(f)\right|^2 \leq W_{xx}(f)\ W_{yy}(f) \tag{3.2.20}$$

3.2.3 Ergodic Random Processes

In practice, only a sample function of the stochastic process is known and even this function is known for only a finite time interval. These processes can be characterized by time averages although the correct approach uses ensemble averages. The general definition, similar to Eq. 3.2.9, is

$$\mathcal{E}[g(x,y)] = \lim_{T\to\infty} (1/2T) \int_{-T}^{+T} g\left(x_k(t), y_k(t)\right)\, dt \tag{3.2.21}$$

where $g(x,t)$ is a random variable over the sample space k. Then

$$\mu_x(k) = \mathcal{E}[x_k(t)], \tag{3.2.22a}$$

$$\psi_x^2(k) = \mathcal{E}[x_k^2(t)], \tag{3.2.22b}$$

$$\sigma_x^2(k) = \mathcal{E}[(x_k(t) - \mu_x(k))^2] = \psi_x^2(k) - \mu_x^2(k), \tag{3.2.22c}$$

$$R_{xy}(\zeta,k) = \mathcal{E}[x_k(t)\ y_k(t+\zeta)] \tag{3.2.22d}$$

and $$C_{xy}(\zeta,k) = \mathcal{E}[(x_k(t) - \mu_x(k))\cdot(y_k(t+\zeta) - \mu_y(k))]. \tag{3.2.22e}$$

The parameters defined by Eqs. 3.2.22 are random variables. A random process is ergodic when all time averages are constants, independent of the sample function on which they are performed. A random process is weakly ergodic when this condition applies only to mean values and first-order correlation functions. A sufficient condition for a random process

to be weakly ergodic is that it is weakly stationary and that the time averages $\mu_x(k)$ and $C_x(\zeta,k)$ are the same for all sample function.

An intuitive physical representation can be associated with the functions described above for random processes. The data may be considered as a combination of a static or time invariant and a dynamic or time variant component. The former is described by the mean value μ_x and the latter by the variance ψ_x^2 or by the standard deviation σ_x. The autocorrelation function is important since it describes the dependence of the data values at one time on the values at another time. The cross-correlation function analyses this dependence for two different types of data. The one-sided power spectral density function $G_{xx}(f)$ may be related to the variance of the data in a frequency interval $(f, f+\Delta f)$

$$G_{xx}(f) = \lim_{\Delta f \to 0} [\psi_x^2(f,\Delta f)/\Delta f] =$$

$$= \lim_{\Delta f \to 0} (1/\Delta f) \left[\lim_{T \to \infty} (1/T) \int_{-T/2}^{+T/2} x^2(t,f,\Delta f)\, dt \right] \qquad (3.2.23)$$

3.2.4 Linear Transformations of Random Processes

Another random process $\{y(Q)\}$ is obtained if an operator A is applied to a random process $\{x(P)\}$.

$$\{y(Q)\} = A[\{x(P)\}] \qquad (3.2.24)$$

where P is a point in a general space (space-time) and Q may be either a point in the same or another space. The operator is linear if

$$A\left[\sum_i a_i x(P_i)\right] = \sum_i a_i A[\, x(P_i)] \qquad (3.2.25)$$

where the a_i are arbitrary constants. Equation 3.2.25 expresses both

the additivity and the homogeneity of the linear operation. The operator A commutes with the expected value operator

$$E[\{y(Q)\}] = E[A(\{x(P)\})] = A[E(\{x(P)\})]. \tag{3.2.26}$$

A time invariant operator A will transform any weak, or strongly, stationary random process into another weakly, or strongly, stationary random process. The gaussian character of a random process is also conserved by linear transformations.

3.3 Linear Systems

3.3.1 Time and Frequency Characteristics

In the context of this chapter, a system is a device which transforms physical data. This transformation is described by Eq. 3.2.24 where x(P) and y(Q) are the input and output data. A system is said to be linear if the corresponding operator is linear and is said to have constant parameters if the operator is time invariant. Such systems are described by convolution integral type transformations, (Bremermann, 1965).

$$y(t) = h(t) * x(t) = \int_{-\infty}^{+\infty} h(\zeta)\, x(t-\zeta)\, d\zeta \tag{3.3.1}$$

where the impulse response h(t) is the output of the system when the excitation is a delta pulse

$$h(t) = h(t) * \delta(t). \tag{3.3.2}$$

A system is physically realizable if it respects the causality principle, i.e., it responds only to past inputs. This implies that

$$h(t) = 0 \text{ for } t < 0. \tag{3.3.3}$$

The system is stable if a bounded input function produces a bounded output function. A sufficient condition requires the impulse response function to be absolutely integrable.

$$\int_{-\infty}^{+\infty} |h(t)|dt < \infty \tag{3.3.4}$$

The same information regarding a linear system is provided by either the impulse response or the frequency response function

$$H(f) = \mathcal{F}\{h(t)\} \ . \tag{3.3.5}$$

The input-output relationship is obtained by applying the Fourier transform operator to Eq. 3.3.1. The mathematical complexity is reduced in the frequency domain.

$$Y(f) = H(f) \bullet X(f) \tag{3.3.6}$$

Occasionally it is convenient to express the frequency transfer function in polar coordinates

$$H(f) = |H(f)| \exp[-j\Phi(f)] \tag{3.3.7}$$

where $|H(f)|$ is the gain of the system and $\Phi(f)$ is the phase factor of the system. Physical realizability implies that

$$H(-f) = H^*(f). \tag{3.3.8}$$

The overall transfer function of cascaded linear systems is

$$H(f) = \prod_i H_i(f). \tag{3.3.9}$$

3.3.2 Random Processes and Linear Systems

The random excitation of a linear system produces a random output. This transformation is also described by Eqs. 3.3.1 and 3.3.6. It was shown in Sec. 3.2 that any linear operator commutes with the expected value operator. Consequently the mean of the output is equal to the output of the mean. It follows from the commutation relation that

$$R_{xy}(\zeta) = h(\zeta) * R_{xx}(\zeta) \tag{3.3.10a}$$

and $$R_{yy}(\zeta) = h(\zeta) * h^*(-\zeta) * R_{xx}(\zeta). \tag{3.3.10b}$$

The Fourier transforms of Eqs. 3.3.10 describe the "propagation" of spectral density functions

$$W_{xy}(f) = H(f)\, W_{xx}(f) \tag{3.3.11a}$$

and $$W_{yy}(f) = |H(f)|^2\, W_{xx}(f), \tag{3.3.11b}$$

These relationships are also valid for one-sided spectral density functions.

The linearity of a system can be verified easily by analysing the coherence function between the input and the output.

$$\gamma^2_{xy}(f) = |W_{xy}(f)|^2 / W_{xx}(f)\, W_{yy}(f) =$$

$$= |G_{xy}(f)|^2 / G_{xx}(f)\, G_{yy}(f) \tag{3.3.12}$$

where $W_{xx}(f)$ and $W_{yy}(f)$ are non-delta functions and nonzero. This coherence function is unity over the entire domain for linear systems. In practice this function may be less than unity due to the existence of more than one input or due to noisy measurements. Bendat and Piersol (1971) have treated the problem of multiple-input linear systems.

CHAPTER IV

BASIC EPR INSTRUMENTATION

4.1 Basic Design Concepts for EPR Spectrometers

EPR spectrometers, in common with all other spectrometers, consist of four basic elements: 1) source of electromagnetic radiation, 2) sample irradiation cell, 3) dispersive component and 4) radiation detector. These elements determine the various characteristics of the system and EPR spectrometers are classified according to their basic features.

Experimentally, it is customary to use a highly monochromatic source of radiation. The dispersive function is accomplished by immersing the sample in a pseudosteady magnetic field. The detector extracts the information concerning the response of the sample to the combined effect of the exciting radiation field and the dispersing magnetic field. The irradiation cell should be designed to enhance the interaction of the radiation field with the sample. This is achieved by making the cell a resonant circuit whose parameters are functions of the sample properties. A resonant sample cell is not essential but non-resonant cells are rarely if ever used (Alger, 1968; Wilmshurst, 1967).

An electrical network having an equivalent resonant behaviour is the RLC series circuit which can be completely described by its impedance $Z(\omega)$,

$$Z(\omega) = R_o + j(L_o\omega - 1/C_o\omega), \tag{4.1.1a}$$

resonant frequency ω_o,

$$\omega_o = (L_oC_o)^{-1/2} \tag{4.1.1b}$$

and its quality factor Q_o

$$Q_o = L_o\omega_o/R_o = 1/\omega_o C_o R_o. \tag{4.1.1c}$$

The subscript "o" indicates an intrinsic parameter. The values of these parameters depend on the physical properties of the sample within the volume enclosed by the resonant cell. It is usual to neglect the effect of the sample on R and C. Its effect on the inductance L is described by

$$L = L_o(1 + \eta\chi) \tag{4.1.2}$$

where $\chi = \chi' - j\chi''$ and η, the filling factor, is a measure of the efficiency with which the sample interacts with the radiation field. Substituting Eq. 4.1.2 into Eqs. 4.1.1 gives

$$Z(\omega) = (R_o + L_o\omega\eta\chi'') + j[\omega L_o(1 + \eta\chi') - 1/C_o\omega_o] \tag{4.1.3a}$$

$$\omega_c = [L_o C_o(1 + \eta\chi')]^{-1/2} = \omega_o(1 + \eta\chi')^{-1/2} \tag{4.1.3b}$$

$$Q_c = [\omega_c C_o(R + L_o\omega_c\eta\chi'')]^{-1} . \tag{4.1.3c}$$

It can be shown that the variation of these parameters is proportional to the susceptibility components.

$$(d\omega_c/\omega_c) = -(1/2)\eta\chi' \tag{4.1.4a}$$

$$d(1/Q) = \eta\chi'' \tag{4.1.4b}$$

Most EPR spectrometers are designed to measure the absorption component χ'' by detecting the variation in the quality factor Q of the resonant sample cell. They are called "absorption" spectrometers, while "dispersion" spectrometers detect χ' by measuring the variation in the resonance frequency of the sample cell. It is preferable to design an

EPR spectrometer so that it can perform both measurements.

4.2 Spectrometer Sensitivity and the Choice of Operating Parameters

The sensitivity was defined in Chapter I as a measure of the capability of an experimental system to extract information about a phenomenon in the presence of sources of error. These error sources diminish the reliability of the information. The sensitivity is determined by the minimum "intensity" of the studied phenomenon for which information can be extracted with a non-zero probability. The resolution is another parameter characterizing this information extraction process. The resolution measures the capability of the experiment or apparatus to distinguish different "adjacent" events occuring in the phenomenon studied. The resolution can be incorporated in the broad, general, definition of sensitivity. Another very important parameter characterizing an experiment (system) is the economic cost of extracting the information. A compromise must be made between sensitivity, resolution and cost and this affects the choice of an EPR spectrometer's operating parameters.

The sensitivity is usually described by the minimum detectable susceptibility χ in magnetic resonance experiments. A theoretical minimum is determined by the condition that the power carrying the information (Eq. 2.3.13) should be at least equal to the thermal noise power

$$P_{inf} = \omega\chi'' B_1^2 = kT\Delta f = P_{th.noise} \qquad (4.2.1)$$

The implications of this condition have been analysed extensively for all possible sample cells. These analyses have been summarized by Poole (1967) and Wilmshurst (1967) amongst others. A resonant cell enhances the effective value of the rotating field B_1. It can be shown that the minimum detectable susceptibility is given by

$$\chi_{min} = (C/\eta Q_o)\cdot(kT\Delta f/P_i)^{1/2} \qquad (4.2.2)$$

where Q_o is the intrinsic quality factor of the resonant call, P_i is the power of the electromagnetic radiation incident on the sample cell, η is the sample filling factor of the cell and C is a numerical factor dependent on the polarization of the electromagnetic radiation field. The minimum detectable number of paramagnetic ions for systems obeying Curie's law and Bloch's equations is

$$N_{min} = [C/\eta Q_o]\ [kT_d\Delta f/P_i]^{1/2}\ [3kT_o/\beta^2 J(J+1)]\ [\Delta\omega/\omega] \qquad (4.2.3)$$

where β is the Bohr magneton, $\Delta\omega/\omega$ is the fractional linewidth $[(\Delta B/B) = (\Delta\omega/\omega)]$, T_o is the sample temperature and T_d is the detector temperature.

In magnetic resonance, the resolution is defined as the smallest detectable variation of the dispersing element. This minimum detectable change is characterized by the minimum detectable linewidth or as the minimum "distance" between adjacent lines which are discernable. The resolution depends strongly on the broadening phenomena discussed in Chapter II. From an engineering viewpoint, it is necessary to consider only instrumentation broadening.

Equation 4.2.3 and the definition of resolution lead to the following requirements for a reliable information extraction: 1) low sample and detector temperatures, 2) highly stable and monochromatic electromagnetic radiation fields of very high frequency, 3) highly stable and homogeneous magnetic fields of high intensity, 4) high values for the quality factor of the resonant cell, 5) large filling factor and 6) large sample volume. Alger (1968) has shown that the sensitivity is a complicated function of the frequency (or the magnetic field B) since both η and Q_o are frequency dependent. Nevertheless, the assumption that the sensitivity is an

increasing function of ω or B is almost generally valid.

These requirements are well satisfied if microwave frequencies are used because the necessary magnetic fields of O(3T) are readily available with a good homogeneity over a volume of $O(5cm^3)$. This space is large enough to permit the introduction of a low-temperature dewar enclosing a resonant cell (cavity) with a high quality factor. Moreover, relatively inexpensive, high quality microwave components are available from 1-40GHz. The concept of "quality" plays an important role since the noise generated in oscillators and detectors exceeds thermal noise and limits the sensitivity of an EPR spectrometer.

4.3 Radiation Sources

Microwave generators have been designed using various physical principles. The frequency limitation of conventional vacuum tubes and transistors is ∿5GHz at present. Magnetrons can generate high power pulses and are useful in pulsed experiments up to 100GHz. Backward wave oscillators have the advantage of enjoying a broad bandwidth compared with other microwave generators. References to literature describing various EPR spectrometers using these devices have been given by Poole (1967).

Most EPR spectrometers use reflex klystron oscillators which can be both mechanically and electrically tuned in frequency. This is very important since a control system can then stabilize the oscillation frequency. The klystrons used in EPR spectroscopy generate O(100mW) with relatively low noise power. This noise is extremely important since it has been shown (Buckmaster and Dering, 1966; Strandberg, 1972) that it ultimately limits the sensitivity of EPR spectrometers. This noise can be analysed in various ways. Dering (1967) summarized the classical approach while Wilmshurst (1967) and Gray (1972) used a phasor description

because they considered it to be more intuitive. Strandberg (1972) provided a mathematical treatment of the oscillator noise effect which will be followed in this thesis.

A general expression for the wave generated by an oscillator is

$$e(t) = E_o[1 + a(t)] \cos[\omega_o t - \phi(t)] \tag{4.3.1}$$

where ω_o is the oscillator frequency and $a(t)$ and $\phi(t)$ are random processes which describe the amplitude and phase modulation noise. If $a(t)$ and $\phi(t)$ are small perturbations, then Eq. 4.3.1 becomes

$$e(t) = E_o \cos(\omega_o t) + E_o a(t) \cos(\omega_o t) + E_o \phi(t) \sin(\omega_o t) \tag{4.3.2}$$

which is the familiar form in communication theory. The random processes $a(t)$ and $\phi(t)$ can be characterized in the real time domain by their auto- and cross-correlation functions or, in the frequency domain, by their power- and cross-spectral density functions $W_{AM}(f)$, $W_{PM}(f)$ and $W_{AMPM}(f)$. These definitions follow from the theory presented in Chapter III. The response of an EPR spectrometer to a noisy excitation can be analyzed using the outline in Sec. 3.3.2. This analysis will be discussed in Sec. 5.2.1 and experimental results will be given to substantiate it. The experimental procedures involved in the measurement of $W_{AM}(f)$ and $W_{PM}(f)$ are discussed in Sec. 8.6.2. The frequency and not the phase is the most important parameter in magnetic resonance so it is customary to analyse $W_{FM}(f)$ - the power spectral density function of the frequency modulation noise - instead of W_{PM}. The relation between the two is

$$W_{FM}(f) = (2\pi f)^2 W_{PM}(f) \tag{4.3.3}$$

since

$$\omega = \omega_o + d\phi(t)/dt. \tag{4.3.4}$$

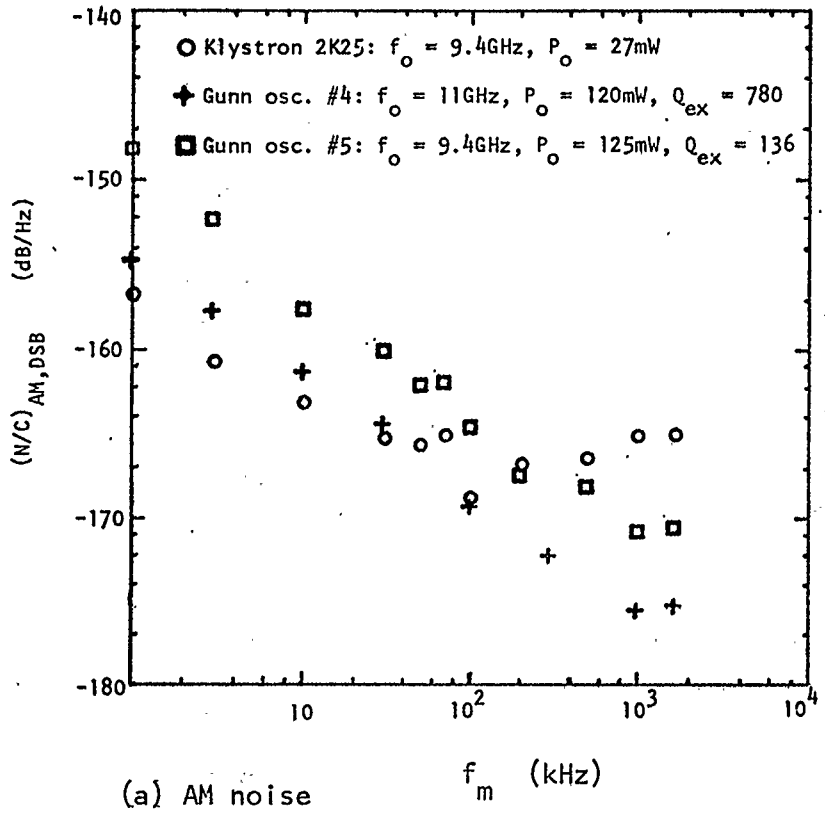

(a) AM noise

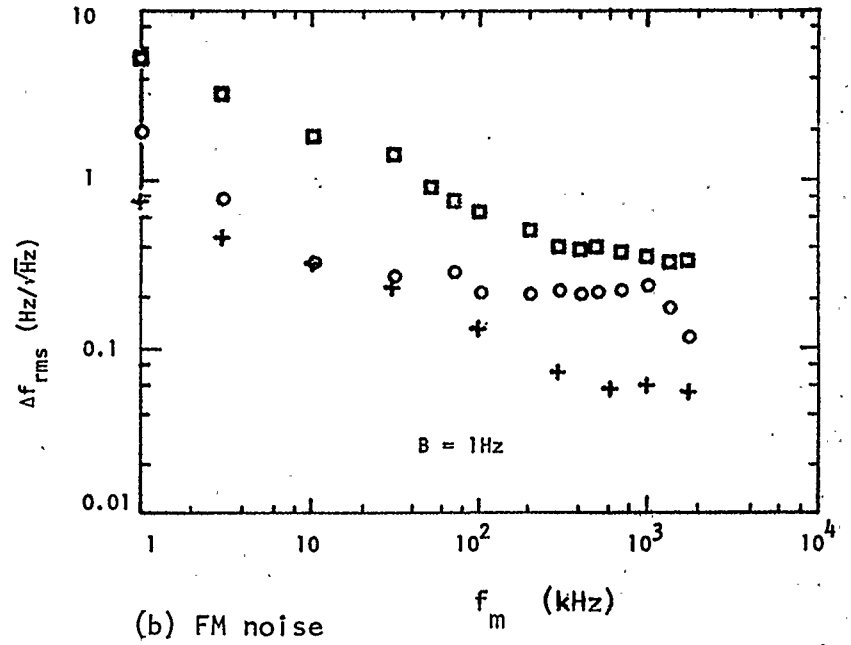

(b) FM noise

FIGURE 4.1 Graphs of the measured noise spectra of two Gunn oscillators and a 2K25 klystron (Ohtomo, 1972).

Typically, $W_{AM}(f)$ is O(-120dB/Hz) compared to the carrier, while $W_{FM}(f)$ is O(-150dB/Hz) at ∿1MHz from a 10GHz carrier. Although these values appear extremely small, they limit the sensitivity of an EPR spectrometer when the power input to the resonant cell is O(100mW).

Recently, solid-state Gunn and avalanche diode microwave generators have been used in EPR spectrometers (Walsh et al., 1970). A theoretical and experimental analysis of their noise properties has been made by Ohtomo (1972). Figure 4.1 summarizes some of his experimental results. However, the use of a 2K25 reflex klystron for comparison is unfair since it is an obsolete design noted for its noisy behaviour. Although noisier than the contemporary klystrons, these solid-state microwave generators are preferable for use in EPR spectrometers where convenience and cost and not sensitivity is of primary importance since they have smaller size, simpler power supply requirements, easier electronic tuning and lower overall cost.

The maser oscillator is the ideal microwave generator as far as the noise problem is concerned. It is a virtually noise-free generator, particularly when operated at liquid helium temperatures, enabling EPR spectrometers incorporating them to have near theoretical sensitivity (Mollier, 1972). Unfortunately, the power generated by these maser oscillators are $O(10^{-12}W)$ so that the effective sensitivity is rather poor. They are useful only for samples which saturate at very low power levels. In general, the cost of these oscillators is prohibitively high and this outweighs their advantages. Buckmaster and Skirrow (1972) have discussed the sensitivity of EPR spectrometers using maser and parametric preamplifiers.

4.4 Resonant Sample Cells

The microwave analog of a tuned circuit is the resonant cavity (Harvey, 1963) which is an enclosure consisting of high conductivity walls of dimensions comparable to the resonant wavelength. Resonance occurs when a standing wave interference pattern is formed within the cavity so that the energy stored is enhanced by the multiple reflections between the cavity walls. These standing waves patterns are a function of the dimensions and shape of the cavity. A cavity is described by its 1) resonant frequency, 2) quality factor, 3) mode and 4) methods of coupling and tuning.

The most general definition of the quality factor of a resonator is

$$Q = 2\pi \frac{(\text{energy stored})}{(\text{energy dissipated per cycle})} . \qquad (4.4.1)$$

This definition leads to Eq. 4.1.3c when the resonator consists of lumped-parameter circuit elements. Other "partial" quality factors can be defined corresponding to specific ways of energy dissipation. The resultant quality factor is

$$(1/Q) = (1/Q_u) + (1/Q_\varepsilon) + (1/Q_c) = (1/Q_o) + (1/Q_c) \qquad (4.4.2)$$

where Q_u, the unloaded Q-factor, accounts for the ohmic losses in the cavity walls, Q_ε accounts for the dielectric losses inside the cavity, Q_c accounts for the losses due to coupling the cavity to external circuits and $(1/Q_o) = (1/Q_\varepsilon) + (1/Q_u)$. The design of microwave cavities is discussed extensively by Slater (1950) amongst others.

The transfer function of a microwave resonator is a very important factor in sensitivity studies. It depends on the way in which the cavity

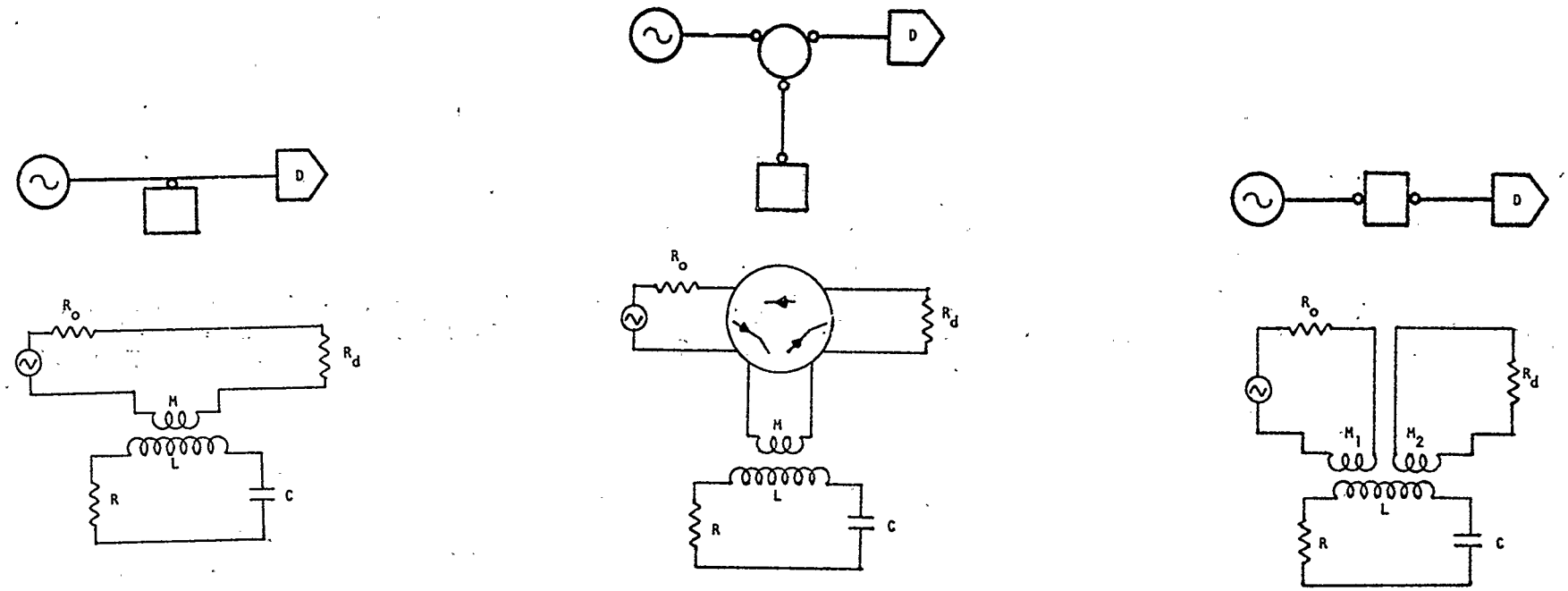

(a) Transmission spectrometer

(b) Reflection spectrometer with circulator

(c) Absorption spectrometer

FIGURE 4.2 Diagrams of the basic microwave spectrometer configurations and their equivalent lumped parameter circuits.

is connected to the external circuit. From this point of view, resonant cavities are classified as transmission, reflection and absorption cavities and, consequently, microwave spectrometers are classified according to the type of sample cell employed. Figure 4.2 shows diagrams of these spectrometers and their equivalent lumped parameter circuits. A circulator or magic-T must be used with a reflection cavity in order to decouple the oscillator from the cavity, the cavity from the detector and the detector from the oscillator. The bimodal cavity is a special type of transmission cavity in which the input and output ports are excited by orthogonal modes and thus they are ideally decoupled. Coupling occurs only when the orthogonality of the two modes is disturbed as when a magnetic resonance occurs. Both the reflection cavity — circulator system and the bimodal cavity are band rejection circuits. The former is a narrow band filter while the latter is broad band by definition.

The choice of the suitable cavity is determined by the performance desired from the spectrometer. This performance is described by the sensitivity, resolution and cost parameters. Wilmshurst (1967) has shown that the sensitivity is independent of the type of cavity chosen if the generator and cavity are perfectly stable and noiseless. A more detailed analysis is necessary because such an ideal is not realizable. The following discussion concerns reflection cavities since they are used commonly.

The transfer function of a cavity can be obtained using the lumped parameter equivalent circuit, but this approach is of limited value since it is only a first-order approximation. Microwave circuit theory (Slater 1950) provides a more precise method of analysis. The voltage transfer

function $\Gamma(f)$ of a reflection cavity is

$$\Gamma(f) = (Z - Z_o)/(Z + Z_o) \tag{4.4.3}$$

where Z_o is the characteristic impedance of the waveguide mode and Z is the impedance of the cavity. Z and Z_o are related to the cavity parameters by

$$Z/Z_o = [1/Q_c] \;/\; [1/Q_o + j(f/f_r - f_r/f)] \tag{4.4.4}$$

where f_r is the cavity resonant frequency. Using Eq. 4.4.4, Eq. 4.4.3 becomes

$$\Gamma(f) = \frac{(1/Q_c - 1/Q_o) - j(f/f_r - f_r/f)}{(1/Q_c + 1/Q_o) + j(f/f_r - f_r/f)} \tag{4.4.5}$$

If $f \simeq f_r$, then

$$\Gamma(f) = \frac{(1-\beta)^2 - [2\beta Q_o(f-f_r)/f_r]^2}{(1+\beta)^2 + [2\beta Q_o(f-f_r)/f_r]^2} - j\,\frac{4\beta Q_o(f-f_r)/f_r}{(1+\beta)^2 + [2\beta Q_o(f-f_r)/f_r]^2} \tag{4.4.6}$$

where $\beta = (Q_c/Q_o)$ is called the coupling factor. The term

$$\Gamma_o = (Q_o - Q_c)/(Q_o + Q_c) = (1 - \beta^2)/(1 + \beta)^2 \tag{4.4.7}$$

is the reflection coefficient at resonance ($f=f_r$). The cavity is matched when $Q_o = Q_c$ so that $\beta=1$ and $\Gamma_o=0$.

The correct method of analysing an EPR spectrometer involves time-varying linear systems since the magnetic resonance phenomenon is detected through the variation of $\Gamma(f)$. The change in $(1/Q_o)$ is proportional to χ'' while the change in f_r is proportional to χ' as was shown in Sec. 4.1. It is more straightforward to use an equivalent generator to

represent the resonance phenomenon since a "temporal" analysis is too complicated. The sensitivity is optimized when

$$\frac{\partial^2 \Gamma(f)}{\partial f_r^{\,2}} = 0 \qquad\qquad \frac{\partial^2 \Gamma(f)}{\partial (1/Q_o)^2} = 0 \tag{4.4.8}$$

These conditions require that the cavity should be operated at the magnetic resonance frequency ($f_{osc} = f_r$), critically coupled ($\beta = 1$) and have the highest possible Q. These are the conditions for maximum signal; the conditions for minimum noise propagation will be discussed in Chapter V.

4.5 Radiation Detectors

The magnetic resonance phenomenon causes a variation in the resonant cell parameters. This is equivalent to modulating the wave emitted by the microwave generator. The power variation is proportional to the absorption component χ'' while the phase variation is proportional to the dispersion component χ'. Since χ'' and χ' are related by the Kramers-Kronig relations, the cavity output wave consists of an in-phase amplitude modulated component due to the absorption χ'' and a quadrature-phase amplitude modulated component due to the dispersion χ'. The role of the receiver is to detect these modulation envelopes and to transform them in a convenient form for interpretation.

The simplest demodulator is a bolometer, whose temperature is proportional to the incident power. Theoretically, bolometers could be ideal detectors since the only noise present is the inherent thermal (Johnson) noise. In practice they are not ideal since account must be taken of their thermal capacity C and time constant τ. Schmidt and Solomon (1966)

have shown that the effective noise power is

$$P_n = (4kT_o^2 C\Delta f/\tau)^{1/2} \tag{4.5.1}$$

where Δf is the bandwidth considered. The noise power decreases rapidly at low temperatures so that the device is sensitive to powers O(5pW) in a 1Hz bandwidth. This leads to a theoretical EPR sensitivity of about 10^5 spins at 4K in the absence of oscillator noise. In addition to the liquid helium restriction the bolometer has two major disadvantages which limit its use in EPR spectrometers. The value of τ must be chosen so as to be a compromise between low P_n and fast response and it can detect only the absorption mode.

The solid-state diode is the commonest type of demodulator used in EPR spectrometers. The point-contact diode was the earliest version but backward or Schottky-barrier diodes have been developed recently. These diodes have two distinct operating regions. The diode operates as a quadratic (square law) demodulator when the incident power is less than $\sim 1\mu W$,

$$v_{out} \sim v_{in}^2 \sim P_{in}, \tag{4.5.2}$$

and as a linear demodulator when the incident power exceeds $\sim 10\mu W$,

$$v_{out} \sim v_{in} \sim P_{in}^{1/2} . \tag{4.5.3}$$

The demodulator is incapable of distinguishing between absorption and dispersion in either mode of operation. The demodulation process is phase sensitive only when the diodes are operated as mixers. Mixing occurs when two different waves are incident on the diode, one of which has an amplitude which drives the diode into the linear region. In a

first approximation the mixer operates like a multiplier. The signal from the cavity is

$$s_{in}(t) = s_a(t)\cos(\omega_o t) + s_d(t)\sin(\omega_o t) \tag{4.5.4}$$

where $s_a(t)$ and $s_d(t)$ are the slow-varying envelopes proportional to the absorption and dispersion components respectively and ω_o is the microwave frequency. When this signal is mixed with a wave of amplitude v_o and frequency ω_1 the output voltage of the mixer is

$$s_{out}(t) \simeq s_{in}(t)v(t) = [s_a(t)\cos(\omega_o t) + s_d(t)\sin(\omega_o t)]v_o\cos(\omega_1 t+\phi) \tag{4.5.5}$$

where ϕ is the relative phase between $s_{in}(t)$ and $v(t)$. The low frequency components are

$$s_{out}(t) \sim v_o s_a(t)\cos[(\omega_o-\omega_1)t-\phi] + v_o s_d(t)\sin[(\omega_o-\omega_1)t-\phi]. \tag{4.5.6}$$

The demodulation is synchronous (homodyne or synchrodyne) when $\omega_o = \omega_1$. The absorption ($\phi = 0$) or dispersion ($\phi = \pi/2$) can be detected by varying the value of ϕ. Heterodyne demodulation occurs if $\omega_o \neq \omega_1$. The signals $s_a(t)$ and $s_d(t)$ are shifted in the frequency domain to the intermediate frequency $\omega_{i.f.} = |\omega_o-\omega_1|$. $s_a(t)$ and $s_d(t)$ must be detected by a further demodulation at the intermediate frequency. Buckmaster and Dering (1967) showed that it is preferable to use synchrodyne demodulation at all signal processing frequencies.

Solid-state diodes have three major types of noise since they are multi-electrode (multi-layered) devices. These are 1) the inherent thermal noise which is frequency independent at microwave frequencies, 2) the shot noise, which is caused by the random arrival of independent charge carriers

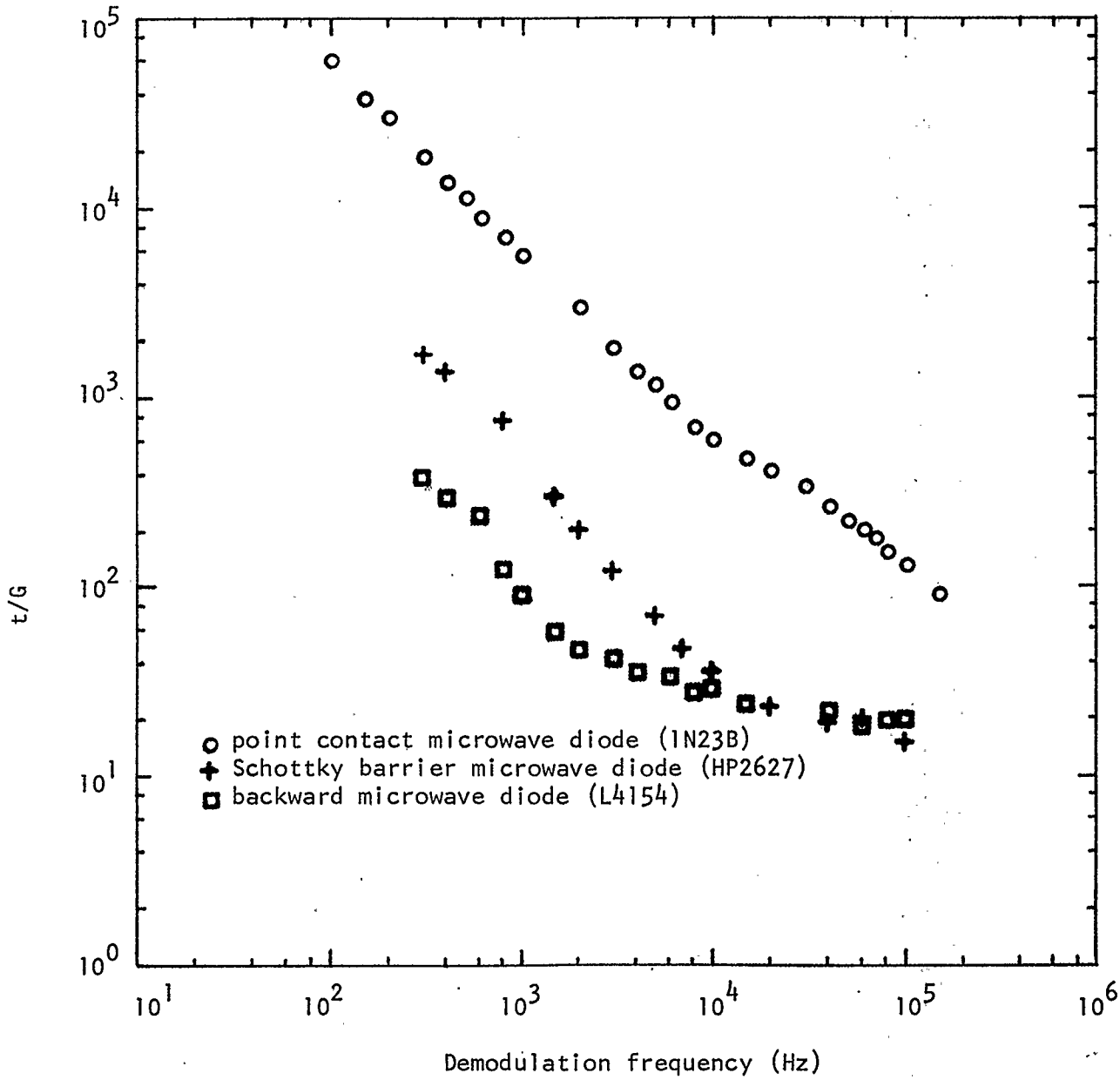

FIGURE 4.3 Graph of the figure of merit (t/G) as a function of the demodulation frequency for selected 1N23B, HP2627 and L4154 diodes operated with optimum microwave bias (Buckmaster and Rathie, 1971-11).

Facing Page 51

and 3) the so-called (1/f) noise. The shot noise is proportional to the d.c. diode current and so to the incident microwave power. Thermal noise and shot noise cannot be distinguished since they are basically white, but their powers can be controlled through the temperature or d.c. current respectively. (1/f) noise nature is not understood completely, however its frequency dependence is given by

$$P_n \sim 1/f^n \tag{4.5.7}$$

where $n \simeq 1$ (Buckmaster and Rathie, 1971-II). The frequency where the (1/f) and white noise powers are approximately equal is called the "knee" of noise power as a function of frequency. Considerable effort has been expended to decrease the (1/f) noise power and hence to decrease the "knee" frequency. Backward and Schottky-barrier diodes are preferable to classical point-contact diodes since they have lower "knee" frequencies. Figure 4.3 (Buckmaster and Rathie, 1971-II) compare the noise power frequency distribution of these three types of diodes.

4.6 Dispersive Elements; Additional Noise Sources

The steady external magnetic field B plays the role of dispersive element in EPR spectrometers. This role could be played by the frequency of the microwave generator, however it is very difficult to vary the resonant frequency of the sample resonant cell over a wide frequency range and to synchronize this frequency with the frequency of the microwave generator.

Magnetic fields suitable for EPR experiments can be generated by air-core solenoids, iron-core magnets and superconducting solenoids. The air-core solenoids are the cheapest and lightest and the magnetic field is proportional to the winding current. Unfortunately, the fields thus

obtained are limited to ∿0.5T. Iron-core magnets are used extensively. They can generate magnetic fields up to ∿3.5T so that g ≃ 2 resonances can be studied up to ∿100GHz. However, the working volume is very restricted above ∿2T and water cooling is required. Superconducting solenoids are used to generate magnetic fields in excess of ∿3T. They use very little power and give fields having a very high stability over long periods of time, but consume appreciable quantities of liquid helium and additional coils are required to sweep and modulate the magnetic field.

The inhomogeneity and instability or noise of the magnetic field do not limit the EPR spectrometer sensitivity directly but drastically restrict its resolution. Ideally, the magnetic field and the microwave frequency should be stabilized to the same degree.

Other noise sources which may limit the EPR spectrometer sensitivity are microphonics and mechanical vibrations. They degrade the sensitivity if their frequency components appear within the detector bandwidth. They are due to mechanical resonances, cooling fans, vacuum pumps or the bubbling of cyrogenic fluids and have audio-frequency components. Mechanical and thermal instabilities are inevitable in adjustable components such as cavity matching and tuning devices, bridge matching, microwave oscillator synchronizer, magnetic field stabilizer, etc. They appear at the output as a very low frequency noise and cause drift and baseline instability. The sensitivity may also be degraded by spurious electrical transients.

CHAPTER V

NOISE MINIMIZATION IN AN EPR SPECTROMETER

This chapter discusses methods of minimizing the noise level to increase the sensitivity. This objective can be achieved by improving each component to reduce its "noise production" and by minimizing the effect of this noise on the final signal. The latter objective is usually achieved by shifting the signal to less noisy frequency regions. Since several noise sources are present in an EPR spectrometer, a careful assessment of the relative importance of each of them is necessary to distinguish clearly the "roots of evil". It is useless to spend any effort to improve a component whose noise contribution plays no important role in limiting the sensitivity. An experimental assessment of the noise situation in an EPR spectrometer is reported in Chapter VIII, but some of the conclusions drawn there are given in this chapter in order to present an unitary picture of the problems involved in an optimum design of an EPR spectrometer.

5.1 Reduction of Detector Noise

Solid-state diodes operated as microwave mixers are the detectors commonly used in EPR spectrometers. The signal appears in the low frequency region where (1/f) noise predominates if the basic configuration discussed in Chapter IV is employed. This problem can be avoided by arranging that the output signal from the first demodulator is not in the noisy region of the detector diode. The various methods of achieving this objective will be discussed briefly.

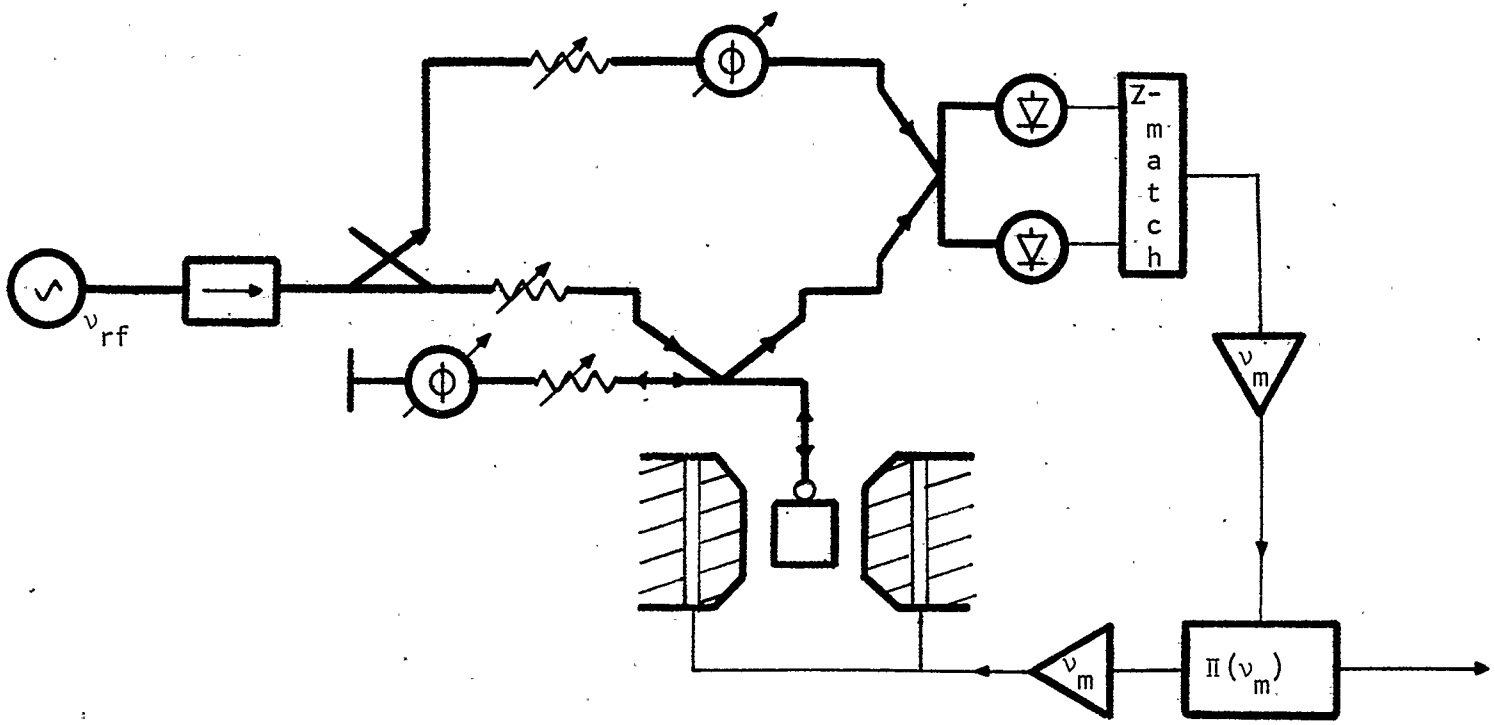

FIGURE 5.1 Block diagram of a homodyne EPR spectrometer

5.1.1 Synchrodyne (Homodyne) Configuration

The synchrodyne configuration is used widely to minimize the effect of the (1/f) diode noise. The nonlinear relationship between the static magnetic field and the resonance signal permits "signal components" to appear at the harmonics of the modulation frequency when the magnetic field is modulated. The relationship between these components and the signal which would appear in the absence of the field modulation is a very complicated function of the many parameters affecting the modulation process. Buckmaster and Dering (1968) have shown that the nth "harmonics" (a_n, d_n) are proportional to the product of the n-th derivative of the original lineshape function and the modulation amplitude B_ω

$$\left[a_n, d_n\right] \sim B_\omega^n \left(\frac{d}{dB_\omega}\right)^n \left[\chi'' , \chi'\right] \tag{5.1.1}$$

when $(B_\omega/B_\Delta)<<1$ and B_Δ is the half width at half maximum amplitude.

Figure 5.1 is a diagram of a typical synchrodyne configuration. Unfortunately, this approach requires the modulation of the static magnetic field at the sample, which may be troublesome at higher frequencies. It can be shown that the signal to noise ratio at the output is proportional to the modulation frequency up to the "knee" frequency provided that diode noise is the limiting sensitivity factor. It is very difficult to produce a magnetic field of sufficient amplitude at frequencies above $\sim$ 1 Hz inside a microwave cavity because Foucault currents are induced in the walls. An internal modulation loop, extremely thin conducting walls have been used to solve this problem,

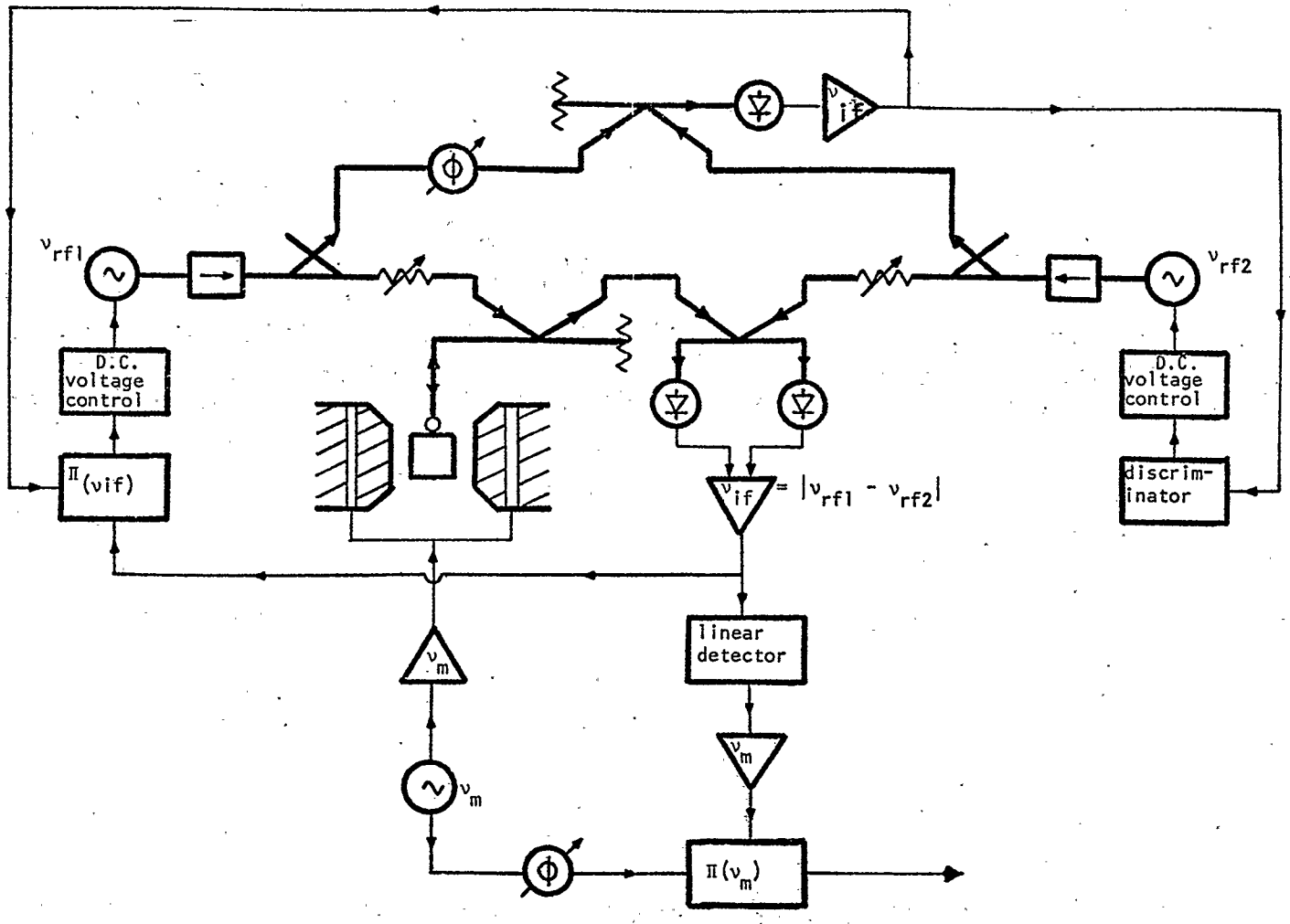

FIGURE 5.2 Block diagram of a superheterodyne spectrometer with frequency stabilization.

(Alger, 1968), however the system is much more complicated and less reliable at low temperatures due to increased microphony. The resolution of the system may be limited if the magnetic field modulation frequency exceeds the linewidth of the resonance but this is rarely a problem. The synchrodyne configuration enjoys the advantages of relative simplicity and lack of severe stability problems in comparison with other configurations explaining its almost universal adoption.

5.1.2 Superheterodyne and Pseudosuperheterodyne Configurations

The superheterodyne configuration employs two separate microwave oscillators so that the signal at the output of the microwave diode mixer appears at the difference frequency of the two oscillators. Detection at the intermediate frequency shifts the signal to zero center frequency. Figure 5.2 is a diagram of the superheterodyne configuration. This design suffers from its complexity because the signal oscillator frequency should be stabilized relative to the cavity resonant frequency and the intermediate frequency must be also stabilized to prevent baseline drift.

The superheterodyne configuration is useful when a) the absorption χ' or dispersion χ'' must be measured, b) the linewidth is less than 10μT or exceeds 10mT, c) very high sensitivity is required, and d) in ENDOR experiments. The advantages of the superheterodyne configuration can be achieved with a minimum of its disadvantages by using a single oscillator in a pseudoheterodyne configuration. This oscillator generates both the "signal oscillator" and the "local oscillator" waves. The frequency of one of these waves must be shifted by a modulation process.

The frequency shift of the local oscillator wave can be achieved in various ways. Ruban (1963) and Buckmaster and Dering (1967) used a single sideband generator (two ferrite modulators operating in anti-phase) to obtain a frequency shift up to 150 kHz More recently, Buckmaster and Gray (1971) have used a phase modulator which is more efficient.

The other approach requires the modulation of the wave in the signal arm. The frequency, phase or amplitude of this wave should not be modulated before entering the resonant cell because of the filtering action of the cell. Methods of amplitude modulating the power output of the resonant cell have been described by many authors. Praddaude (1967) used a Faraday rotation modulator to achieve 100kHz sidebands; Faulkner and Whippey (1966) used a microwave point-contact diode modulator driven with a 460kHz square wave and, more recently, Clerjaud and Lambert (1971) made use of a PIN-diode modulator. This latter modulator has the best characteristics. The system described by Clerjaud and Lambert is very simple and easy to build but it is doubtful that it can achieve a very high performance since nothing is done to prevent the effect of the klystron noise as do the systems devised by Buckmaster et al or Praddaude.

These amplitude modulation techniques have the disadvantage of introducing at least a 3dB loss in signal power. This causes a significant loss of sensitivity when the usable signal wave power is limited. Nevertheless, it is possible to overcome this effect in a system suggested by Wilmshurst (1967). The use of a PIN diode instead of a point-contact diode in the configuration described by Faulkner and Whippey produces a square wave phase modulation since a PIN diode is equivalent

to a short circuit when forward biased and to an open circuit when reverse biased.

It should not be forgotten that all these modulation techniques require the use of devices which introduce nonlinearities and additional noise. Special devices and techniques must be used to minimize these effects. This increases the complexity of the system which the pseudo-heterodyne configuration was supposed to avoid.

5.1.3 Low Noise Preamplifiers

Low noise microwave preamplifiers can be used to increase the signal and its additive noise prior to the receiver with the object of improving the overall noise figure of the detection system. To be useful, these preamplifiers should have a much lower (equivalent) noise temperature than the detector. The applications in EPR of either parametric preamplifiers ($t \approx 100\text{-}20K$) or maser preamplifiers ($t \approx 10\text{-}1K$) have been described by Poole (1967) and Wilmshurst (1967) amongst others. The maser is more interesting since its use would appear to produce the ultimate sensitivity. Buckmaster and Skirrow (1972) have analysed this problem thoroughly. They showed that the advantage of using a maser preamplifier is superfluous in EPR studies of samples which saturate at signal power levels in excess of $O(1\mu W)$, but that they are useful for samples that saturate below $O(0.1\mu W)$ since this is also the saturation threshold of the preamplifier. Experimental proof of this assertion is given by Hardin and Uebersfeld (1971).

Low noise preamplifiers are not useful unless the receiver noise is dominant and its influence can be reduced by using such a preamplifier with sufficient gain. In general this is not the situation since the sensitivity is ultimately limited by the oscillator noise.

5.2 Reduction of Microwave Oscillator Noise

The analysis of oscillator noise effects is very complex compared to receiver noise effects. Various techniques have been used to describe oscillator noise and, in particular, its frequency instability. An intuitive approach using concepts such as background noise, noise pedestal, mean and rms frequency fluctuation has been followed by Bosch and Gambling (1961-1962) amongst others. Wilmshurst (1967) used phasor techniques in his analysis of the influence of different noise components on the sensitivity of EPR spectrometers. Teaney *et al* (1961) noted and Buckmaster and Dering (1967) proved experimentally that oscillator noise is the factor that limits the sensitivity of an EPR spectrometer at high cavity power levels. These investigations were quite simplistic in their disregard of the unique and complex nature of the oscillator noise. A more correct analytical approach which recognizes noise as a random process affecting both the amplitude and the phase of the microwave was used by Strandberg (1972).

5.2.1 Oscillator Noise Propagation in the Signal Arm

The propagation of oscillator noise in the signal arm can be studied correctly by analysing the output of the reflection cavity, whose frequency transfer function is given by Eq.4.4.6, when the input is a wave described by Eq.4.3.2. The effect of various mixers and

synchronous demodulators can be accounted for by introducing a new transfer function cascaded with a band-pass filter centered around the frequency $f=kf_m$ of the detected harmonic of the magnetic field modulation frequency f_m. A synchronous detector makes the bandwidth of this filter equal to the very narrow bandwidth of the low-pass filter located after the final stage of detection. If the a.m. and p.m. noise are uncorrelated, then the noise power spectral density at the input to the final detector is

$$W_N = |G(f)|^2 P_o \left[|Z_{AM}(f)|^2 W_{AM}(f) + |Z_{PM}(f)|^2 W_{PM}(f) \right] \tag{5.2.1}$$

where P_o is the oscillator power and $G(f)$, the transfer function of the other circuit components, is frequency independent in the bandwidth of interest. If the reflection cavity is nearly matched ($\beta \simeq 1$ and $\Gamma_o \simeq 0$) and at resonance ($f_{osc} \simeq f_r >> f_m$) then

$$|Z_{AM}(f)|^2 = Q_o^2 S^2 \sin^2\phi + \Gamma_o^2 + Q_o^2 f^2/f_o^2 \cos^2\phi \tag{5.2.2a}$$

$$|Z_{PM}(f)|^2 = (\Gamma_o^2 + Q_o^2 f^2/f_o^2)\sin^2\phi + Q_o^2 S^2 \cos^2\phi \tag{5.2.2b}$$

where $S=(f_o-f_r)/f_o$ is a factor measuring the relative stability carrier frequency-resonant cavity frequency and ϕ represents an overall phase angle between the signal and the reference wave. The absorption component is detected when $\phi=0$ while the dispersion component is detected when $\phi=\pi/2$. Eqs.5.2.1 and 5.2.2 describe all the ways in which the signal oscillator noise can limit the spectrometer sensitivity and indicate the importance and frequency dependence of the various parameters governing the oscillator noise propagation.

It is instructive to rearrange these equations to show how the absorption and dispersion components are affected by oscillator noise.

$$W_N^{abs} = W_N^{\phi\simeq 0} \simeq P_o|G(f)|^2 \; [(\Gamma_o^2 + Q_o^2 f^2/f_o^2) + \phi^2 Q_o^2 S^2] \; W_{AM}(f) + $$
$$+ \; P_o|G(f)|^2 \; [Q_o^2 S^2 + \phi^2(\Gamma_o^2 + Q_o^2 f^2/f_o^2)] \; W_{PM}(f) \tag{5.2.3a}$$

$$W_N^{disp} = W_N^{\phi\simeq\pi/2} \simeq P_o|G(f)|^2 \; [(\Gamma_o^2 + Q_o^2 f^2/f_o^2)(\pi/2-\phi)^2 + Q_o^2 S^2] \; W_{AM}(f) + $$
$$+ \; P_o|G(f)|^2 \; [(\pi/2-\phi)^2 Q_o^2 S^2 + (\Gamma_o^2 + Q_o^2 f^2/f_o^2)] \; W_{PM}(f) \tag{5.2.3b}$$

It should be noted that several contradictions with the general consensus of requirements for higher sensitivity appear in these equations. While the signal is proportional to Q in the absence of saturation, the noise due to the signal oscillator is also an increasing function of Q so that a compromise must be achieved. This compromise depends on many factors including the oscillator noise level, the receiver noise level, the final detection frequency and the saturation power level. The f^2 dependence of some of the terms of $|Z(f)|^2$ contradicts the experimental folklore that the system sensitivity is proportional to the magnetic field modulation frequency. This belief takes into account the fact that the noise power of the receiver decreases with increasing sideband frequency but overlooks the fact that this is valid only up to the "knee" frequency and disregards the role of oscillator noise and its frequency dependence. Again, a frequency compromise is

required according to each experimental situation.

Equations 5.2.2 and 5.2.3 stress the importance of critically matching the resonant cavity to make the noise terms depending on Γ_o negligible. This shows that configurations in which the cavity is not matched or the sample cell bridge is unbalanced in order to provide the microwave reference for the diode detector are not optimum and should not be used.

5.2.2 Frequency Stabilization

Equations 5.2.2. and 5.2.3 indicate that there are two different problems involved in the concept of frequency stabilization. Absolute stabilization reduces the f.m. noise, and hence W_{PM}, while relative stabilization is necessary to maintain the difference between the oscillator frequency and the resonant cavity frequency as small as possible.

The absolute stabilization can be achieved either by phase or frequency discrimination relative to a standard frequency. This reference frequency is determined by either a very stable high-Q resonant cavity (Pound, 1946) or a high stability monochromatic quartz crystal oscillator (Pascaru, 1964). Buckmaster and Dering (1966) and Dering (1967) have discussed the various schemes in detail. They also discussed the problem of relative stabilization using the sample cavity as a reference cavity in a Pound stabilizer. The stabilization should be independent of the microwave power into the sample cavity or, at least, it should be effective when the power exceeds a certain minimum value. The optimum approach is to combine absolute stabilization using a high stability, monochromatic quartz crystal reference oscillator and

relative stabilization using the sample resonant cavity as the reference. Such systems have been described by Buckmaster and Dering (1966) and Buckmaster and Gray (1971).

Frequency stabilization is a profound and complex problem because it affects the performance of EPR spectrometers in various ways. The stability of the resonant frequency of the sample cell also needs consideration. Strandberg (1972) proposed the use of a wide bandwidth relative stabilization system instead of the usual narrow bandwidth absolute and/or relative stabilization systems. Thus it is possible to reduce the factor S to zero and to decrease the relative f.m. noise power so that the sensitivity of the EPR spectrometer will increase. Unfortunately, this proposal overlooks the fundamental role played by the frequency of the electromagnetic wave in magnetic resonance phenomena. This frequency must not drift with the cavity resonant frequency or follow its rapid fluctuations since this would affect the system resolution and degrade its sensitivity. Care must be taken to ensure that a satisfactory compromise is achieved.

It would be interesting to invert the procedure by stabilizing the resonant frequency of the sample cell to a high stability, monochromatic signal oscillator because the frequency at which the EPR transitions are measured should be constant. This procedure is feasible since high-Q varactor and PIN diodes have become available and should be evaluated both theoretically and experimentally.

5.2.3 Phase Stabilization

An analysis of Eqs.5.2.3 shows the importance of the operating phase angle ϕ (0 or $\pi/2$). The correct interpretation of the information

carried by the output signal depends on this angle as does the reduction of oscillator noise effects. The problem of distinguishing between absorption and dispersion spectra will be treated in Chapter IX.

The effect of phase instability has not been granted much attention, except by Praddaude (1967), since it is not a first-order effect and the phase stability of the waveguide components is usually quite good. A stabilization loop using a phase modulator can be introduced when required. The frequency response functions given in Eqs.5.2.2 are sensitive to the phase when the input wave is either amplitude or pulse modulated. This is the basic idea of Praddaude's system, but a simpler system using only one phase modulator for both the frequency and the phase stabilization can be devised.

5.2.4 Bimodal Cavity

Teaney, Klein and Portis (1961) showed experimentally that oscillator noise could be reduced by using a bimodal cavity as a resonant cell. The following discussion assumes that the resonant cell has two orthogonal modes. This orthogonality ensures a high degree of isolation between the modes, and thus attenuates the amount of oscillator noise reaching the detector. Very interesting designs have been described by Nishina and Danielson (1961), Hyde and Freed (1968) and Franconi (1969, 1970) amongst others.

A bimodal cavity is a reciprocal two-port resonant cell. The ports are activated by two orthogonal modes having the same resonant frequency. In theory, the modes and thus the ports should be perfectly isolated unless disturbed by a magnetic resonance phenomenon, a Faraday rotation or some other perturbing phenomena. Off-diagonal components of

the susceptibility tensor permit a transfer of power from the input to the output mode. Attempts to derive a frequency transfer function for a bimodal cavity have been made by Teaney et al (1961) and Liu, Nishina and Good (1961). The former derivation assumed that a lumped parameter equivalent circuit could be used, while the latter is pertinent only to that particular geometrical configuration, although quite general in principle.

These transfer functions cannot be easily measured experimentally. A clearer and deeper understanding of the function of this type of cavity is required. It can be considered as a transmission cavity with isolated input and output ports so that it is a band-reject filter. The advantage of this filter is its wide bandwidth due to the frequency independence of the orthogonality between modes. The combination of a reflection cavity with a magic bridge or a circulator is also a band-reject filter but has a very narrow bandwidth. Then, an equation similar to Eq.4.4.6 is a valid expression for the frequency response function of a bimodal cavity.

$$T_{bm}(f) = \frac{(1-\beta_{eff}) - j[2\beta_{eff}Q_{eff}(f-f_r)/f_r]}{(1+\beta_{eff}) + j[2\beta_{eff}Q_{eff}(f-f_r)/f_r]} \qquad (5.2.4)$$

where f_r is the resonant frequency of both modes, β_{eff} is the effective coupling coefficient and Q_{eff} is the effective quality factor. These three parameters can be easily measured experimentally. For the narrow bandwidth filter $Q_{eff} = Q_o$ and a conflict arises between the high signal requirement that Q_o is as large as possible for maximum signal and the requirement that Q_{eff} is as small as possible to reject oscillator noise. This conflict does not appear for the bimodal cavity

since Q_o, the quality factor for an individual mode, and Q_{eff} which describes the bandwidth of the orthogonality are different. They can be optimized separately and no compromise is necessary. Such an ideal filter for which $Q_{eff} = 0$ and $\beta_{eff} = 1$ will reject all the oscillator noise.

Unfortunately, ideal bimodal cavities cannot be realized. Moreover, the introduction of the sample distorts the necessary orthogonality and various tuning and matching devices are necessary since the distortion changes from sample to sample and the tuning devices usually affect both modes. This, along with its bulkiness, are the main disadvantages of the bimodal cavity. The bulkiness arises because the two orthogonal oscillating magnetic fields must be also orthogonal to the static magnetic field. The problems of achieving a small volume and an effective "match" are treated extensively in the literature but no mention has been made regarding the bandwidth of the cavity. The assumption that the modes are othogonal at all frequencies is not valid in practice. Noise coupling via the resonance phenomenon has never been mentioned also. This mechanism has not been observed because the sensitivity is determined incorrectly as the ratio of the signal amplitude to the noise r.m.s. amplitude measured far from the signal.

The advantages of a bimodal cavity are uncontestable in principle, but a more complete study of its practicality remains to be done. The use of bimodal cavity in pulse experiments is another field of interest.

5.2.5 Local oscillator Noise—Balanced Mixer

The previous sections have discussed the propagation and reduction of oscillator noise in the signal channel. Additional noise arrives at the receiver through the reference, or "local oscillator" channel. The quotation marks indicate that the role of local oscillator is played *de facto* by the signal oscillator in single oscillator systems.

F.m. oscillator noise plays no influence in the reference channel besides introducing a second-order phase uncertainty since no frequency dependent device is used. A.m. noise is a first-order effect and its influence should be reduced. A magic-T balanced mixer is the simplest and best technique since the a.m. local oscillator noise components appear in antiphase and, hence, they cancel. The degree of cancellation depends on the diode match to the waveguide, the mechanical symmetry of the bridge arms and an identity of diode characteristics (Poole, 1967). It is necessary to use some form of mechanical tuning and amplitude attenuation to satisfy these conditions, but such an involved design of a good balanced mixer is justified by the advantages it provides.

The cancellation of a.m. noise is, in a first-order approximation, valid over a relatively large bandwidth contrary to the statement of Wilmshurst (1968). Wilmshurst's (1967) statement that a balanced mixer reduces f.m. noise is also not justified either theoretically or experimentally.

5.3 Reduction of Mechanical, Thermal and Electrical Transients Effects

The mechanical, thermal and electrical transients form a special class of noise sources. They are difficult to identify and locate in

either space or frequency and, moreover, they are not always repeatable. These effects usually produce noise components which are negligible compared to those due to the receiver or oscillator. They become increasingly important only when the latter components are decreased. A good mechanical and electrical environment is required. Various noise sources must be identified and located both in space and in frequency before a systematic attempt is made to minimize their effect. The procedure depends on the nature of the noise sources (Alger, 1968).

Frequently, the solution consists of shifting the detection bandwidth to noise-free frequency regions when elimination is impossible.

The long-term thermal instability and drift lead to loss of resolution and baseline instability. This effect can be reduced by employing magnetic field modulation techniques and both relative and absolute stabilization of the oscillator frequency.

5.4 Conclusions

The noise sources affecting the performance of an EPR spectrometer have been analyzed. It is concluded that a compromise is usually necessary to optimize the system. The optimum situation depends on the many experimental parameters and their variation. A complete analysis of the noise is necessary to distinguish the most important noise sources before their influence can be minimized in a systematic approach.

CHAPTER VI

EPR SPECTROMETER PERFORMANCE IMPROVEMENT BY SIGNAL PROCESSING

It was shown in Chapter I that the detection system of an EPR spectrometer consists of a detector for the resonance phenomenon, an information processor and a time base. The radiation detector was analysed with the microwave system because it is technically a part of this system although logically it is a part of the information processor. The information processor consists of transformation, measurement and interpretation processors. This chapter analyses only the transformation processor since the other functions are still performed by the human operator.

The transformation processor brings the data into a form which is optimum for the subsequent analysis. It is usual to assume that the transformations are performed by linear time-invariant processors. This assumption is made for the sake of mathematical simplicity rather than because linear systems have necessarily a superior performance to non-linear systems. It was shown in Sec. 3.3 that time-invariant linear systems are characterized by a convolution integral equation

$$y(t) = \int_T h(t-\tau)\ x(\tau)\ d\tau \qquad (6.0.1)$$

where T is an interval on the time (real variable) axis. If a system yielding a functional z(t) of the input data x(t) is desired, it is necessary to solve Eq. 6.0.1 for h(t) where y(t) = z(t). The solution can be obtained easily using Fourier transform operators if the input data x(t) are deterministic and the interval T is unbounded.

$$H(f) = \frac{Z(f)}{X(f)} \tag{6.0.2}$$

For stochastic input data, Eq. 6.0.2 is invalid and the output data y(t) can only approximate the function z(t). It is then necessary to define adequate criteria according to which this approximation is optimum (Helstrom, 1968).

6.1 Least Mean Square Estimation (Wiener-Kolmogoroff Theory)

The criterion on which the Wiener-Kolmogoroff theory is based requires the mean square error between the actual output y(t) of the linear system and the desired signal z(t) to be minimized.

$$e = E\left[|z(t) - y(t)|^2\right] \tag{6.1.1}$$

The advantage of using this criterion is the significant simplification of the mathematical analysis involved although it may not lead to improved performance. According to the orthogonality principle (Papoulis, 1965), Eq. 6.1.1 is equivalent to the condition that the simple error defined as the difference between the desired value $z(t_1)$ and the estimated value $y(t_1)$ is orthogonal to the input data x(t).

$$E[(z(t_1) - y(t_1))\, x(t)] = 0 \quad ; \quad t \in T \tag{6.1.2}$$

Three different problems can be distinguished depending on the position of t_1 relative to the interval T:

- t_1 belongs to T - the smoothing problem in which an estimate of the past is improved on the basis of knowledge of both past and future relative to t_1 values;

- t_1 equals the upper bound of T - the filtering problem in which the present value is estimated on the basis of knowledge of past values;

$-t_1$ exceeds the upper bound of T - the prediction problem in which an estimate of a future value is attempted.

Unfortunately, the solution for the system h(t) can be expressed only as an integral equation. If Eqs. 6.0.1 and 6.1.2 are combined and random process theory is applied, then

$$R_{zx}(t - t_1) = \int_T h(t_1,\tau)R_{xx}(t - \tau)\, d\tau \,. \tag{6.1.3}$$

This Wiener-Hopf type equation can be solved easily only when the interval T covers the entire time domain. The optimum system is time invariant if the random processes involved are stationary. The solution of Eq. 6.1.3 becomes

$$H(f) = \frac{W_{zx}(f)}{W_{xx}(f)} \exp(-j2\pi f t_1) \tag{6.1.4a}$$

while the minimum error is

$$e = R_{zz}(0) - \int_{-\infty}^{+\infty} R_{zx}(\tau)h(\tau)d\tau = \int_{-\infty}^{+\infty} W_{zz}(f) \left[1 - \frac{|W_{zx}(f)|^2}{W_{zz}(f)W_{xx}(f)}\right] df. \tag{6.1.4b}$$

The determination of a functional z(t) of the signal s(t) when this signal is mixed with noise n(t) is an interesting common problem. If the signal and the noise are uncorrelated, then

$$x(t) = s(t) + n(t) \,, \qquad W_{sn}(f) = W_{zn}(f) = 0 \tag{6.1.5}$$

and Eqs. 6.1.4 become

$$H(f) = \frac{W_{zs}(f)}{W_{ss}(f) + W_{nn}(f)} \tag{6.1.6a}$$

and

$$e = \int_{-\infty}^{+\infty} \frac{W_{zz}(f)W_{nn}(f)}{W_{ss}(f) + W_{nn}(f)} \, df \, . \tag{6.1.6b}$$

The realization of this filter H(f) depends on the signal shape. An implementation of such filters on digital computers is discussed in Chapter IX. It is interesting to mention that the least mean square criterion is never used for optimum filter design in EPR instrumentation and that the signal to noise ratio (S/N) maximization criterion is used exclusively.

6.2 Filtering for Enhancement of Sensitivity in the S/N Sense

The S/N maximization criterion is appropriate only in problems where the decision concerns only the presence or absence of a signal which may be buried in noise and no information is required concerning its shape or time of occurrence. The least mean square estimation or other criteria must be used if this latter information is required or additional constraints must be imposed on the S/N maximization criterion.

6.2.1 S/N Definitions

Communication theory usually employs a S/N definition involving powers

$$S/N(P) = \frac{\text{Signal Power}}{\text{Noise Power}} = [S/N(A)_{rms}]^2 = \left[\frac{\text{r.m.s. signal amplitude}}{\text{r.m.s. noise amplitude}}\right]^2 \tag{6.2.1}$$

where the signal power $P[x(t)]$ is defined by

$$P[x(t)] = \lim_{T\to\infty} \frac{1}{2T} \int_{-T}^{+T} |x(t)|^2 \, dt \tag{6.2.2}$$

which is finite and measurable.

EPR experiments produce signals of the finite energy type since their power, as defined by Eq. 6.2.2, is zero while their energy is

$$E[x(t)] = \int_{-\infty}^{+\infty} |x(t)|^2 \, dt. \tag{6.2.3}$$

A more appropriate S/N definition is

$$S/N(E) = \frac{E[\text{signal}]}{P[\text{noise}]} \; . \tag{6.2.4}$$

It is difficult to measure signal energies or noise powers in EPR spectroscopy because they are usually concentrated in a very narrow low-frequency range. Consequently, the S/N is defined in terms of amplitudes instead of either of these two definitions.

$$S/N(A)_u = \frac{(\text{peak amplitude of signal})}{\sqrt{2}\,(\text{r.m.s. amplitude of noise})} \tag{6.2.5}$$

where the subscript "u" denotes a unipolar signal. As mentioned in Sec. 2.4, magnetic resonance spectroscopy lineshapes are Gaussian, Lorentzian or some combination. Ernst (1966) has described some convenient methods of measuring S/N(A) in which the noise power or its r.m.s. amplitude is usually measured in magnetic field or microwave frequency regions far from resonance. This is erroneous for EPR spectrometers in which oscillator noise predominates because the output noise power is higher when the resonance condition is satisfied since then the resonant cavity is less effective in rejecting oscillator noise. The S/N(A) definition given in Eq. 6.2.5 may be considered as equivalent to the S/N(E) definition.

Most EPR spectrometers employ magnetic field modulation and detect the first Fourier coefficient of the lineshape a_1 or d_1. a_1 has a bipolar shape with two extrema of opposite polarity. The appropriate S/N(A)

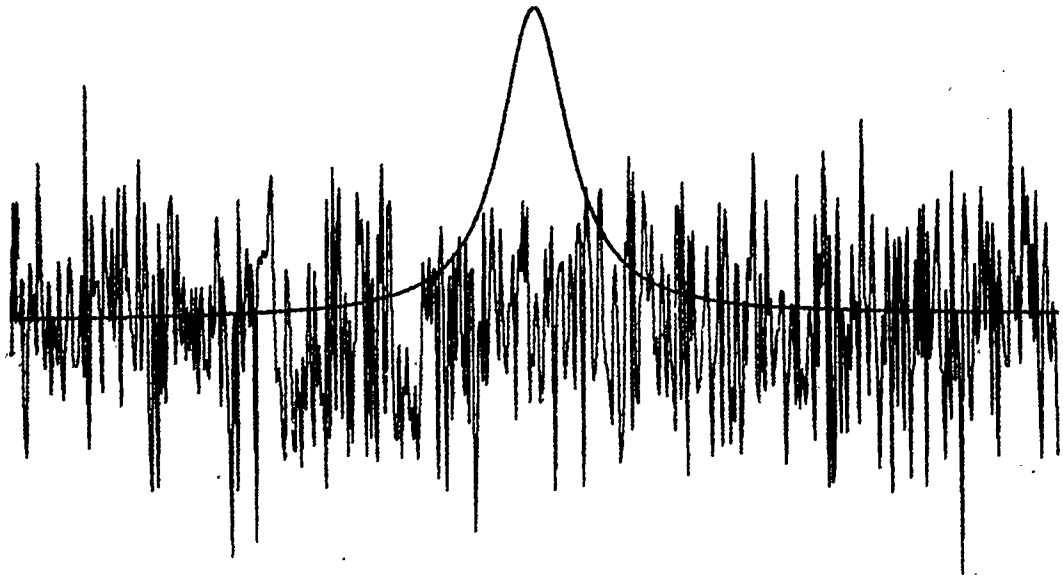

(a) Lorentzian a_0 lineshape; $S/N(A)_u = 2$

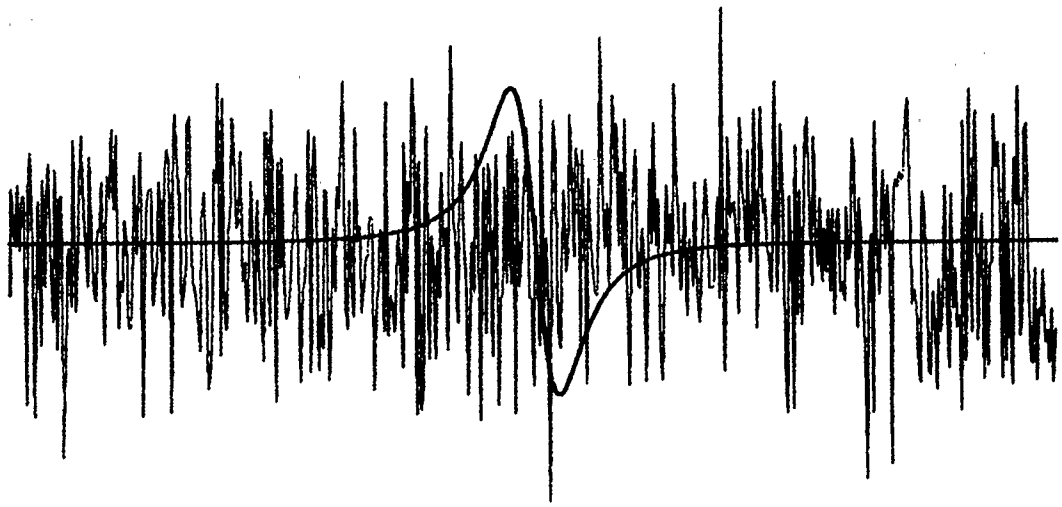

(b) Lorentzian a_1 lineshape; $S/N(A)_b = 2$

FIGURE 6.1 Diagram showing the superposition of lineshape function and noise.

definition is

$$S/N(A)_b = \frac{(\text{positive signal peak amplitude - negative signal peak amplitude})}{(\text{r.m.s. value of difference of noise amplitudes at extrema})} \tag{6.2.6}$$

where the subscript "b" denotes a bipolar signal. When the noise is white this definition simplifies to

$$S/N(A)_b = \frac{(\text{positive signal peak amplitude - negative signal peak amplitude})}{\sqrt{2}\ (\text{r.m.s. amplitude of noise})} \tag{6.2.7}$$

Figure 6.1 illustrates Lorentzian a_0 and a_1 noisy signals having S/N(A) of 2.

EPR signals consisting of many spectral lines present a more complex problem. If the lines are assumed to have the same lineshape f(t) but different amplitudes and locations, then

$$x(t) = \sum_{k,j} A_{k,j} f(t-t_{k,j}) + n(t) = \sum_j g_j(t) + n(t) \tag{6.2.8}$$

where $A_{k,j}$ are the amplitude weighting factors, n(t) is the noise amplitude and $g_j(t) = \sum_k A_{k,j} f(t-t_{k,j})$. The S/N should be defined according to the information desired. The S/N must be defined in terms of the energy carried by a single line if each individual line is to be detected,

$$S/N(E) = \frac{E[f(t)]}{P[n(t)]}, \tag{6.2.9}$$

whereas if a combination $g_j(t)$ of lines is to be detected then the proper S/N definition is

$$S/N(E)_\Sigma = \frac{E[g_j(t)]}{P[n(t)]}. \tag{6.2.10}$$

A hypothetical speech transmission problem is a useful analogy to appreciate the distinction between $S/N(E)_\Sigma$ and $S/N(E)$. A filter to detect single letters in the presence of noise is necessary if all the letters are of interest, whereas a filter designed to detect certain letter patterns is required if only certain words or phrases are of interest. It might be advantageous to use filters which enhance the word energy rather than the letter energy since $S/N(E)_\Sigma \geq S/N(E)$. Single lines and groups of lines are the magnetic resonance analogy of letters and words.

Optimum filtering of complex patterns discards all the information carried individually by the pattern components. This method is not very economic since a special filter must be built for each pattern and the filtering is not 100% effective if the pattern is disturbed by the experimental conditions. $S/N(E)_\Sigma$ filters could be useful to detect the presence of specific paramagnetic ions since each ion has a characteristic spectral pattern. The processing complexity is justified only if the pattern is relatively complicated since the advantage of using the filter to enhance $S/N(E)_\Sigma$ is proportional to the number of spectral lines forming the pattern.

6.2.2 The Matched Filter

The optimum S/N maximization filter is derived in communication theory texts.

$$H_m(f) = c\,\frac{S^*(f)}{W_{nn}(f)}\,\exp(-j2\pi f t_0) \qquad (6.2.11)$$

where $S^*(f)$ is the complex conjugate of the Fourier transform of the signal $s(t)$, c is a constant and the filter lag time t_0 is the instant

at which maximum S/N occurs. It is called the matched filter because its pulse response $h_m(t)$ is a time reversed replica of the signal if the noise is white.

$$h_m(t) = c \cdot s(t_0 - t) \tag{6.2.12}$$

The filter function H(f) and the achievable S/N are different if the signal s(t) is considered to be f(t) or $g_j(t) = \sum_k A_{k,j} f(t - t_{k,j})$. The S/N is obviously greater in the latter case.

The matched filter distorts the signal shape. One of its effects is to broaden the signal. The broadening is symmetric for symmetric lines and no relative peak-shifting occurs. The formulae describing this process for Lorentzian or Gaussian lineshapes are discussed in Sec. 9.2. The shape distortion is more dramatic for lineshapes which can be considered to be derivatives of an original line because a S/N(E) matched filter introduces a further differentiation. This distortion causes problems for experimentalists accustomed to interpreting only a_1 spectra. A method of avoiding this distortion is discussed in Sec. 9.2.

The matched filter is realizable only for signals which can be completed by a time t_0. Unfortunately, magnetic resonance signals do not satisfy this condition.

6.2.3 The RC Filter Approximation of the Matched Filter

It is not easy to realize a good approximation of an optimum filter because it requires the calculation of a realizable transfer function and the synthesis of the corresponding filter as an electrical network. Consequently, it is not surprising that the simple RC low-pass filter is the commonest filter employed in magnetic resonance. It has been analysed

completely by Ernst (1966) who showed that the achievable S/N for a Lorentzian line is almost what can be theoretically achieved using a matched filter. Unfortunately, the RC filter has asymmetric broadening effects and shifts the peak location. These asymmetric lineshape distortions are the major disadvantages of the RC filter. Nevertheless, it has the advantage of being an easily and cheaply realizable On-Line filter.

6.2.4 S/N Filters with Additional Constraints

Constraints additional to S/N maximization must be imposed to minimize the distortion introduced by "normal" filters. A parameter must be defined to measure the specific distortion so that an adequate criterion for acceptable distortion can be formulated.

Ernst (1966) used a relative error ε defined in the mean square sense by

$$\varepsilon^2 = \frac{\int_{-\infty}^{+\infty} |s_i(t) - s_o(t)|^2 \, dt}{\int_{-\infty}^{+\infty} |s_i(t)|^2 \, dt} \tag{6.2.13}$$

where $s_i(t)$ and $s_o(t)$ are the input and output signals. He used the Lagrange multiplier technique to obtain the optimum filter for a symmetrical unipolar lineshape.

$$H_o(f) = \frac{pS_i^2(f) + qS_i(f)}{pS_i^2(f) + W_{nn}(f)} \tag{6.2.14}$$

where $W_{nn}(f)$ is the noise power spectral density and p and q are the multipliers. This filter produces minimum lineshape distortion for a fixed S/N value. The filtering effectiveness depends on the values of p and q. It should be noted that the filters given by Eqs. 6.1.6 and

6.2.14 are not identical, unless $p = 1$ and $q = 0$, because the filter 6.2.14 is specifically designed according to the S/N criterion. This filter transforms into a matched filter if $p = 0$ while its effectiveness is nullified if $p \to \infty$.

The kth moment of the line is another lineshape parameter whose distortion may be restricted in a S/N enhancement filtering.

$$M_k(s_i) = \frac{\int_{-\infty}^{+\infty} t^k s_i(t)\, dt}{\int_{-\infty}^{+\infty} s_i(t)\, dt} = \frac{(j)^k\, s_i^{(k)}(0)}{S_i(0)} \tag{6.2.15}$$

The moment of the signal at the output from a filter h(t) is

$$M_k(s_o) = (j)^k \sum_{\ell=0}^{k} \frac{(\ell)^k\, H^{(\ell)}(0)\, S_i^{(k-\ell)}(0)}{H(0)\, S_i(0)} \tag{6.2.16}$$

and it follows that the first (k-1) moments are conserved if

$$h(t) = \left(\frac{d}{dt}\right)^k g(t) \qquad\qquad H(f) = (2\pi j f)^k G(f) \tag{6.2.17}$$

where g(t) should be chosen so that S/N is also enhanced.

6.3 Filtering for Resolution Improvement

Good resolution is required to locate lines accurately. This measurement is limited by a) noise which blurs the peaks (for unipolar lines) or zero-crossings (for bipolar lines) and b) overlapping of adjacent lines of finite width. The first effect can be minimized by using the procedures outlined in Sec. 6.1 and 6.2. For unipolar lines, it is preferable to cascade a noise minimization filter with a differentiating

filter because zero-crossings can be located with greater precision than extrema. RC filters are not satisfactory for this purpose because they shift the peaks of the lines. This section analyzes the effect of overlapping lines and the methods used for its minimization.

6.3.1 Definition of Resolution Parameters

The general definition of resolution has been given in Chapter I. This section attempts to define a quantitative parameter which can be associated with the concept of resolution. This parameter is usually related in magnetic resonance spectroscopy to the shape of the narrowest line detectable. The most practical and common measure is the full width of the line at half its height (w_{fh}) or the half width at half height (w_{hh}). The main advantage of these measures is the ease of determination, but they are deficient in the sense that they concern only two points on the entire line.

A resolution parameter can be defined as an integral of a functional of the lineshape function. The variance is a possible such definition.

$$w_\sigma^2 = M_2(s_i) - M_1^2(s_i) \tag{6.3.1}$$

Unfortunately, this measure diverges for Lorentzian and certain other lineshapes.

Two other common integral measures refer to the width of a rectangular lineshape whose properties are related to those of the actual lineshape. The equivalent width

$$w_a = \left[\int_{-\infty}^{+\infty} s_i(t)\, dt\right] \cdot \left[\frac{1}{s_i(0)}\right] \tag{6.3.2}$$

is the width of a rectangle having the same height and area as the magnetic

resonance line. The energy width

$$w_e = \frac{\int_{-\infty}^{+\infty} |s_i(t)|^2 dt}{|s_i(0)|^2} = \frac{\int_{-\infty}^{+\infty} |S_i(f)|^2 df}{\int_{-\infty}^{+\infty} S_i(f)\ df} \tag{6.3.3}$$

is the width of a rectangle having the same height and energy as the magnetic resonance line.

6.3.2 The Ideal Filter

Generally, the resolution distortion can be represented by a Fredholm integral equation of the first kind

$$s(x) = \int_{-\infty}^{+\infty} q(x')\ r(x,x')\ dx' \tag{6.3.4}$$

where $r(x,x')$ represents the resolution function and $q(x)$ is the desired undistorted original spectrum. Equation 6.3.4 transforms into a convolution integral equation if the distorting system is linear and x-invariant

$$s(x) = \int_{-\infty}^{+\infty} q(x')\ r(x-x')\ dx' \tag{6.3.5}$$

The solution of Eq. 6.3.5 can be obtained by using Fourier transform operators.

$$q(x) = \mathcal{F}^{-1}\left\{\frac{\mathcal{F}\{s(x)\}}{\mathcal{F}\{r(x)\}}\right\} \tag{6.3.6}$$

This is equivalent to a filtering process whose frequency transfer function is

$$H_r(f) = 1/R(f) = 1/[\mathcal{F}\{r(x)\}] \ . \tag{6.3.7}$$

For spectra consisting of overlapping lines, the ideal original spectrum q(x) and the experimental spectrum s(x) can be represented by sums of delta and lineshape functions respectively

$$q(x) = \sum_k A_k \delta(x-x_k) \tag{6.3.8a}$$

$$s(x) = \sum_k A_k r(x-x_k) \tag{6.3.8b}$$

where it is assumed that the resolution distortion function r(x) is identical for all lines. The ideal filter given by Eq. 6.3.7 will output q(x) as a spectrum of delta lines if s(x) is the input data.

Like other ideal filters, the resolution filter cannot be realized as a synthesis of electrical network elements. Section 6.3.4 discusses practical approaches to its approximation while Sec. 9.3 discusses its simulation by a digital Fourier analyzer.

6.3.3 Limitations of Ideal Resolution Improvement Procedures

For overlapping line spectra, the term "ideal resolution improvement" refers to attempts to reduce the spectrum into a sequence of delta lines. A comparison of the matched filter for the white noise case (Eq. 6.2.11) and the ideal resolution filter (Eq. 6.3.7) shows that these filters are an inverse pair. Consequently, any ideal resolution improvement process leads to a drastic reduction of the S/N due to the favourable weighting of high frequency noise components. A compromise must be established between resolution and sensitivity.

Cohn-Sfetcu *et al* (1970) have shown that the resolution of magnetic

resonance spectra can be improved by transforming a line into a narrower one of the same type because Lorentzian and Gaussian lines are self-convolving functions. For Lorentzian lineshapes

$$\mathcal{F}\left\{\alpha/\pi(\alpha^2+x^2)\right\} = e^{-2\pi\alpha|f|} \tag{6.3.9a}$$

and

$$\mathcal{F}^{-1}\left\{\frac{\mathcal{F}\{\alpha/\pi(\alpha^2+x^2)\}}{\mathcal{F}\{\beta/\pi(\beta^2+x^2)\}}\right\} = (\alpha-\beta)/\pi[(\alpha-\beta)^2+x^2] \tag{6.3.9b}$$

where α and β are the values for w_{hh} for the spectrum line and resolution distortion function respectively. For Gaussian lineshapes

$$\mathcal{F}\left\{(1/\alpha\sqrt{\pi})\ e^{-x^2/\alpha^2}\right\} = e^{-(\pi\alpha f)^2} \tag{6.3.10a}$$

and

$$\mathcal{F}^{-1}\left\{\frac{\mathcal{F}\{(1/\alpha\sqrt{\pi})\ e^{-x^2/\alpha^2}\}}{\mathcal{F}\{(1/\beta\sqrt{\pi})\ e^{-x^2/\beta^2}\}}\right\} = [\pi(\alpha^2-\beta^2)]^{-1/2}\ e^{-x^2/(\alpha^2-\beta^2)} \tag{6.3.10b}$$

where α and β are the half widths at $(1/e)$ of maximum height. Such processings are meaningless if $\beta > \alpha$ for the narrowest line in the spectrum.

Filters can be designed to transform a broad line into a narrower line of different nature if the conservation of the Lorentzian or Gaussian character is not important. A transformation broad Lorentzian into a narrower Gaussian line can be used because the Fourier transform of a Gaussian tends faster to zero than the transform of a Lorentzian line and the filter transfer function

$$H(f) = G(f)/L(f) \sim \exp(-\pi^2\gamma^2 f^2 + 2\pi\beta|f|), \tag{6.3.11}$$

where α and γ are the widths of the Lorentzian and Gaussian lines

respectively, tends to zero at high frequencies.

Cohn-Sfetcu et al. (1971) have analyzed the passage of bandwidth limited white noise through Lorentz — Lorentz and Lorentz — Gauss filters. They showed that the ratio of output and input noise powers is proportional to

$$P_{no}/P_{ni} \sim (1/\beta\Omega)(e^{-4\pi\beta\Omega} - 1) \tag{6.3.12}$$

for the Lorentz — Lorentz filter and

$$P_{no}/P_{ni} \sim (1/\gamma\Omega)\ e^{2\beta^2/\gamma^2} \cdot \mathrm{erf}[\sqrt{2}\pi\Omega\gamma - (\sqrt{2}\beta/\gamma)] \tag{6.2.13}$$

for Lorentz - Gauss filter, where β and γ are the widths of the Lorentzian and Gaussian references lines respectively and Ω is the noise bandwidth.

Using a different approach, Ernst (1966) derived an optimum filter which maximizes the S/N subject to a reduction of the energy width of the line

$$H_o(f) = c\ \frac{(1+p)\ R(f)}{pR^2(f) + W_{nn}(f)} \tag{6.3.14}$$

where p is a parameter determined by the chosen compromise between resolution and S/N. If R(f) is the lineshape function $S_i(f)$, then the ideal resolution improvement filter requires $p = \infty$ while the matched filter requires $p = 0$.

The least mean square error criterion enables the resolution and sensitivity enhancement problems to be approached simultaneously. Franks (1969) has shown that the transfer function of the optimum filter is given by

$$H(f) = \frac{W_{xx}(f)\ R^*(f)}{W_{xx}(f)|R(f)|^2 + W_{nn}(f)} \tag{6.3.15}$$

when the resolution distortion mechanism can be idealized as a linear time-invariant system affecting the signal data x(t) prior to its association with zero mean stationary noise. This filter introduces attenuation in the frequency regions where the noise density exceeds the signal density and tends to behave like an ideal resolution filter in the regions where the noise density is negligible.

6.3.4 Analogue Filters for Resolution Improvement

The analogue methods used commonly in magnetic resonance spectroscopy to increase the resolution are based on the "derivative approach."

One method uses the fact that the apparent line widths of the higher derivatives of a line are smaller than the original line width. The Fourier coefficients a_K (d_K), $K \neq 0$, can be detected using synchronous demodulators at the kth harmonic of the magnetic field modulation frequency. The S/N also decreases since the amplitude of a_K is smaller than the amplitude of a_{K-1}. Halpern and Phillips (1970) claimed that both the resolution and the S/N can be improved if a double magnetic field modulation technique with a cascaded double synchronous demodulation is used. Their claim can be shown to be invalid and no improvement is achieved by the addition of the expensive extra instrumentation.

Another derivative method is based on the theory of Allen et al. (1964). They expanded the filter transfer function defined by Eq. 6.3.7 into a Taylor series

$$H_r(f) = \sum_{k=0}^{\infty} a_k f^k \tag{6.3.16a}$$

where

$$a_k = (1/k!)\left(\frac{d}{df}\right)^k [H_r(f)]_{f=0} \tag{6.3.16b}$$

so that

$$h_r(t) = \sum_{k=0}^{\infty} (-j)^k a_k \delta^{(k)}(t) \ . \tag{6.3.16c}$$

The output lineshape is then

$$r_\delta(t) = \sum_{k=0}^{\infty} (-j)^k \ a_k \left(\frac{d}{dt}\right)^k [r(t)] \ . \tag{6.3.17}$$

The coefficients a_k can be found by solving Eq. 6.3.14a for a particular lineshape. For a Lorentzian lineshape, Eq. 6.3.15 becomes

$$\ell_\delta(t) = \sum_{k=0}^{\infty} (-1)^k \frac{1}{(2k)!} \left(\frac{w_{hh}}{\alpha}\right)^{2k} \left(\frac{d}{dt}\right)^{2k} [\ell(t)] \tag{6.3.18}$$

where $\ell(t)$ is the Lorentzian lineshape and α is the sweep rate.

This method is more complex than the previous one since it yields a weighted mixture of the original line and several of its even derivatives. As expected, the S/N is drastically reduced by this procedure so that a compromise must be made. The method can be implemented directly by mixing the outputs of several differentiating circuits and passing the combined signal through a low-pass filter. Glarum (1965) had the interesting idea of modulating the magnetic field at three different frequencies f_m, $(f_m/3)$ and $(f_m/5)$ and synchronously detecting the spectrometer signal at a frequency f_m = 100kHz. Alternatively, one modulation frequency can be used with three parallel synchronous demodulators at f_m, $3f_m$ and $5f_m$ if the lineshape is bipolar. Even harmonics or subharmonics must be used for unipolar lineshapes.

6.4 Special Digital Processings

The field of digital processings for either sensitivity or resolution

improvement is vast and prolific. This section discusses only some of these procedures. They can be implemented on general purpose digital computers or special digital processors can be used. The latest trend is to build specialized digital computers such as the Hewlett-Packard Fourier Analyzer whose application in EPR spectroscopy is described in this thesis. The use of a digital Fourier analyser as a signal processor is discussed separately in Chapter IX.

An analog-to-digital (A/D) conversion of the data is a necessary preprocessing operation because EPR spectrometers output only analogue signals. Care must be exercised to perform this conversion correctly. The necessary precautions are discussed in Sec. 8.1.

6.4.1 Digital On-Line Filters

A simple type of discrete-time linear filter consists of a relatively small number of single and multiple input amplifiers and fixed delay units. They can be realized ON-LINE by either analogue or digital systems. Non-recursive digital filters approximate Eq. 6.0.1 by a weighted sum of a finite number of past and present input values.

$$y(n) = \sum_{k=0}^{M} h_k x(n-k) \tag{6.4.1a}$$

They can be analysed elegantly using the z-transform (Gold and Rader, 1969) since the transfer function of the system can be expressed as

$$H(z) = \sum_{k=0}^{M} h_k \, z^{-k} \tag{6.4.1b}$$

where $z = \exp(j2\pi f\Delta t)$ and Δt is the unit time delay. Unfortunately, non-recursive filters are very sensitive to truncation errors and require a

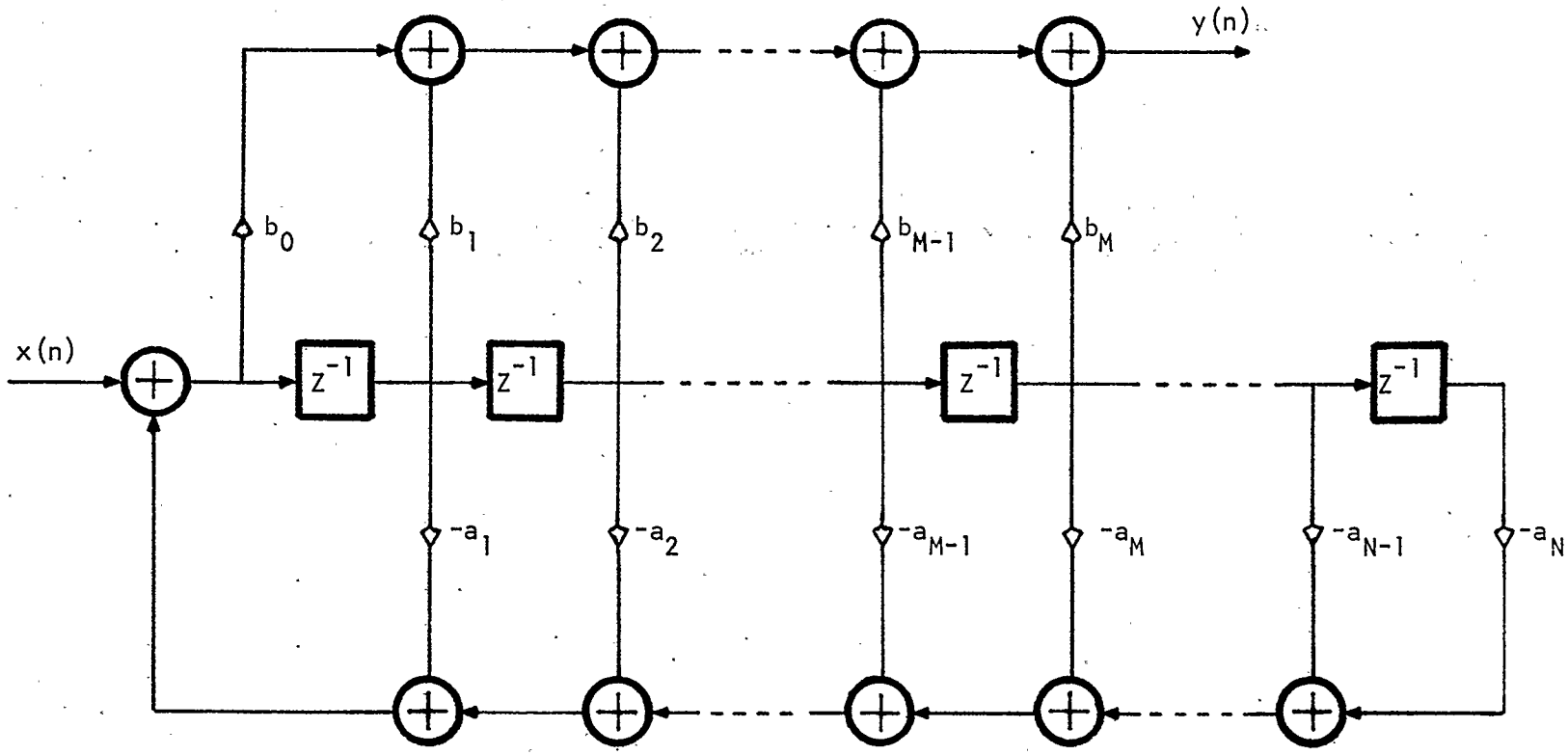

FIGURE 6.2 Block diagram representation of the canonic form for a discrete-time linear filter.

great number of weights (i.e., amplifiers and delay units).

Recursive filters use the feedback principle in summing both input and past output values.

$$y(n) = -\sum_{k=1}^{N} a_k y(n-k) + \sum_{k=0}^{M} b_k x(n-k) \tag{6.4.2a}$$

$$H(z) = \frac{\sum_{k=0}^{M} b_k z^{-k}}{1 + \sum_{k=1}^{N} a_k z^{-k}} \tag{6.4.2b}$$

Figure 6.2 shows the canonic form of a recursive filter. A recursive filter using only the present input value and the preceding output value,

$$y(n) = (1-a)x(n) + ay(n-1), \tag{6.4.3}$$

is the equivalent of an RC low-pass filter provided $a = \exp(-\Delta t/RC)$, $\Delta t \ll RC$ and $f \ll 1/\Delta t$.

6.4.2 Time Averaging

Time averaging is the term used to describe the technique of performing an ensemble averaging over N output signals obtained by succesive fast scans of either the magnetic field or the microwave frequency. Time-averaging separates the signal from noise because of their different autocorrelations properties over multiples of the repetition period T, rather than because of their different frequency locations. The signal adds coherently to give $Ns_i(t)$ while the noise adds as $\sqrt{N}\, n_i(t)$ provided it is uncorrelated over multiples of T. The distinction signal - noise is thus made even if their frequency spectra overlap. Successful use of time averaging requires a good correlation of the scans to prevent resolution

degradation. It is also necessary to use a sufficiently large number of channels to comply with Nyquist's theorem (Eq. 7.2.5) and avoid distortion of the lineshape and loss of resolution.

Bonnet (1965) gave a complete theory of time-averaging procedures. He showed that they can be conveniently cascaded with a low-pass prefiltering realized by the computer by obtaining each sample point for the averaging process through another averaging over M adjacent samples. Ernst (1965), amongst others, has summarized all problems related to magnetic resonance experiments and their optimum timing which may involve passage effects.

Time averaging procedures are advantageous since they, unlike filtering procedures, do not increase the sensitivity (S/N) at the expense of the resolution. Time averaging procedures are not limited to digital techniques. Various analogue storage devices are capable of performing this processing thus eliminating the A/D conversion problems.

6.4.3 Least Square Approximation Techniques

The least square approximation is a curve fitting technique. The goodness-of-fit criterion is implied in the name and it has been discussed in Sec. 6.1. This procedure is based on the selection of a suitable trial function with a sufficiently large number of parameters which are to be optimized in a least square fit.

Two distinct applications can be envisaged in connection with magnetic resonance spectroscopy. Least square smoothing can be used to increase the sensitivity. The trial function g(t) is usually a sum of orthogonal functions $P_k(t)$ whose coefficients are to be optimized

$$g(t) = \sum_{k=0}^{n} a_k \, P_k(t) \; . \qquad (6.4.3)$$

Ernst (1966) has shown that it is equivalent to linear filtering.

The least square approximation can be used to increase the resolution. The trial function is a sum of the linshape functions

$$g(t) = \sum_{k=1}^{n} s(t,a_k,p_k,r_k\ldots) \tag{6.4.4}$$

where the parameters to be optimized in an ideal solution are the lineshape function s(t), the number of lines in the spectrum n, their amplitudes a_k, their positions p_k, their shape peculiarities r_k, etc. Iterative methods for solving systems of such nonlinear equations require extremely large and fast computers. A hundred line spectrum can be "identified" in about 90 years using a medium size second-generation computer. Prior knowledge about the spectrum composition is necessary in order to avoid the time "trap" and the finite probability that the method does not converge. This method of resolving overlapping lines does not affect the sensitivity (S/N) of the measurement, but an excellent (S/N) is necessary if it is to be successful. Ernst and Benz (1970) have shown that the optimum preprocessing is a noise whitening filtering. The least square approximation provides the ultimate precision. Unfortunately, its cost may be prohibitive and the faster and simpler filtering procedures are usually preferred. It is not unusual and, in fact, it is advisable to combine both methods since the filtering procedure can provide initial values for the parameters which are then refined using iterative techniques.

CHAPTER VII

FOURIER ANALYSIS VIA THE FFT ALGORITHM

7.1 The Discrete Finite Fourier Transform (DFT)

The Discrete finite Fourier transform (DFT) is a linear operator relating two sequences of N complex numbers (Cooley *et al*, 1969):

$$X(n) = \mathcal{F}[x(k)] = (1/N) \sum_{k=0}^{N-1} x(k) W_N^{-nk} \qquad (n=0,1,\ldots,N-1) \qquad (7.1.1)$$

where $W_N = \exp(j2\pi/N)$ and

$$\sum_{k=0}^{N-1} W_N^{-nk} W_N^{-mk} = \begin{cases} N & n=m \text{ (modulo N)} \\ 0 & n \neq m \end{cases} \qquad (7.1.2)$$

The inverse DFT is

$$x(k) = \mathcal{F}^{-1}[X(n)] = \sum_{n=0}^{N-1} X(n) W_N^{+nk} \qquad (k=0,1,\ldots,N-1) \qquad (7.1.3)$$

The sequences X(n) and x(k) are periodic with the same period N as W_N^m.

$$X(n) = X(iN+n) \qquad (i=0,\pm1,\pm2,\ldots) \qquad (7.1.4a)$$

$$x(k) = x(iN+k) \qquad (i=0,\pm1,\pm2,\ldots) \qquad (2.1.4b)$$

As a corollary,

$$X^*(\pm n) \longleftrightarrow x^*(\mp k) \qquad (7.1.5)$$

where the double headed arrow indicates a Fourier pair relationship.

The behaviour of the Fourier transform to "time" or "frequency" shifts is an important characteristic.

$$x(i-k) \leftrightarrow W_N^{-in}\, X(n) \tag{7.1.6a}$$

$$W_N^{mk}\, x(k) \longleftrightarrow X(n-m) \tag{7.1.6b}$$

$\delta(k)$, the DFT equivalent of a δ-pulse, is defined by

$$\delta(k) = \begin{cases} 1 & k=0 \text{ (modulo N)} \\ 0 & k \neq 0 \end{cases} \tag{7.1.7}$$

so that

$$\delta(k) \leftrightarrow 1/N \tag{7.1.8a}$$

$$1 \longleftrightarrow \delta(n) \tag{7.1.8b}$$

The DFT of a product of sequences is called a cyclical convolution because it is periodic and not linear like the convolution defined through the "normal" (continuous, infinite) Fourier transform:

$$x_1(k)\; x_2(k) \longleftrightarrow \sum_{m=0}^{N-1} X_1((m))X_2((n-m)) =$$

$$= \sum_{m=0}^{N-1} X_1((n-m))X_2((m)) =$$

$$= X_1((n)) \circledast X_2((n)) \tag{7.1.9a}$$

$$(1/N)\; X_1((k)) \circledast X_2((k)) \longleftrightarrow X_1(n)\; X_2(n) \tag{7.1.9b}$$

where $((n))$ means the index is modulo N.

A corollary of Eqs.7.1.5 and 7.1.9 which is equivalent to Parseval's theorem is

$$(1/N) \sum_{k=0}^{N-1} |x(k)|^2 = \sum_{n=0}^{N-1} |X(n)|^2 \tag{7.1.10}$$

Equations 7.1.6 and 7.1.10 distinguish the Fourier transform amid the entire class of Hadamard transforms (Whelchel and Guinn, 1968).

The transforms of the stretched and sampled sequences,

$$\text{Stretch}_M\{k:x\} = \begin{cases} x(i/M) & i=kM \quad k=0,1,\ldots N-1 \\ 0 & \text{otherwise} \end{cases} \tag{7.1.11a}$$

$$\text{Sample}_M\{k:x\} = x(kM) \qquad k=0,1,\ldots,(N/M-1) \tag{7.1.11b}$$

are

$$\text{Stretch}_M\{k:x\} \longleftrightarrow (1/M)\ X(n) \qquad n=0,1,\ldots NM-1 \tag{7.1.12a}$$

$$x(k) \longleftrightarrow \text{Stretch}_M\{n:x\} \qquad k=0,1,\ldots NM-1 \tag{7.1.12b}$$

and

$$\text{Sample}_M\{k:x\} \longleftrightarrow \sum_{p=0}^{M-1} X(n+pN/M) \tag{7.1.13a}$$

$$(1/M) \sum_{i=0}^{M-1} x(k+iN/M) \longleftrightarrow \text{Sample}_M\{n:X\} \tag{7.1.13b}$$

This concludes a summary of the DFT.

7.2 The Relationship Between the Fourier Transform and the DFT

The relationship between the Fourier transform defined in Eqs.3.1.5 and the DFT defined in Eqs.7.1.1 - 7.1.3 is determined by the fundamental differences between the domains on which the functions and their transforms are defined. This domain is the continuous, infinite group of complex numbers for the Fourier transform and the discrete and finite (N) set of integers for the DFT.

In practice, the collection of physical data is limited to finite time intervals. The finite Fourier transform is defined by

$$X(f,T) = \int_{-T/2}^{+T/2} x(t) \exp(-j2\pi ft)\, dt. \qquad (7.2.1)$$

As $T\to\infty$, the finite Fourier transform $X(f,T)$ approaches the Fourier transform $X(f)$. Care must be taken since

$$X(f,T) = \int_{-\infty}^{+\infty} v(t)\, x(t) \exp(-j2\pi ft)\, dt = V(f) * X(f) \qquad (7.2.2)$$

where the rectangular data window $v(t)$ is unity in the interval $|t| \leq T/2$ and zero otherwise. Rectangular data windows lead to "leakage" through the sidelobes of their Fourier transform. This undesirable phenomenon cannot be always neglected. The usual approach (Bergland, 1969) is to taper the physical data $x(t)$ using a more convenient window. Finite time spectral density functions defined through the finite Fourier transform of sample functions are used to analyse stationary random processes.

$$W_{xy}(f,T) = E[W_{xy}(f,T,k)] = E[(1/T)\ X_k^*(f,T)\cdot Y_k(f,T)] \qquad (7.2.3)$$

The properties of an infinite discrete Fourier transform can be best established using the shah function $\text{///}(t)$. An infinite sequence of equidistant data may be considered as the product of the original continuous data function and the shah function.

$$x(t)\ \text{///}(t) = x(t) \sum_{k=-\infty}^{+\infty} \delta(t-k\Delta t) = \sum_{k=-\infty}^{+\infty} x(k\Delta t)\delta(t-k\Delta t) \qquad (7.2.4)$$

The relationship between the Fourier transform of the sequence $\sum x(k\Delta t)$ and $X(f)$ is given by

$$\sum_{k=-\infty}^{k=+\infty} x(k\Delta t) \longleftrightarrow F_s \sum_{m=-\infty}^{+\infty} X(f-mF_s) \qquad (7.2.5)$$

where $F_s = 1/\Delta t$ is the sampling frequency. Eq.7.2.5 is referred to as the sampling-in-time-domain theorem. It immediately leads to the famous Nyquist theorem which states that a continuous function $x(t)$ is determined uniquely by the sequence $\sum x(k\Delta t)$ provided its Fourier transform is nonzero only on the region $|f| \leq F_s/2$. A similar sampling theorem exists in the frequency domain

$$\sum_{n=-\infty}^{+\infty} X(n\Delta f) \longleftrightarrow T \sum_{i=-\infty}^{+\infty} x(t-iT) \qquad (7.2.6)$$

where $T=1/\Delta f$ is the repetition time interval.

The finite discrete Fourier transform can be defined by combining Eqs.7.2.5 and 7.2.6 and taking only the principal terms.

$$X(n\Delta f) = \sum_{k=0}^{N-1} \Delta t\ x(k\Delta t)\ \exp(-j2\pi kn/N) \longleftrightarrow \sum_{n=0}^{N-1} \Delta f\ X(n\Delta f)\ \exp(j2\pi kn/N) = \qquad (7.2.7)$$

$$= x(k\Delta t)$$

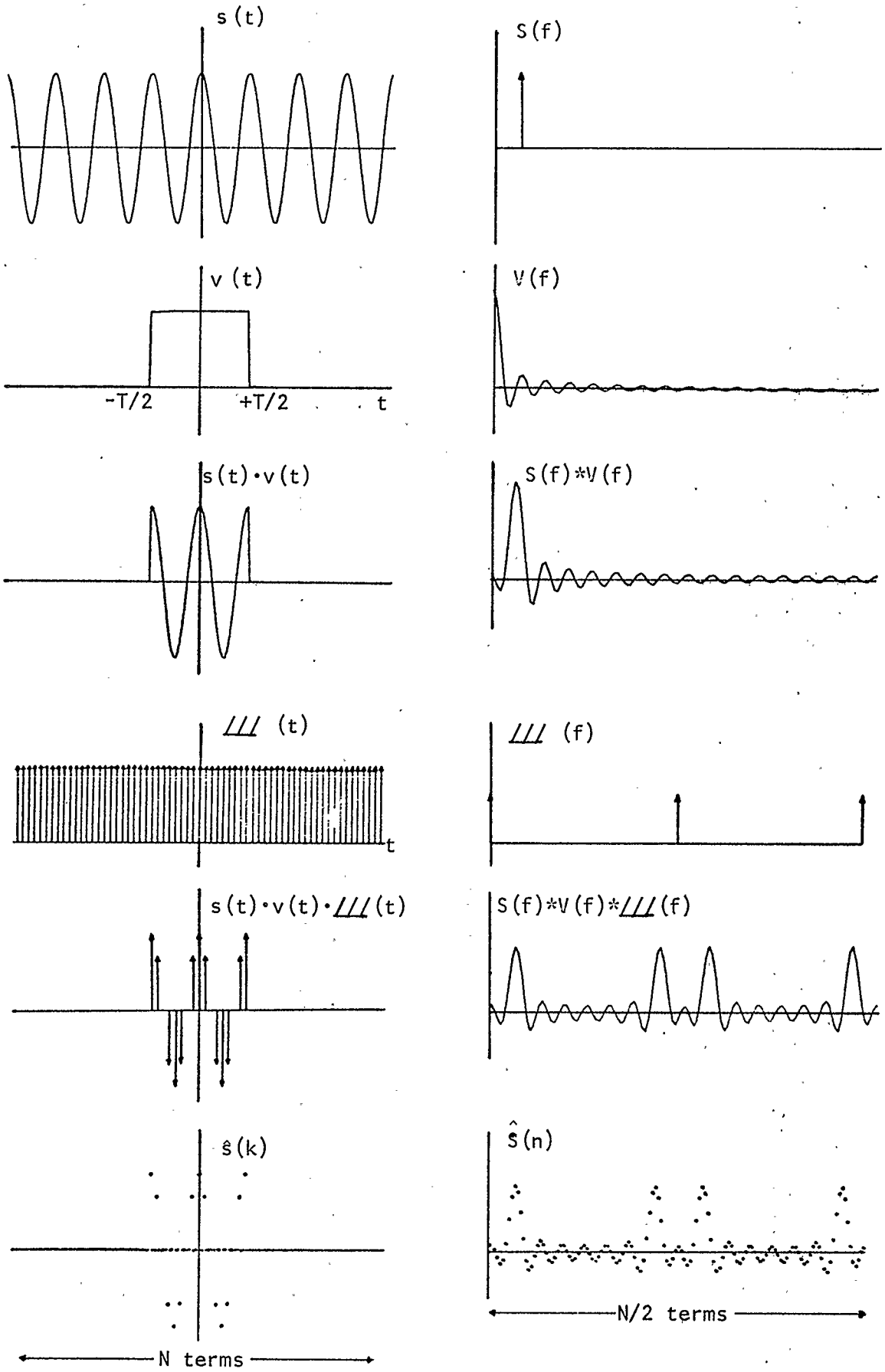

FIGURE 7.1 Diagrams illustrating the relationship between the discrete Fourier transform and the continuous infinite Fourier transform. For simplicity, the Fourier transforms are presented only for $f \geq 0$, because $X(-f) = X(f)$ for the functions illustrated.

where $T=N\Delta t$ and $F_s=N\Delta f$. These relations are similar to the definition of DFT by Eqs.7.1.1 - 7.1.3 except that a factor 1/T is missing in the expression for X(n). This difference is unimportant mathematically but it is important physically since it changes the dimensionality.

An illustration of the problems involved in this relationship is given in Fig.7.1.

7.3 Estimates via DFT

7.3.1 Spectral Density Functions Estimates

The theory presented previously shows that

$$\tilde{W}_{xx}(n\Delta f) = T|X(n)|^2 \tag{7.3.1}$$

an estimate of the power spectral density of a stationary ergodic random process.

If the process is Gaussian, then the normalized standard error of this estimate (Bendat and Piersol, 1971) is

$$\varepsilon_r = \frac{\sigma[\tilde{W}_{xx}(f)]}{W_{xx}(f)} = \sqrt{2/m} \tag{7.3.2}$$

where m represents the degrees of freedom of the estimate. For the simple estimate of Eq.7.3.1 m=2 and $\varepsilon_r=1$ which is unacceptable. This can be corrected by performing the average operation involved in the definition of a spectral density function. Frequency smoothing can be achieved by averaging p neighbour points.

$$\hat{W}_{xx}(n\Delta f) = (1/p)\sum_{i=0}^{p-1} \tilde{W}_{xx}((n+i)\Delta f) \tag{7.3.3}$$

so that m=2p. Ensemble averaging takes the mean value of the estimate of q separate sample sequences.

$$\hat{W}_{xx}(n\Delta f) = (1/q) \sum_{i=0}^{q-1} \tilde{W}_{xx,i}(n\Delta f) \tag{7.3.4}$$

so that m=2q. If both averages are performed, then

$$m=2pq \qquad \text{and } \varepsilon_r=\sqrt{1/pq} \tag{7.3.5}$$

which results in an appreciable improvement in the estimate of a spectral density function. This theory also applies for cross-spectral density functions.

The problem of reducing the leakage due to the finite nature of the transform still remains. As mentioned above, a possible solution is to use a suitable nonrectangular data window. The Origin Hanning (HØ) data window is commonly used but other data windows (Parzen, Tukey, cosine-bell, etc.) have been also proposed (Bergland, 1969; Bendat and Piersol, 1971). The HØ data window is

$$D_{H\emptyset}(K\Delta t) = \begin{cases} [1 + \cos(\pi k/N)]/2 & k=0,1,\ldots,N \\ 0 & k>N \end{cases} \tag{7.3.6}$$

This data window is equivalent to frequency smoothing since

$$\overline{W}_{xx}(n\Delta f) = 0.25\,\hat{W}_{xx}((n-1)\Delta f) + 0.5\,\hat{W}_{xx}(n\Delta f) + 0.25\,\hat{W}_{xx}((n+1)\Delta f) \tag{7.3.7}$$

7.3.2 Linear System Identification

Spectral density functions estimated via the DFT can be used with Eqs.3.3.11 and 3.3.12 to identify linear systems.

$$\hat{H}(n\Delta f) = \hat{W}_{xy}(n\Delta f) / \hat{W}_{xx}(n\Delta f) \tag{7.3.8}$$

$$\gamma^2_{xy}(n\Delta f) = |\hat{W}_{xy}(n\Delta f)|^2 / \left[\hat{W}_{xx}(n\Delta f)\hat{W}_{yy}(n\Delta f)\right] \tag{7.3.9}$$

Smoothed estimates of the spectral density functions should be used. It can be shown that the random error in the frequency response function estimates tends to zero as both $m \to \infty$ and $\gamma^2_{xy}(f) \to 1$.

7.3.3 Linear System Simulation (Filtering)

As shown in Sec.3.3 a linear time invariant system is represented by a convolution integral operator in the time domain. In the frequency domain, the operation is equivalent to the multiplication of the input by the frequency response function of the system.

$$y(t) = h(t) * x(t) \tag{7.3.10a}$$

$$Y(f) = H(f) \cdot X(f) \tag{7.3.10b}$$

The simplicity of the input-output relationship in the frequency domain is a strong argument for using the DFT representation to simulate a linear system. This is particularly advantageous when even a crude physical approximation of an optimum filter is not available.

A discrete simulation like

$$Y(n) = H(n) \cdot X(n) \tag{7.3.11}$$

is easily synthesized on a digital computer but care must be taken because of the special nature of the DFT and the periodical character of the cyclical convolution. This frequency-sampling realization of

the filter H(f) is equivalent to a finite impulse response filter of duration N samples which is a combination of a cascade of a comb filter and a parallel bank of N complex pole resonators. A more detailed analysis of this filter simulation is presented in Chapter IX.

7.4 The Fast Fourier Transform (FFT) Algorithm

The classical algorithm for the DFT requires approximately N^2 real multiply-add operations making it prohibitive to implement on a large scale. The development of the FFT algorithm (Cooley and Tukey, 1965) has made extensive use of the DFT techniques possible. The many variations of FFT algorithms stress either the economy of time or memory (Rabiner et al, 1972). They are all based on the principle of performing Fourier transforms whose dimensions are the composite factors of N.

If $N = \prod_{i=1}^{P} r_i$ then only $4N \sum_{i=1}^{p} r_i$ operations are required.

It is advisable to choose $N=2^p$ for binary digital computers so that a direct implementation of the FFT is immediately possible. The processing time is decreased by a factor N/8p. The same procedure applies for the inverse transform. The computation time of the FFT of two real-valued records can be shortened by a factor of two if they are considered as the real and imaginary parts of a complex record.

$$z(k) = x(k) + jy(k) \tag{7.4.1a}$$

$$X(n) = [Z(n) + Z^*(N-n)]/2 \tag{7.4.1b}$$

$$Y(n) = -j[Z(n) - Z^*(N-n)]/2 \tag{7.4.1c}$$

Computation errors associated with the FFT algorithm have been studied by Welch (1969), Weinstein (1969) and Welchel and Guinn (1970) amongst others. The finite length of the words in a digital computer is the general source of these errors. Various systems are used to represent the numbers in a digital computer. In fixed point representations, the position of the decimal (or binary) point is assumed fixed. In floating point representation the number is formed by two fixed point numbers, the mantissa and the exponent, while the exponential base is a constant of the representation. The block floating point representation is a mixture of the previous two representations in the sense that only one exponent is associated with all the numbers in the array. Roundoff error or truncation error is caused by rounding or truncating the products or sums formed within the digital computer. In many cases these errors are well modeled as random processes. Overflows are very rude errors caused by the impossibility of the computer to represent a computational result which is too large for the arithmetic (representation) used. This is a more stringent problem when fixed point arithmetic is used, as is the case with the majority of hardware implementations of the FFT algorithm.

Welch (1969) has analysed the fixed point accuracy of the power of two FFT algorithm. For $N=2^p$ there are p stages of computations involving one or two arrays of N numbers. There are three ways of keeping these arrays properly scaled so that no overflow can occur. An automatic scaling (right shifting one bit) at each iteration is the simplest but the least accurate method. The most accurate method tests each operation for overflow and consequently scales the entire array prior to

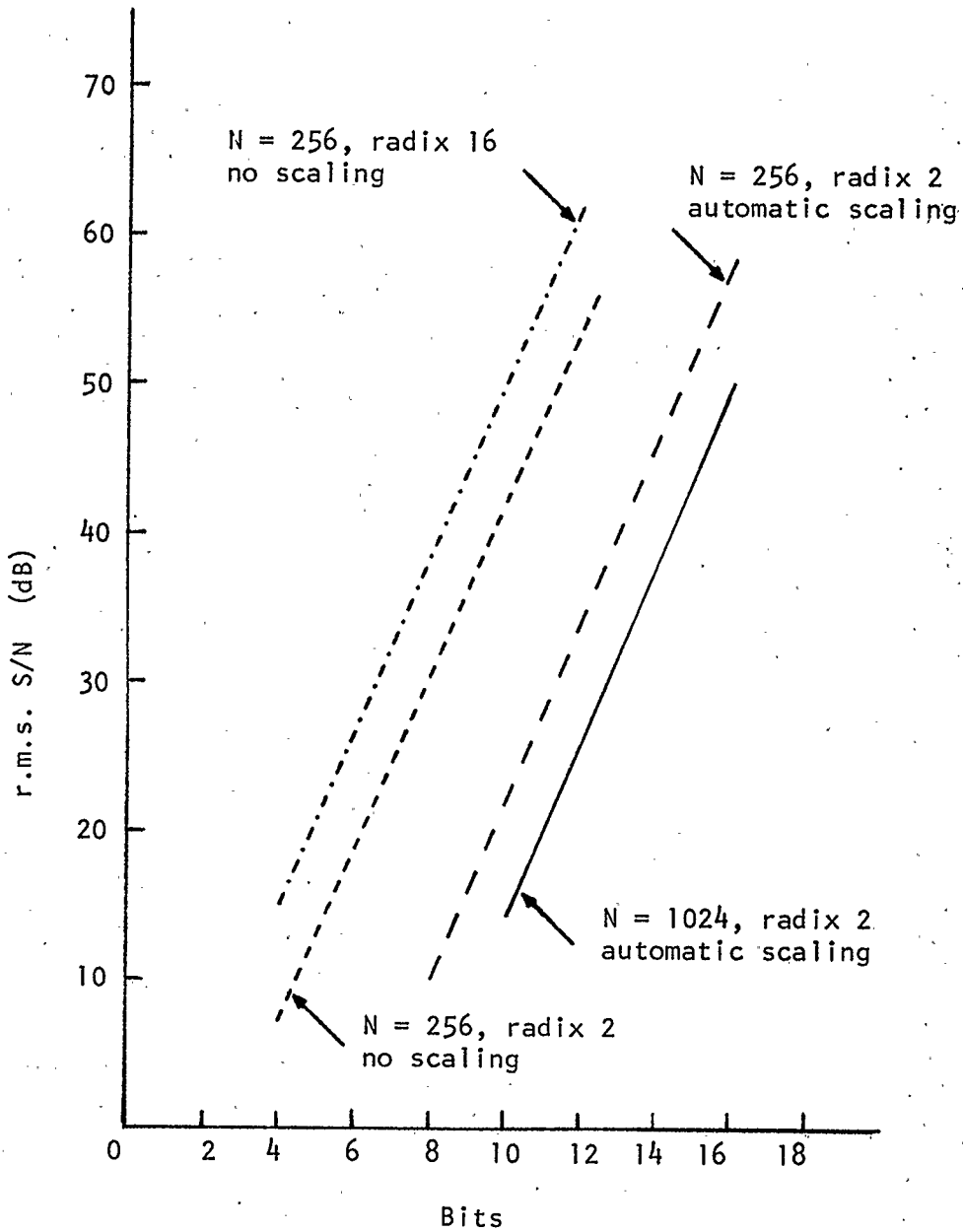

FIGURE 7.2. Figure illustrating the dependence of fixed-point FFT computation errors on the number of bits, length of sequence N, radix and scaling used in implementing the FFT algorithm (Welchel and Guinn, 1970).

each overflow occurence. This leads to an appreciable speed reduction. An intermediate method controls the array at every stage and scales it only when an overflow might occur. Welch has shown that an upper bound for the ratio of the r.m.s. of the error to the r.m.s. of the answer increases as $\sqrt{N}$ when the FFT algorithm is implemented in fixed point arithmetic. The lower bound of this ratio increases as $\log_2 N$, which is the rate of increase when floating point arithmetic is used (Weinstein, 1969). Weinstein has found experimentally that for non-random rounding of "half-way" numbers the error has a greater than linear increase with $\log_2 N$, while for truncation the increase rate is close to $(\log_2 N)^2$ rather than to $\log_2 N$. Welchel and Guinn (1970) have analyzed the error propagation for high-radix (4 and 16) FFT algorithms, showing that such high-radix transforms may be advantageous due to the smaller number of multiplications. Figure 7.2 summarizes some of their results.

CHAPTER VIII

NOISE MEASUREMENTS IN EPR SYSTEMS

The principles of optimum EPR spectrometer design were reviewed in Chapter V, where the propagation of noise in an EPR spectrometer was analysed theoretically. This chapter gives the experimental evidence to substantiate this theory. A digital method of measuring the noise power spectral density, which was first described by Haslett et al. (1971) is employed. This method was discussed theoretically in Chapters IV and VII. This thesis gives the first data which compares directly the limiting effect on an EPR spectrometer sensitivity of the microwave oscillator and microwave diode detector noise in the low frequency region as a function of various parameters. The influence of the oscillator noise is studied for the both absorption and dispersion phases.

It is fortuitous that contemporary instrumentation for a.m. and f.m. microwave oscillator noise measurements (Ondria, 1967; Ashley et al., 1968) is identical with a reflection cavity, synchrodyne, EPR spectrometer using a balanced microwave detector. The measurements described in this chapter were performed to obtain a realistic assessment of microwave oscillator and diode detector noise influence in EPR spectrometers (Buckmaster and Cohn-Sfetcu, 1972-1). Nevertheless, it was possible to draw conclusions regarding specific methods of microwave device noise measurements because the microwave instrumentation is identical. A new, faster method of determining the in situ figure of merit of a microwave detector is described in Sec. 8.6.1. Section 8.6.2 analyses the recent literature concerning microwave oscillator noise measurements. It is concluded that the complexity involved in such measurements is not fully appreciated.

8.1 Instrumentation Employed

Care must be taken to correctly digitize the data since a digital method is employed to measure the noise power spectral density. Sampling and quantization are the two separate and distinct operations involved in an analogue-to-digital (A/D) conversion.

Sampling, which is the process of defining the times at which the data are to be observed has been discussed in Sec. 7.2. Equation 7.2.5 requires that the folding frequency satisfies

$$f_f = F_s/2 = 1/(2\Delta t) \geq F_{max.data} \tag{8.1.1}$$

where Δt is the sampling interval. This condition can be satisfied by choosing Δt sufficiently small. The limit to Δt is set by technical problems in the design of A/D converters. A filter should be used before the sampling device to eliminate data components at frequencies above the Nyquist limit. An antialiasing filter consisting of a 8-pole Butterworth low-pass filter (Rockland 1042F-01) with a cut-off frequency of about $0.9f_F$ has been employed in processing the data reported in this thesis.

Quantization is the conversion of data values into digital form. The quantization error (noise) in an ideal conversion with a uniform probability distribution has an r.m.s. amplitude of $\sim 0.29\Delta x$, where Δx is the quantizing increment (Bendat and Piersol, 1971). This noise is negligible when an A/D converter with a sufficient number of bits is used at full dynamic range. For example, the signal-to-noise ratio would be $\sim$67dB for a 10 bit A/D. Other error sources in an A/D conversion are jitter, inherent nonlinearities and finite quantization time.

The A/D conversion in the system used was performed by the 10 bit

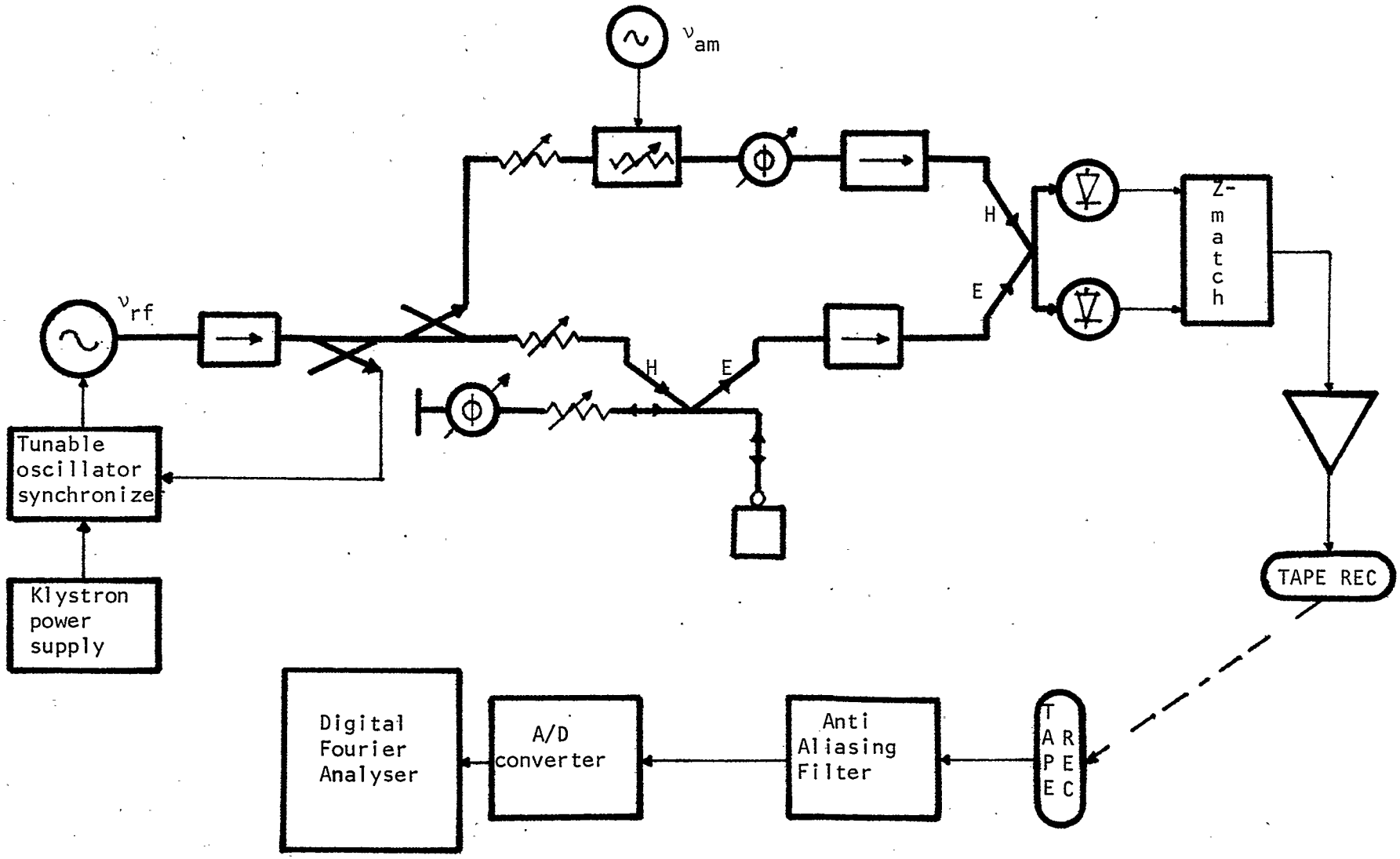

FIGURE 8.1 Block diagram of the 9GHz EPR spectrometer and the associated noise power spectrum density measurement configuration.

A/D converter incorporated in the digital Fourier analyser (HP5450A).

Figure 8.1 is a block diagram of the instrumentation used for most of the measurements described in this chapter. The microwave system is a 9GHz synchrodyne EPR microwave configuration described by Buckmaster and Dering (1965). A transformer provides the impedance match between the microwave detector and the preamplifier (PAR-CR4). The detector is balanced by separate stub tuners and microwave attenuators. An amplitude modulator is incorporated in the reference channel connected to the H-arm of the balanced detector to simplify the method of obtaining an a.c. detector balance. The importance of this balance has been ignored by most experimentalists although it was emphasized by Buckmaster and Dering (1967). The a.c. balance should be obtained at the EPR spectrometer intermediate frequency. A tape recorder was required since the EPR spectrometer and the Fourier analyzer were located in separate buildings.

Unless otherwise stated, the number of samples in a record, N, was 256, while the number of ensemble averages, q, was 100. The spectrum analysed was limited to 0.1 - 20kHz by the bandwidth of the impedance-matching transformer. Origin Hanning frequency smoothing was used. The computing procedure calculates Eqs. 7.1.1 and 7.3.1 q times and then uses the result to calculate Eqs. 7.3.4 and 7.3.7.

8.2 Measurements of Diode Noise Effects in EPR Spectrometers

The power spectral density of the noise in an EPR spectrometer relative to the input of the preamplifier has been measured under various conditions. Initially, the system noise was measured with zero microwave power incident on the detector diodes. This noise will be referred to as post-detector system noise in the following discussion and is the back-

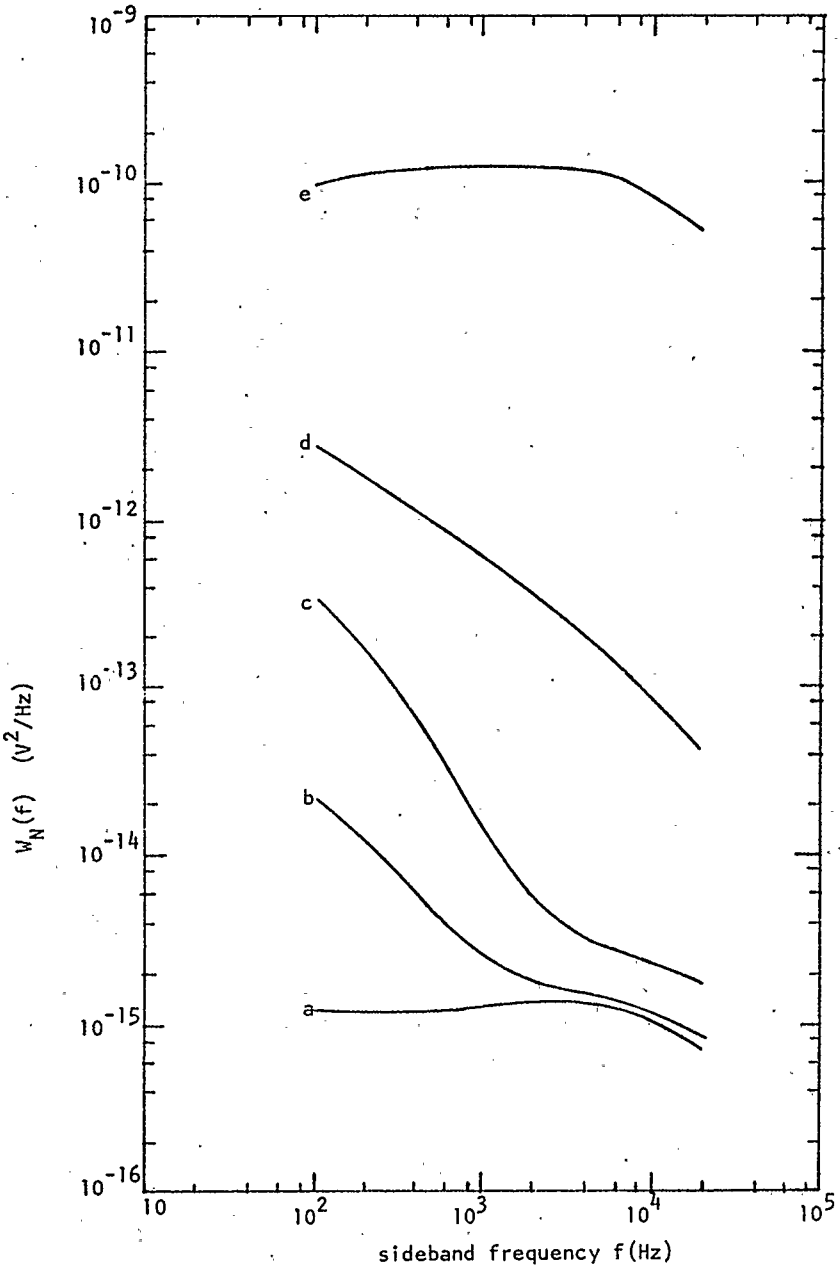

FIGURE 8.2 Graphs showing the smoothed power spectral density functions of the noise in a reflection cavity EPR spectrometer when (a) no microwave power is incident on a balanced mixer using backward diodes; (b) optimum microwave local oscillators unmodulated or a.m. noise modulated is incident on this mixer; (c) same as (b) but for unbalanced mixer (unmodulated); (d) same as (b) but using silicon point-contact diodes, (unmodulated); (e) same as (c) for a.m. noise modulated local oscillator power.

ground noise to which the microwave oscillator and diode noise are added. The background noise should be lower than that produced by the microwave noise sources if a good post-detector system is used. Curve (a) of Fig. 8.2 is the power spectral density of the background noise in the instrumentation described in Sec. 8.1.

The noise spectra for backward diodes (Philco L4154) and silicon point-contact diodes (1N23WE) are given in Fig. 8.2b and Fig. 8.2d respectively. It was necessary to use different impedance matching transformers for each type of diode. The (1/f) character of the noise due to these diodes when microwave power was incident on the reference arm of the mixer is easily verified. The "knee" for backward diodes is O(1kHz) when the incident microwave power is ∿0.2mW. The "knee" frequency for silicon point-contact diodes is above the upper frequency limit of the measurements reported in this thesis.

8.3 Measurements of Microwave Oscillator Noise Effects in EPR Spectrometers.

8.3.1 Local Oscillator Effects

The effect of local oscillator noise has been discussed in Sec. 5.2.5. It was shown that its effect can be minimized by employing a balanced microwave mixer detector. Experimental data has been obtained to substantiate this statement. Curves (b), (c) and (d) in Fig. 8.2 compare the power spectral density of the noise using balanced and unbalanced mixers. Local oscillator noise is dominant when backward diodes are employed with an unbalanced mixer. A balanced mixer is not essential when using silicon point-contact diodes and the sideband frequency is lower than the "knee" frequency since the diode (1/f) noise exceeds that of the local oscillator.

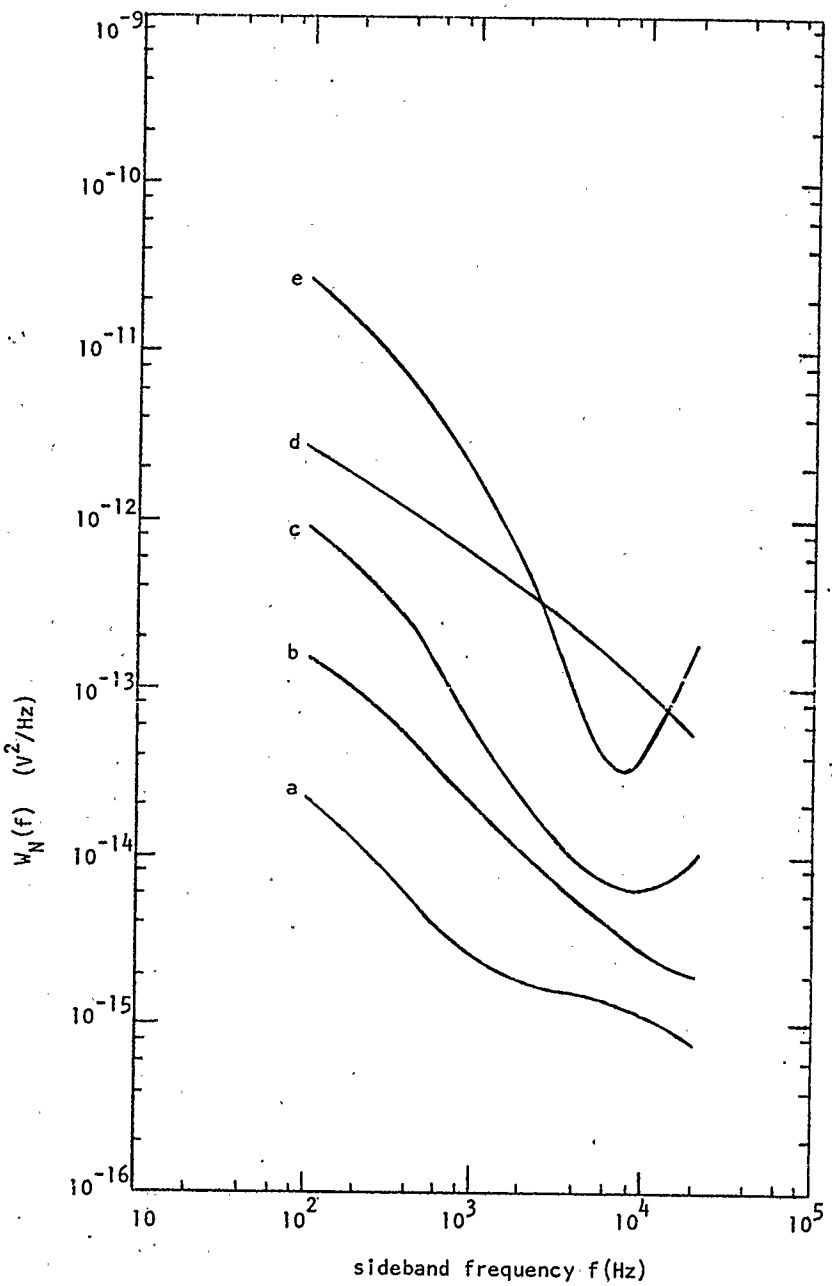

FIGURE 8.3 Graphs showing the smoothed power spectral density functions of the noise in a reflection cavity EPR spectrometer for the absorption phase when (a) only optimum microwave local oscillator power is incident on a balanced mixer using backward diodes, (b) 50mW power incident on sample cavity with Q = 2000; (c) same as (b) but Q = 5000; (d) same as (b) but for silicon point-contact diodes; (e) same as (b) but Q = 9300.

The response of balanced and unbalanced mixer detectors to pseudo-white noise amplitude modulation of the reference microwave power has been measured to test experimentally Wilmshurst's assertion (1968). Figure 8.2e indicates that this artificially introduced noise is the dominant noise component when an unbalanced mixer is used although the modulation depth was only about -50dB. The effect of this artificial noise could not be detected when a balanced mixer detector was used which clearly demonstrates the advantage of a balanced detector.

8.3.2 Signal Oscillator Noise Effects

The analysis of the signal oscillator noise propagation in an EPR spectrometer was presented in Sec. 5.2.1. The objective of a first series of measurements was to verify experimentally the validity of Eqs. 5.2.3. The most important conclusions of Strandberg's theoretical analysis were that the overall noise increases at higher frequencies as f^2 and the oscillator noise is magnified by Q^2.

Figure 8.3 shows the noise power spectral density function of the EPR system noise for the absorption phase. A pair of backward diodes and three cavities with different Q factors were used to obtain curves (b), (c) and (e). Curve (d) gives this function when silicon point contact diodes and a cavity with Q=2000 are used. The power incident on the microwave bridge was 50mW. The contribution of oscillator noise is not significant below 20kHz when silicon point-contact diodes are used. This noise is the dominant component with backward diodes. The f^2 shape and the influence of the cavity Q are noticeable. The lowest Q cavity is typical of that used in EPR spectrometers designed in this laboratory. A number of discrete peaks due to harmonics of the power line frequency were observed in the low frequency portion of the noise spectra.

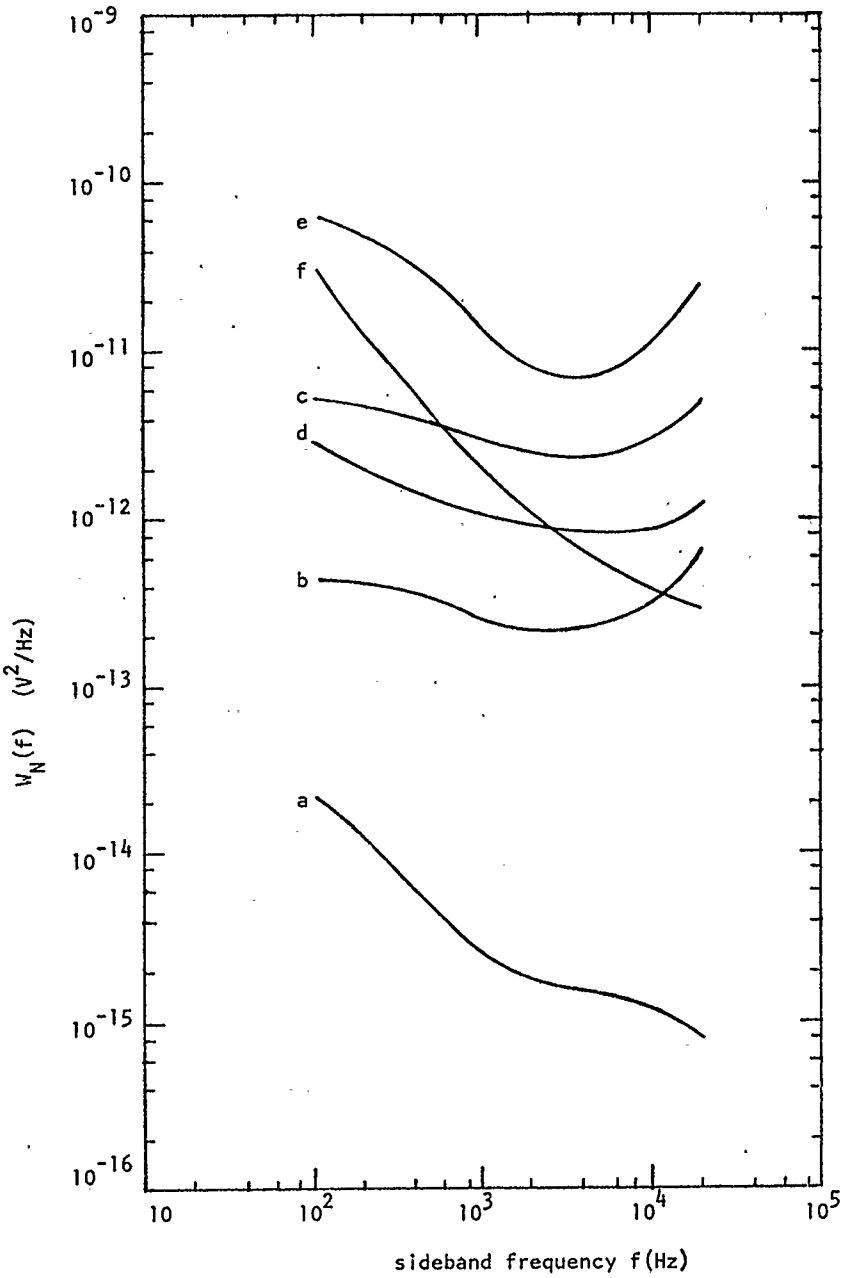

FIGURE 8.4 Graphs showing the smoothed power spectral density function of the noise in a reflection cavity EPR spectrometer for the dispersion phase when (a) only optimum microwave local oscillator power is incident on a balanced mixer using backward diodes; (b) 50mW power incident on sample cavity with Q = 2000; (c) same as (b) but Q = 5000; (d) same as (b) but for silicon point-contact diodes; (e) same as (b) but Q = 9300; (f) same as (b) but with microwave oscillator synchronizer feedback loop open.

The noise power spectral density functions measured for dispersion phase using the same microwave configurations are presented in Fig. 8.4. In addition, curve (f) presents the noise power spectral density obtained with the microwave oscillator synchronizer loop open under the same conditions as for curve (b). The effect of using this type of synchronizer (Microwave System MOS-1/f) is most pronounced below ∿2kHz. It has no effect above this frequency since its internal 3dB bandwidth is ∿1kHz. A comparison of the theoretical predictions (Eqs. 5.2.3) with these experimental measurements shows that Kurokawa's conclusions (1968) concerning the noise of phase locked injection-current oscillators also apply to klystron oscillators. He showed that phase locking a microwave oscillator to a MHz crystal oscillator enhances the frequency stability and reduces f.m. noise but increases the a.m. noise.

The measurements made do not confirm the general assumption of pseudo-white a.m. sideband noise near the carrier. On the contrary, the noise increases with decreasing frequency from 10^1 - 10^3 Hz. This may explain the decrease in S/N with increasing power observed in superheterodyne EPR spectrometers using magnetic field modulation frequency in this range (Buckmaster and Gray, 1971).

8.4 Spurious Mechanical and Electrical Oscillations and Transients

Measurements of noise in an EPR spectrometer also permit the detection of spurious mechanical and electrical oscillations. A mechanical resonance was detected at 3.125kHz during the measurements reported in Sec. 8.3. It appeared in the long waveguide connecting the cavity to the magic-T and was easily suppressed after it was located.

Transients are more difficult to detect because they occur randomly. However, they are less troublesome than other noise sources and do not

play a significant role in limiting the sensitivity unless their frequency of occurrence is very high.

8.5 The Optimum Design of EPR Spectrometers

Conclusions regarding the optimum design for EPR spectrometers have been discussed in Chapter V and summarized by Buckmaster and Cohn-Sfetcu (1972-II).

A digital Fourier analyser enables fast, accurate and reliable absolute noise measurements to be performed from 0 - 10^5 Hz. This is the frequency range of importance in the design of EPR spectrometers. The method reported in this chapter permits the *in situ* evaluation of the noise in EPR spectrometers enabling the microwave configuration and operating parameters such as the microwave reference power, magnetic field modulation frequency, cavity Q factor, etc. to be optimized.

Conversely, the sensitivity of various EPR systems can be assessed objectively and absolutely independent of such variables as filling factor, sample, magnetic field modulation amplitude, type and cut-off frequency of the output filter which are under the control of the experimentalist.

8.6 Analysis of Microwave Device Noise Measurement Methods

8.6.1 A New Method of Determining the Quality of a Microwave Diode Detector

Buckmaster and Dering (1965) demonstrated that EPR spectrometer sensitivity measurements could be used to determine the figure-of-merit of microwave silicon point-contact diodes and that such measurements were in good agreement with direct determinations of the power conversion gain and noise factor of these diodes. These studies were extended by Buckmaster and Rathie (1971) to include backward

diodes and Schottky barrier diodes.

The figure of merit (t/G) is the parameter most commonly used to characterize the performance of a microwave detector diode. The noise temperature ratio, t, is the ratio of the excess diode noise power to the thermal noise power in the same bandwidth. The frequency dependence of t is given by

$$t = 1 + A_L P_{rf}/f \tag{8.6.1}$$

where P_{rf} is the incident microwave power and A_L is a constant if the diode is operated in the linear region. The power conversion gain

$$G = P_{if}/(m^2 P_{rf}) \tag{8.6.2}$$

is a measure of the efficiency with which the diode transforms the microwave signal power P_{rf} into power at the sideband (intermediate) frequency P_{if} and m is the voltage modulation index at the sideband frequency.

The figure of merit (t/G) is an important parameter in the noise factor F which measures the overall noise performance of microwave systems (Van der Ziel, 1954).

$$F = (Gs + t + F_{amp} - 1)/G \tag{8.6.3}$$

where s is the excess noise temperature ratio of the microwave oscillator and F_{amp} is the noise factor of the intermediate frequency amplifier.

It is conventional to measure t and G in separate test apparata. The conventional method of measuring t uses a calibrated reference microwave noise source. The disadvantage of this procedure is that the system noise factor is not optimized directly as an <u>in situ</u> part of the instrumentation system employing the microwave diode. The accepted measurement

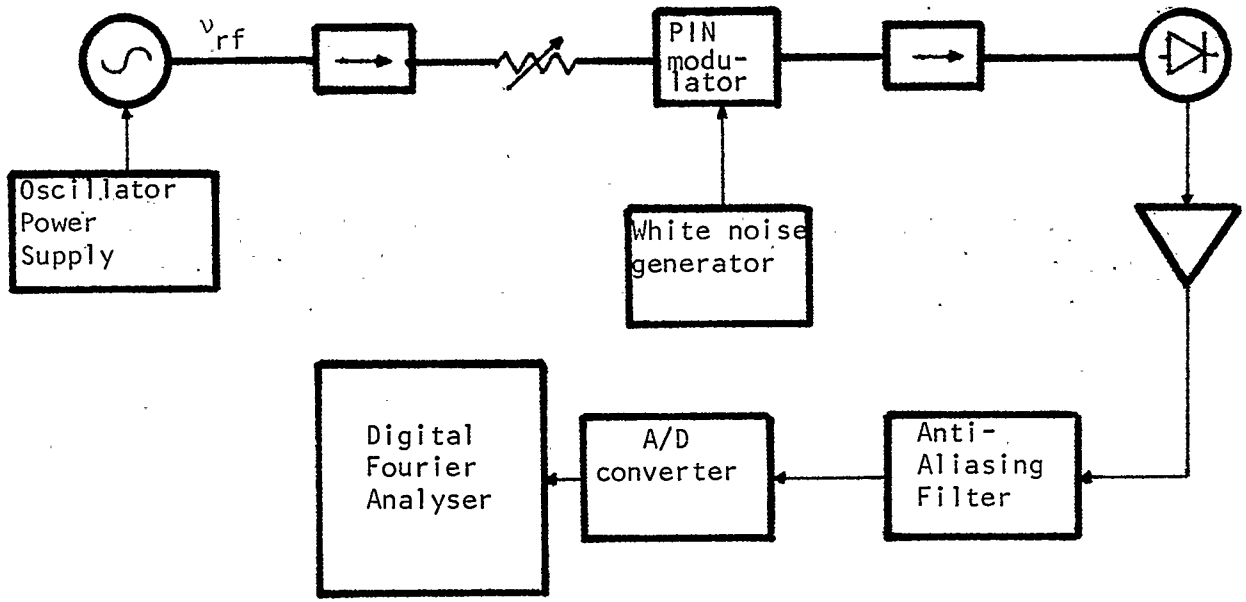

FIGURE 8.5 Block diagram of the basic configuration for microwave detector performance measurement.

procedures are tedious since they are usually of the point-by-point type. Typically, the spot frequency determination made does not cover completely the frequency range of interest.

The digital Fourier analyser as a computer of power- and cross-spectral density functions for random processes is an extremely valuable tool for the rapid determination of the figure of merit over the low frequency region of sideband frequencies. This region extends from d.c. to the maximum frequency permitted by the A/D converter used.

The in situ determination of the figure-of-merit of microwave diode detectors is made possible by inserting a PIN diode a.m. modulator driven by a white noise generator before the detector. Figure 8.5 is a block diagram of the simplest measurement system. The PIN diode modulator is preferable since its modulation index is essentially frequency independent. It is recommended that the microwave ports of the modulator be buffered with isolators to minimize extraneous interactions with the remainder of the system due to the imperfect match of the modulator.

The noise temperature ratio $t(f,P_{rf})$ is

$$t(f,P_{rf}) = W_n(f,P_{rf})/W_n(f,0) \tag{8.6.4}$$

where $W_n(f,P_{rf})$ is the noise power spectral density of the detector at the sideband frequency f when a microwave power R_{rf} is incident on the detector. The power conversion gain $G(f,P_{rf})$ is

$$G(f,P_{rf}) = \frac{W_n^{am}(f,P_{rf},m)}{P_{rf}m^2/R_o} \tag{8.6.5}$$

where R_o is the input impedance of the microwave detector and $W_n^{am}(f,P_{rf},m)$

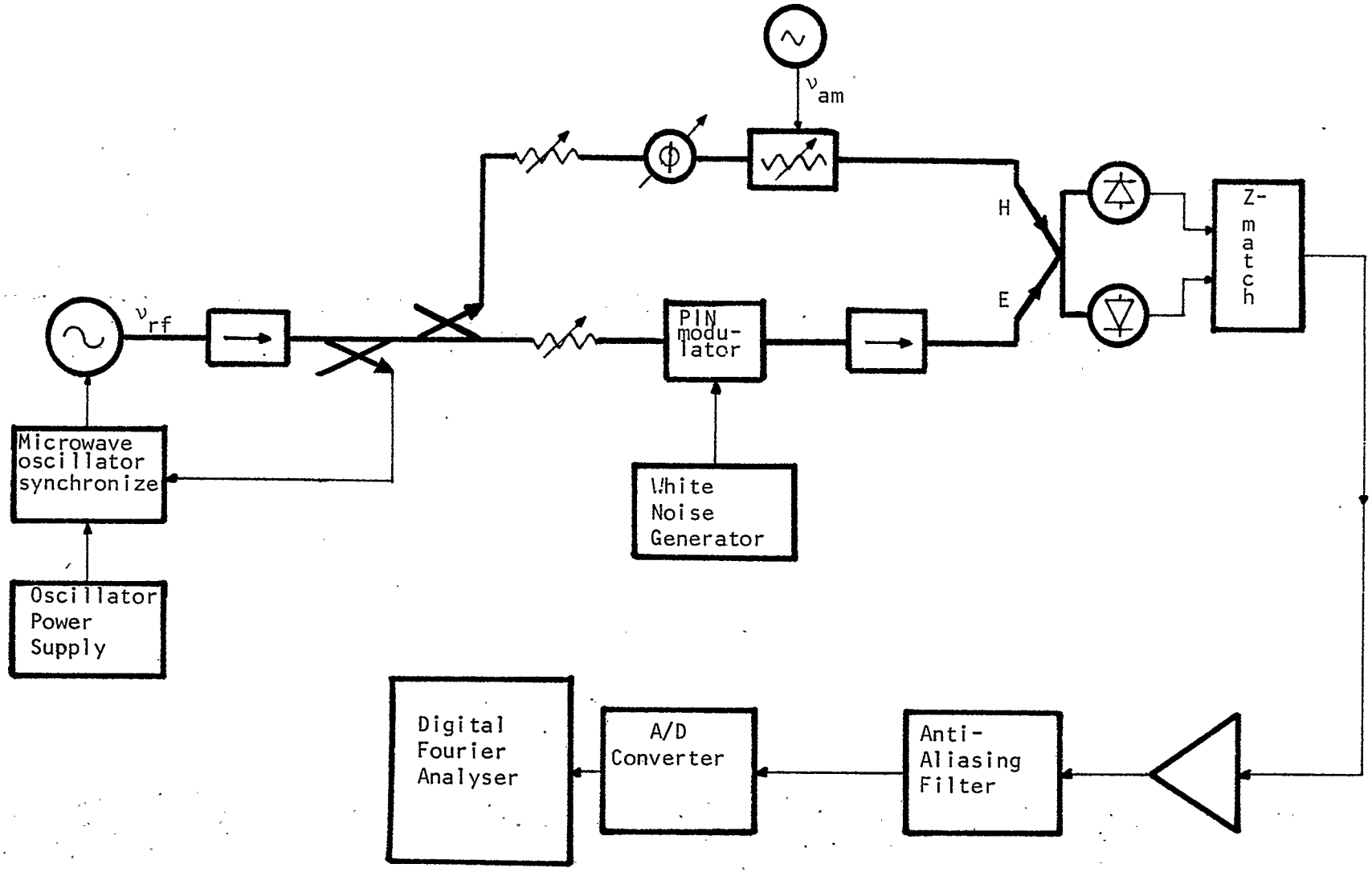

FIGURE 8.6 Block diagram of the instrumentation for measuring the performance of balanced microwave mixer detectors.

is the system noise power spectral density when the a.m. modulator is driven by the white noise generator. The microwave power can be measured by conventional means. R_o is the characteristic impedance of the waveguide if the detector is matched. The figure-of-merit is computed from these two in situ measurements.

It was shown in Sec. 4.5 that it is preferable to use the microwave diode as a mixer. The local oscillator or reference wave has a constant amplitude sufficient to drive the mixer diode into its linear region. The microwave power arriving at the mixer via the signal arm, P_{rf}^{so}, is small and variable compared to the local oscillator power. In EPR, it depends on the strength of the magnetic resonance phenomenon and on the microwave sample cavity balance. The local oscillator power, P_{rf}^{lo}, should be adjusted independently to optimize the performance of the mixer.

The optimum performance of a microwave diode mixer can be determined by measuring (t/G) over the frequency range of interest for different local oscillator power levels while the signal oscillator power is maintained at a constant low level.

Care must be taken to account for the effect of a.m. microwave oscillator noise particularly when the noise performance of backward or Schottky barrier diodes is studied since oscillator noise can exceed the diode noise due to these diodes. The measurements of (t/G) for microwave diodes in unbalanced mixer detectors should be viewed with suspicion unless it is demonstrated that the oscillator noise is negligible. Local oscillator noise can be minimized by using a balanced mixer. The composite figure-of-merit of the two diodes in the mixer is then measured, but it is this composite parameter which appears in the system noise factor and must be optimized.

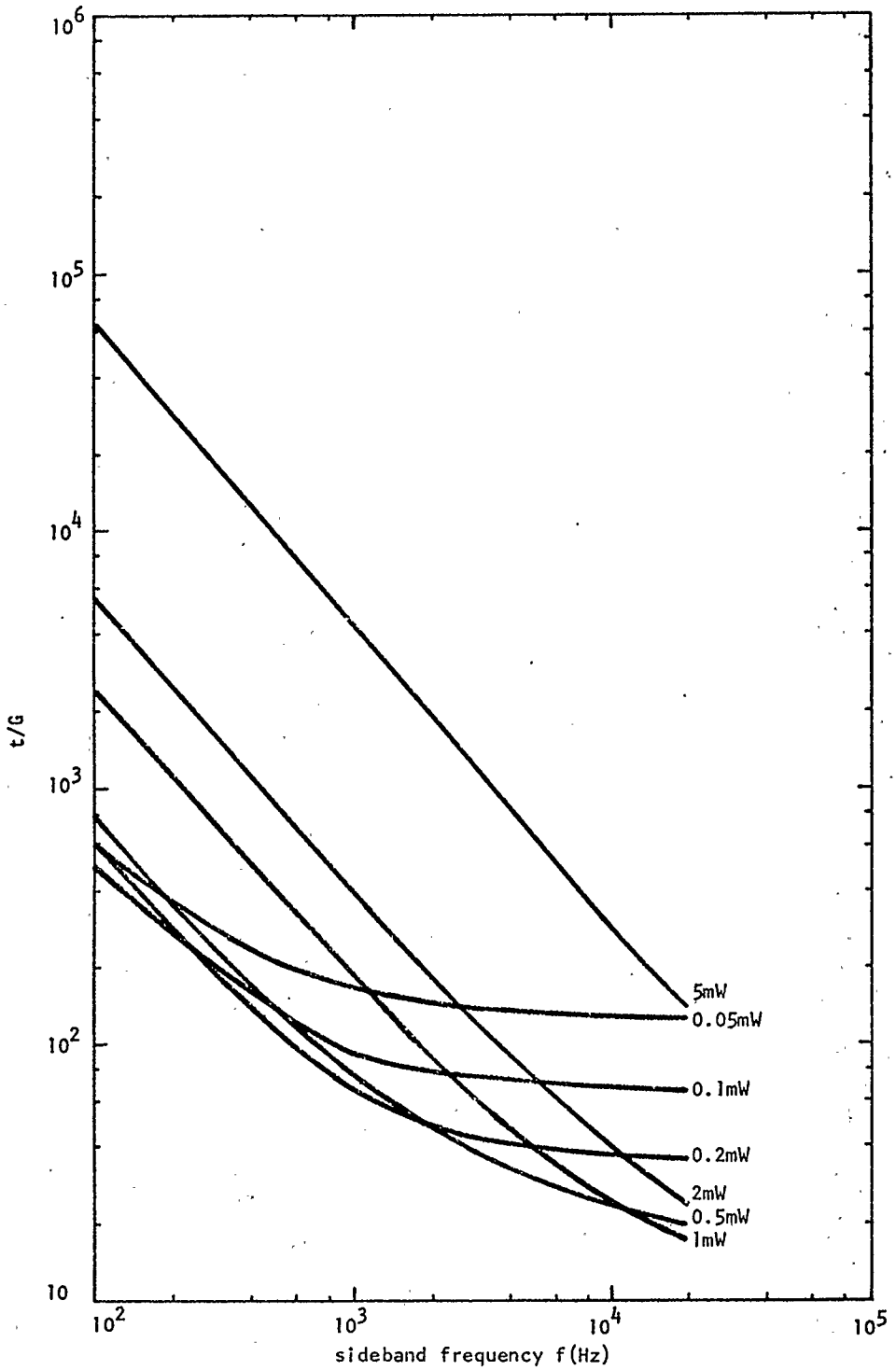

FIGURE 8.7 Graph of the figure of merit (t/G) as a function of the sideband (demodulation) frequency for a pair of L4154 backward diodes operated at various microwave local oscillator powers.

A block diagram of the instrumentation employed is given in Fig. 8.6. The role of the impedance-match transformer has been explained in Sec. 8.1. It may be considered as an integral part of the balanced detector, or account must be taken of its frequency dependent gain since

$$W_n^o = |H_{tr}(f)|^2 \, W_n^i \tag{8.6.6}$$

then

$$(t/G)_i = |H_{tr}(f)|^2 \, (t/G)_o \tag{8.6.7}$$

where $(t/G)_o$ and $(t/G)_i$ are the figures of merit for the diode mixer with and without the transformer respectively. $H_{tr}(f)$ can be determined accurately <u>in situ</u> using the linear system identification procedure outlined in Secs. 3.3 and 7.3.2. Unfortunately, this would have decreased the available measurement bandwidth by a factor of two, when the A/D converter incorporated in the HP5450A Fourier Analyser was used. The procedure was simplified by assuming, with good theoretical and experimental reasons, that the background system noise is white, i.e., $W_n(f,0) = W_o = \text{const.}$ Then $(t/G)_i$ can be measured as

$$(t/G)_i = \frac{P_{rf}^{so} m^2 / R_o}{W_o} \cdot \frac{W_n(f, P_{rf}^{lo})}{W_n^{am}(f, P_{rf}^{lo}, P_{rf}^{so}, m)} \tag{8.6.8}$$

Figure 8.7 presents $(t/G)_i$ curves measured as a function of the sideband frequency for different levels of local oscillator power when two Philco L4154 backward diodes were employed in a balanced mixer. The signal oscillator power was maintained at 1μW. The impedance matching transformer had been designed on the basis of previous measurements reported by Buckmaster and Rathie (1971-11). The graphs are calculated in two

overlapping segments each consisting of 128 points. The points are separated by ∿200Hz in the high frequency section, while the resolution in the lower frequency section is ∿20Hz. The curves in Fig. 8.7 represent a smooth version of the actual data. The noise power spectral density functions were obtained by using an ensemble averaging over q = 200 sample records.

8.6.2 Discussion of Microwave Oscillator Noise Measurement Methods

The microwave configurations used in EPR spectroscopy and in microwave oscillator noise measurements are identical. Ashley *et al.* (1968) and Ondria (1968) outlined the principle of using a synchrodyne configuration to measure oscillator noise. One channel contains a carrier supression filter which is usually a reflection cavity — circulator configuration. The carrier suppressor filter is bypassed for a.m. oscillator noise measurements to prevent the conversion of f.m. noise into a.m. noise (Eq. 5.2.3a). Nevertheless, Ondria considers that the filter is advantageous even for a.m. noise measurements. Both papers emphasize the importance of using a balanced mixer detector. More recently, a.m. and f.m. noise measurement techniques have also been discussed by Ohtomo (1972) and Fickart *et al.* (1972).

Generally, these analyses assume that the circuit elements are ideal. Thus the resulting noise propagation equations are not very complicated, but not very profound either. Strandberg (1972) gave the first detailed analysis of the noise propagation in which account was taken of the non-ideal characteristics of the reflection cavity — circulator or magic-T combination. The conclusions of this analysis were presented in Chapter V. The a.m. and f.m. noise components are shown to become mixed if $\phi \neq 0$ or $\pi/2$ or if the microwave cavity is not perfectly matched and stable.

Fickart et al. (1972) attempted a critical assessment of the limitations of the synchrodyne configuration but their final noise propagation equation is also valid only for an ideal configuration

$$W_n(\omega) = W_{FM}(\omega)/(\omega^2 + \omega_o^2/Q_o^2) \tag{8.6.9a}$$

for dispersion ($\phi = \pi/2$) and

$$W_n(\omega) = W_{AM}(\omega)(\omega Q_o/\omega_o)^2/[1 + (\omega Q_o/\omega_o)^2] \tag{8.6.9b}$$

for absorption ($\phi = 0$). These formulae differ from those of Strandberg. Fickart et al. (1972) draw attention to the limitations set by real cavities and balanced detectors and present graphs showing the ideal frequency dependence of $W_n(\omega)$ from Eqs. 8.6.9 as well as deviations from these ideal dependences, but no theoretical evidence is given to show how these latter curves were obtained. They conclude that Ondria's suggested use of the carrier suppressor filter for a.m. noise measurements is not practical in the frequency region between the cavity 3dB points even under ideal conditions. It is interesting to note that they consider a balanced mixer as a linear detector which performs an addition of the input voltages and not as a multiplier.

In general, only d.c. methods of balancing the mixer are discussed in the literature (Ohtomo, 1972). It has been found in the study reported in this thesis that it is not sufficient to assume that a d.c. balance implies an a.c. balance and that care must be exerted to achieve the latter condition.

CHAPTER IX

THE DIGITAL FOURIER ANALYSER AS AN EPR INFORMATION PROCESSOR

This chapter discusses the simulation of linear systems by a digital computer using the FFT algorithm. Linear systems which enhance the sensitivity and/or the resolution of EPR spectra have been analysed theoretically in Chapter VI, while the discrete Fourier transform (DFT) and the FFT algorithm have been discussed in Chapter VII.

Fundamentally, frequency sampling (DFT) simulation of a linear system is an OFF-LINE processing because the entire signal (sequence) must be known before the actual computation is commenced. It has the advantage of being a higher fidelity simulator of ideal systems than ON-LINE processors since physical realizability is not a limitation. But this OFF-LINE character makes it difficult to use DFT filters in closed-loop systems where feedback decisions are required immediately. Nevertheless, the advent of the FFT algorithm has shortened the computation time to such an extent that, for practical purposes, a Fourier transform processor may be considered as a pseudo ON-LINE processor. It has been successfully included in a large variety of closed-loop systems. An application in NMR was reported by Ernst (1969) and will be discussed in Sec. 9.4.

9.1 DFT Simulation of Linear Systems - Limitations

Section 7.3.3 mentioned the possibility of using the DFT to compute the convolution integral describing a time-invariant linear system,

$$y(t) = h(t) * x(t) = \int_{-\infty}^{+\infty} h(t-\tau)\, x(\tau)\, d\tau \qquad (9.1.1a)$$

$$Y(f) = H(f)\cdot X(f) \ . \tag{9.1.1b}$$

The discrete time equivalent of Eq. 9.1.1a is

$$y(i\Delta t) = \Delta t \sum_{k=-K}^{+K} h((i-k)\Delta t)\cdot x(k\Delta t) \tag{9.1.2a}$$

while the DFT equivalent of Eq. 9.1.1b is

$$Y(n\Delta f) = N\ H(n\Delta f)\ X(n\Delta f)\ , \quad n=0,\ldots,N-1. \tag{9.1.2b}$$

The finite length of the sequences in Eqs. 9.1.2 permits the discrete simulation of only finite impulse response systems, i.e., systems whose impulse response is zero outside some finite limits.

An important distinction between Eqs. 9.1.1 and 9.1.2 arises because of the periodic character of the DFT. Section 7.2 showed that if $x(t)$ and $X(f)$ are a Fourier transform pair,

$$x(t) \longleftrightarrow X(f), \tag{9.1.3a}$$

then the DFT relates finite sequences of the aliased versions of $x(t)$ and $X(f)$,

$$T\ x_a(k\Delta t) \longleftrightarrow X_a(n\Delta f), \tag{9.1.3b}$$

where

$$x_a(t) = \sum_{p=-\infty}^{+\infty} x(t+pT), \tag{9.1.4a}$$

$$X_a(f) = \sum_{r=-\infty}^{+\infty} X(f+rF_s), \tag{9.1.4b}$$

$T=N\Delta t$ and $F_s = 1/\Delta t = N\Delta f$. Cooley <u>et al</u>. (1967) have analysed the errors due to aliasing effects in a DFT simulation of a convolution integral.

They defined an aliasing error

$$\varepsilon_x(f) = X_a(f) - X(f) \tag{9.1.5}$$

and showed that

$$\varepsilon_y(f) = X(f)\varepsilon_h(f) + H(f)\varepsilon_x(f) \tag{9.1.6}$$

which is small provided that $\varepsilon_h(f)$ and $\varepsilon_x(f)$ are small and $X(f)$ and $H(f)$ are bounded. This condition can be satisfied by choosing F_s sufficiently large (i.e., Δt sufficiently small) so that

$$\begin{aligned} H(f) &\simeq 0 \\ & \qquad \text{for } f \geq F_s/2 \\ X(f) &\simeq 0 \end{aligned} \tag{9.1.7}$$

Section 8.1 analysed the conditions necessary for a proper A/D conversion of the input signal $x(t)$.

The cyclic character of the discrete convolution (Eqs. 7.1.9) is another error source in a DFT computation of a convolution integral. Rewriting Eq. 9.1.2b as

$$N\,H(n)\cdot X(n) \longleftrightarrow \sum_{k=0}^{N-1} h((i-k))\cdot x((k)) = \sum_{k=0}^{i} h((i-k))\cdot x((k)) + \sum_{k=i+1}^{N-1} h((i-k))\cdot x((k)) \tag{9.1.8}$$

shows that the second summation is generally undesirable and represents an error. This "wrap-around" error may be eliminated enabling a portion of the sequence $y(i)$ to be obtained from an acyclic convolution if both sequences $x(i)$ and $h(i)$ are augmented with zeros so that they have the same length N, which is at least as great as one less than the sum of the lengths of the two sequences. Usually, the input data is much longer than the filter sequence; therefore sectioning techniques are used to

reduce the required computation time and memory. The longer sequence is sectioned into pieces whose discrete convolutions can be computed separately. Helms (1967) has described the "overlap-add" and "select-save" methods of recombining the results of these convolutions.

Finite word length effects are another class of errors associated with a DFT simulation of a linear system. Section 7.4 analysed scaling and rounding or truncating errors related to the FFT algorithm. The errors affecting the signal X(n) appear as a noise component which is usually white. The filter transform H(n) is affected by a parameter quantization error which may lead to drastic alterations of the output data. These finite word length effects will be analysed separately for each type of EPR signal processing.

9.2 DFT Processing for Sensitivity Improvement

The theory of sensitivity improvement procedures was analysed in Secs. 6.1 and 6.2. The maximization of the S/N and the minimization of the mean square error were the two criteria used to derive analytical expressions for the frequency transfer functions of the optimum filters (Eqs. 6.1.8; 6.2.5; 6.2.9 and 6.2.11b). Since these transfer functions tend to zero at high frequencies the conditions of Eq. 9.1.7 are easily satisfied and the aliasing errors can be made negligible provided that the correct procedure for the filter simulation mentioned in Sec. 9.1 is followed. The scaling and rounding errors are also negligible since the noise introduced by them is negligible compared to the noise accompanying the signal if the number of word bits is sufficiently high and N is not too large. Sensitivity enhancement filters can be simulated without difficulty even if block floating point arithmetic is used, while the precautions described by Oppenheim and Weinstein (1969) must be followed

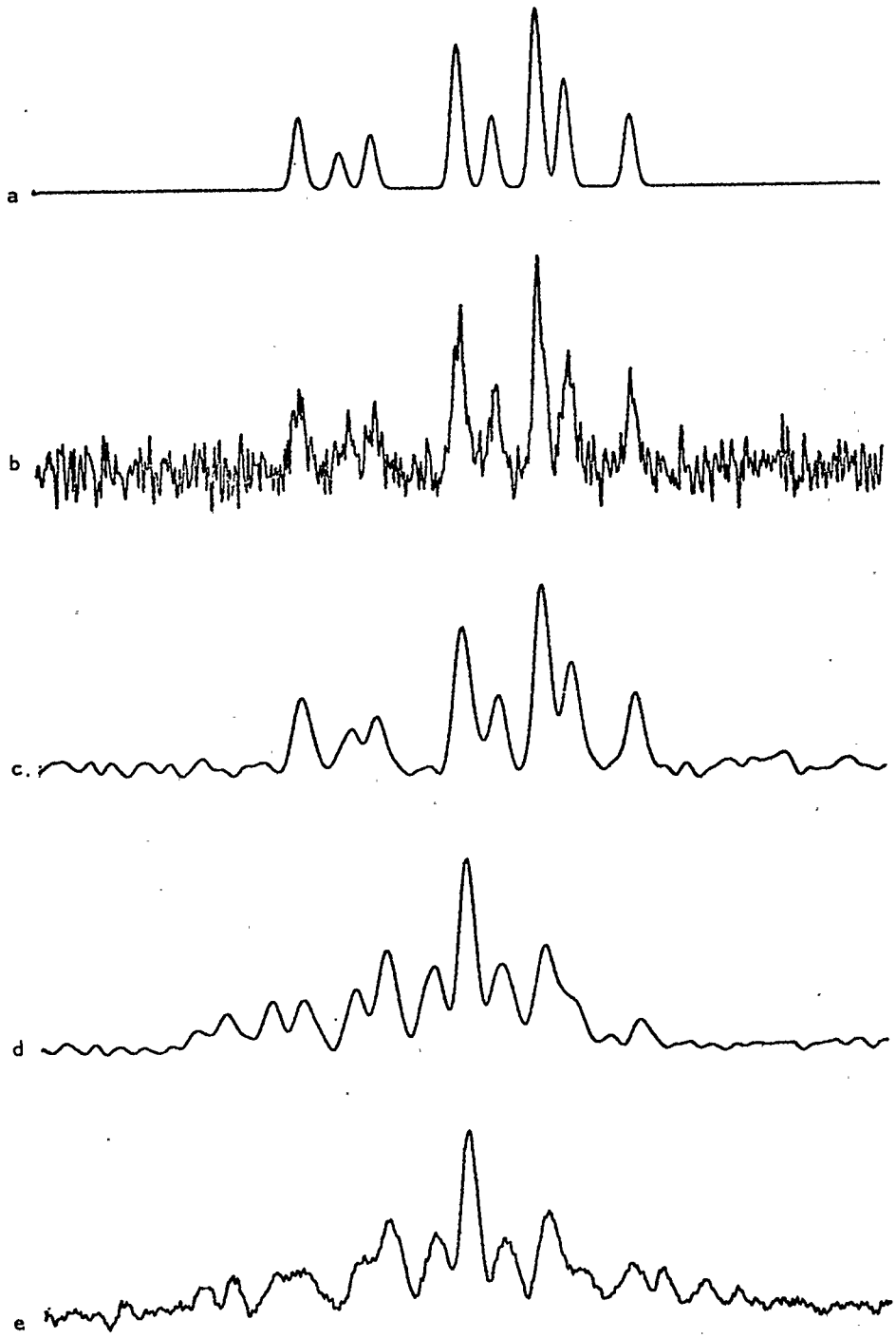

FIGURE 9.1 Examples of the effect of various optimum S/N filters on a unipolar lineshape spectrum: (a) hypothetical spectrum of Gaussian lines composed of 3-, 4- and 1-line patterns; (b) same spectrum with added white noise so that $S/N(A)_u=1$ for the smallest line; (c) output of the $S/N(E)$ matched filter; (d) output of the $S/N(E)_\Sigma$ matched filter for the 4-line pattern and (e) output of the Bryson's filter (cross-correlator). The processing was performed on HP5450 Fourier analyser with N=512.

to prevent an overflow, if fixed-point arithmetic is used. The remainder of this section analyses some particular problems related to filters for EPR signals.

Section 6.2 showed the importance of distinguishing clearly between different S/N definitions. A hypothetical spectrum formed of 8 Gaussian lines having the same width but different amplitudes has been synthesized and then filtered to illustrate this point. Figure 9.1 shows the results of different S/N processings performed by the HP5450A Fourier Analyser. Curve (a) is the original spectrum composed of 3-, 4- and 1-line patterns. Curve (b) pictures the same spectrum with added white noise whose r.m.s. amplitude is such that the smallest line in the spectrum has a $S/N(A)u \simeq 1$. Curve (c) is the output of the $S/N(E)$ matched filter. The S/N is maximized while each line broadens but the patterns are not modified. The filter output signal changes completely when $S/N(E)_{\Sigma}$ filters are used. Curve (d) is the output of the filter designed to "search" for the 4-line pattern while curve (e) is the output of the filter suggested by Bryson (1971), i.e., a cross-correlator of two noisy signal records. As mentioned in Sec. 6.2, such pattern filters disregard all the information unrelated to the presence of the desired pattern. Accordingly, Bryson's filter is capable of delivering information concerning only the presence of a signal but nothing about the lineshape, amplitude or time of occurrence of that signal. Bryson's claim that no a priori knowledge and no comparison is needed to determine the concentration of the paramagnetic sample from the peak of the cross-correlation is incorrect because this peak is proportional to the energy of the signal while the number of spins is proportional to the area under the absorption curve.

The line broadening is an undesirable effect inherent in matched filtering. Caprini et al. (1970) showed that this effect can be reduced

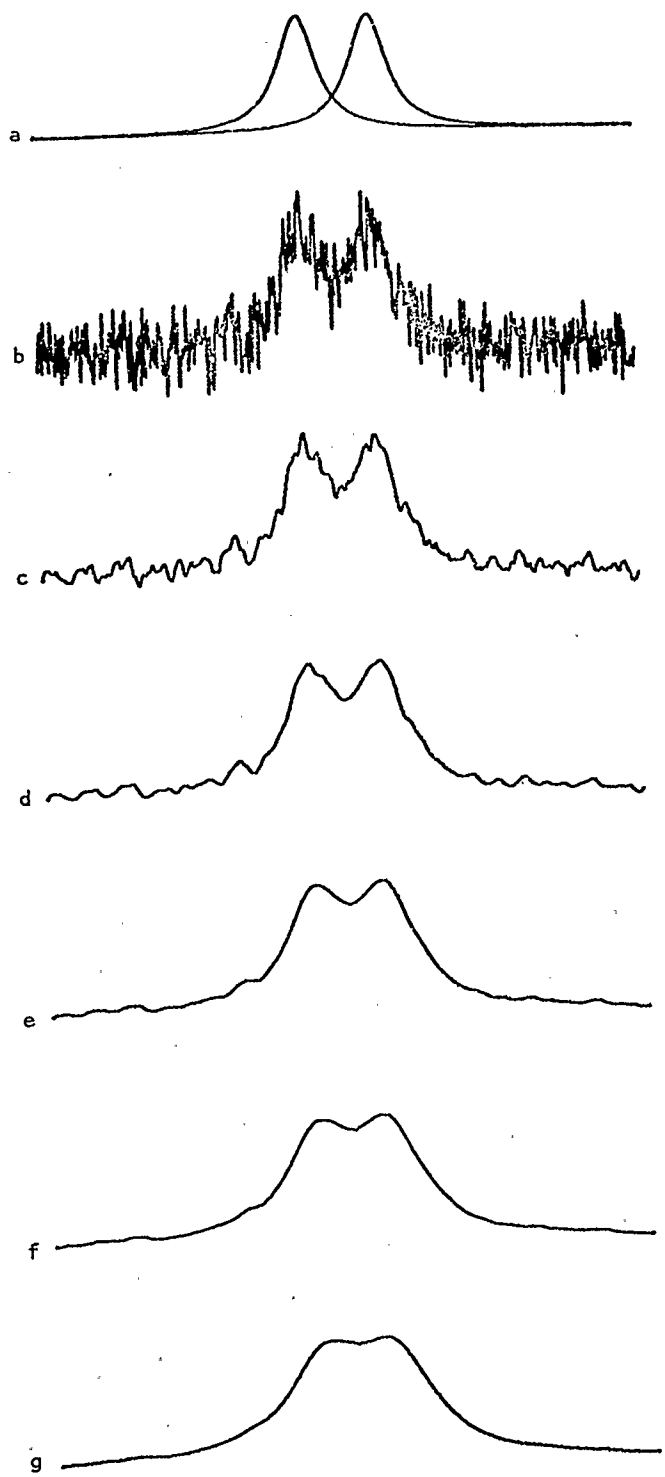

FIGURE 9.2 Illustrations of the broadening effect of a matched filter; (a) the two Lorentzian lines (w_{hh}=20) composing the spectrum; (b) the noisy signal; the output signals from matched filters for Lorentzian lines with (c) w_{hh}=2; (d) w_{hh}=5; (e) w_{hh}=10; (f) w_{hh}=15; (g) w_{hh}=20. The processing was performed on HP5450A with N=512.

by using filters matched for narrower lines of the same type. Accordingly, the S/N will not be maximized but the resolution will not be degraded as much either. This filtering is equivalent to a cross-correlation with lines narrower than those in the spectrum. The equation describing this procedure for Lorentzian lines is

$$[n(t)+s(t)]*h(t) = \left[n(t) + \sum_k A_k \frac{\alpha_k}{\alpha_k^2+(t-t_k)^2}\right] * \left[\frac{\beta}{\beta^2+t^2}\right] =$$

$$= n(t)*h(t) + \sum_k A_k \frac{(\alpha_k+\beta)}{(\alpha_k+\beta)^2+(t-t_k)^2} \qquad (9.2.1a)$$

while for Gaussian lines the equation is

$$[n(t)+s(t)]*h(t) = \left[n(t) + \sum_k \frac{A_k}{\sqrt{\alpha_k}} e^{-(t-t_k)^2/\alpha_k^2}\right] * \left[\frac{1}{\sqrt{\beta}} e^{-t^2/\beta^2}\right] =$$

$$= n(t)*h(t) + \sum_k \frac{A_k}{\sqrt{\alpha_k^2+\beta^2}} \exp - \frac{(t-t_k)^2}{\alpha_k^2+\beta^2}$$

$$(9.2.1b)$$

If the noise imput is white and limited to a bandwidth Ω, then the ratio of the output and input noise powers is

$$(P_{no}/P_{ni}) \sim (1/\beta\Omega)[1-\exp(-4\pi\beta\Omega)] \qquad (9.2.2a)$$

for Lorentzian lines and

$$(P_{no}/P_{ni}) \sim (1/\beta\Omega)\ \mathrm{erf}(\sqrt{2}\pi\beta\Omega) \qquad (9.2.2b)$$

for Gaussian lines. Figure 9.2 shows the results of filtering two noisy Lorentzian lines separated by three half line widths in filters matched for lines narrower than the signal line.

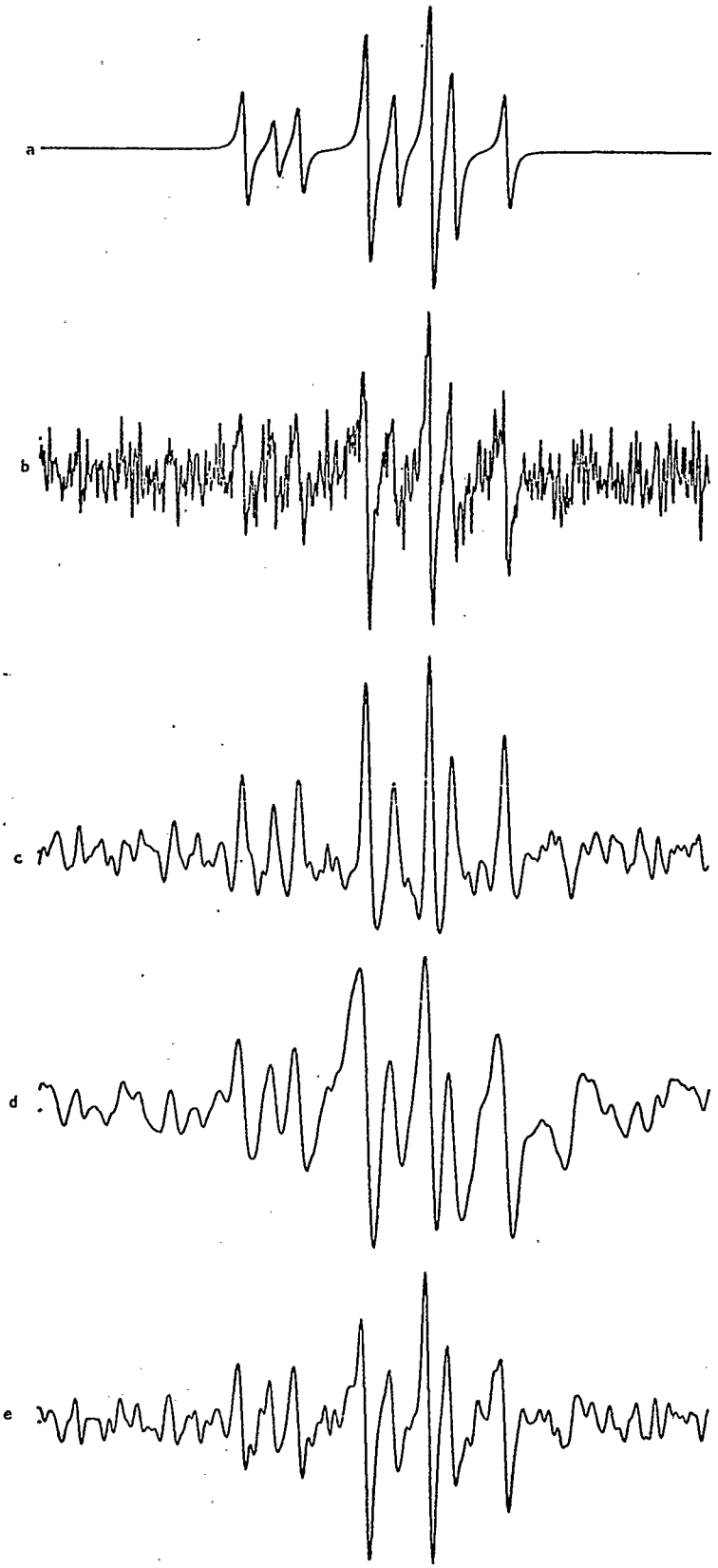

FIGURE 9.3 Illustrations of the effects of various optimum filters on a_1 spectra: (a) hypothetical spectrum of derivatives of Lorentzian lines grouped in 3-, 4- and 1-line patterns; (b) same spectrum with added noise so that $S/N(A)_b=1$ for the smallest line; (c) output of the $S/N(E)$ matched filter; (d) output of the matched filter for the undiferentiated line; (e) output of the linear mean square estimator. The processing was performed on HP5450A with N-512.

Caprini et al. (1970) have shown that the output of filters matched for a_I lineshapes is proportional to a_{II} lineshapes if the signal is Gaussian or Lorentzian. More generally, if a line can be considered as a derivative of an original line, then the matched filter will "double" the differentiation. For example, if the input signal is the kth derivative of a Lorentzian line of width α,

$$s_i(t) = \ell_\alpha^{(k)}(t) = \left(\frac{d}{dt}\right)^k [\ell_\alpha(t)] = \left(\frac{d}{dt}\right)^k [\alpha/\pi(\alpha^2 + t^2)], \tag{9.2.3a}$$

$$S_i(f) = (j2\pi f)^k \mathcal{F}\left\{\ell_\alpha(t)\right\} = (j2\pi f)^k \exp(-2\pi\alpha|f|), \tag{9.2.3b}$$

then the matched filter has a transfer function

$$H_m(f) \sim S_i^*(f) \tag{9.2.3c}$$

and the filter output signal is

$$S_o(f) = S_i(f)\, H_m(f) \sim (j2\pi f)^{2k} \exp(-4\pi\alpha|f|) \tag{9.2.3d}$$

$$s_o(t) \sim \ell_{2\alpha}^{(2k)}(t). \tag{9.2.3e}$$

Since this additional differentiation may introduce difficulties in interpreting complicated spectra, Caprini et al. proposed using filters matched for the original, undifferentiated line instead of the actual signal line. The broadening effect for Gaussian or Lorentzian lines is described by Eqs. 9.2.1 and the same solutions mentioned above can be used to minimize this effect. The possible alternative processings are illustrated in Fig. 9.3, where the spectrum has the same pattern as that in Fig. 9.1 but has an a_I shape.

Figure 9.3(e) is the output of the linear mean square estimator (Eq. 6.1.8). It is noted that no broadening or shape changing occurs

since this filter preserves information concerning the lineshape and hence it may be preferable to S/N filters when studying lineshapes. Moreover, it was also shown in Sec. 6.3 that a linear mean square estimator is a filter capable of increasing both sensitivity and resolution.

9.3 DFT Processing for Resolution Improvement

The theory of resolution enhancement procedures has been analysed in Sec. 6.3 where it was shown that these procedures are equivalent to solving a convolution integral equation (Eq. 6.3.5)

$$s(t) = \int_{-\infty}^{+\infty} q(\tau)\, r(t-\tau)\, d\tau \,. \tag{9.3.1}$$

Fourier transform techniques provide an immediate solution to Eq. 9.3.1,

$$Q(f) = S(f)/R(f), \tag{9.3.2}$$

so that a DFT realization of resolution filters looks very promising.

Unfortunately, a DFT approach to this problem is limited to cases where aliasing errors and finite word length effects can be neglected. This is not possible for EPR ideal resolution improvement filters. Cooley *et al.* (1967) have analysed the effect of aliasing errors associated with DFT deconvolutions and showed that

$$\varepsilon_q(f) = \frac{S(f)\varepsilon_r(f) + R(f)\varepsilon_s(f)}{R_a(f)} \,. \tag{9.3.3}$$

The aliasing error $\varepsilon_q(f)$ is unacceptable if $R(f)$ tends to zero as for EPR lineshapes.

Alternatively, the solution given by Eq. 9.3.2 can be considered as a convolution problem, i.e., a linear filtering with a filter frequency

transfer function $H(f) = 1/R(f)$. Viewed as a filtering problem, a correct DFT simulation requires $H(f)$ to tend to zero (Eq. 9.1.7) which is impossible if $R(f)$ tends to zero as it happens for EPR lineshapes. Moreover, the rounding and scaling errors are enhanced significantly in a convolution process where $H(t)$ is an increasing function of f as in EPR. This effect can be minimized by using relatively short sequences (i.e. small values of N) and operating in floating point double precision arithmetic. These quantization errors lead to a contradiction inherent in a DFT solution of a resolution enhancement problem because Δt should be chosen sufficiently small and N sufficiently large to prevent distortion of the signal shape and loss of resolution while N should be kept small to minimize the finite word length effects.

Ernst (1966) predicted that oscillations (wiggles) would appear on the output of a resolution enhancement filter due to the particular way in which a δ function is approached in a Fourier transform

$$\delta(x) = \lim_{p\to\infty} \int_{-p}^{+p} \exp(j2\pi fx)\, df = \frac{1}{\pi} \lim_{p\to\infty} \frac{\sin(px)}{x} \qquad (9.3.4)$$

It is interesting to mention that Cohn-Sfetcu et al. (1970), who first used the FFT algorithm to enhance the resolution of magnetic resonance signals, incorrectly attributed the output oscillatory-like noise to this effect. This was incorrect because Ernst's theory applies only for truncated continuous Fourier transforms, whereas the delta function is defined without a "limiting" operation (Eqs. 7.1.7 and 7.1.8) in relation to the DFT. The output oscillatory-like noise should be attributed to the enhancement of scaling and rounding errors.

The solutions mentioned in Sec. 6.3 which compromise between resolution enhancement and S/N degradation are capable of reducing the

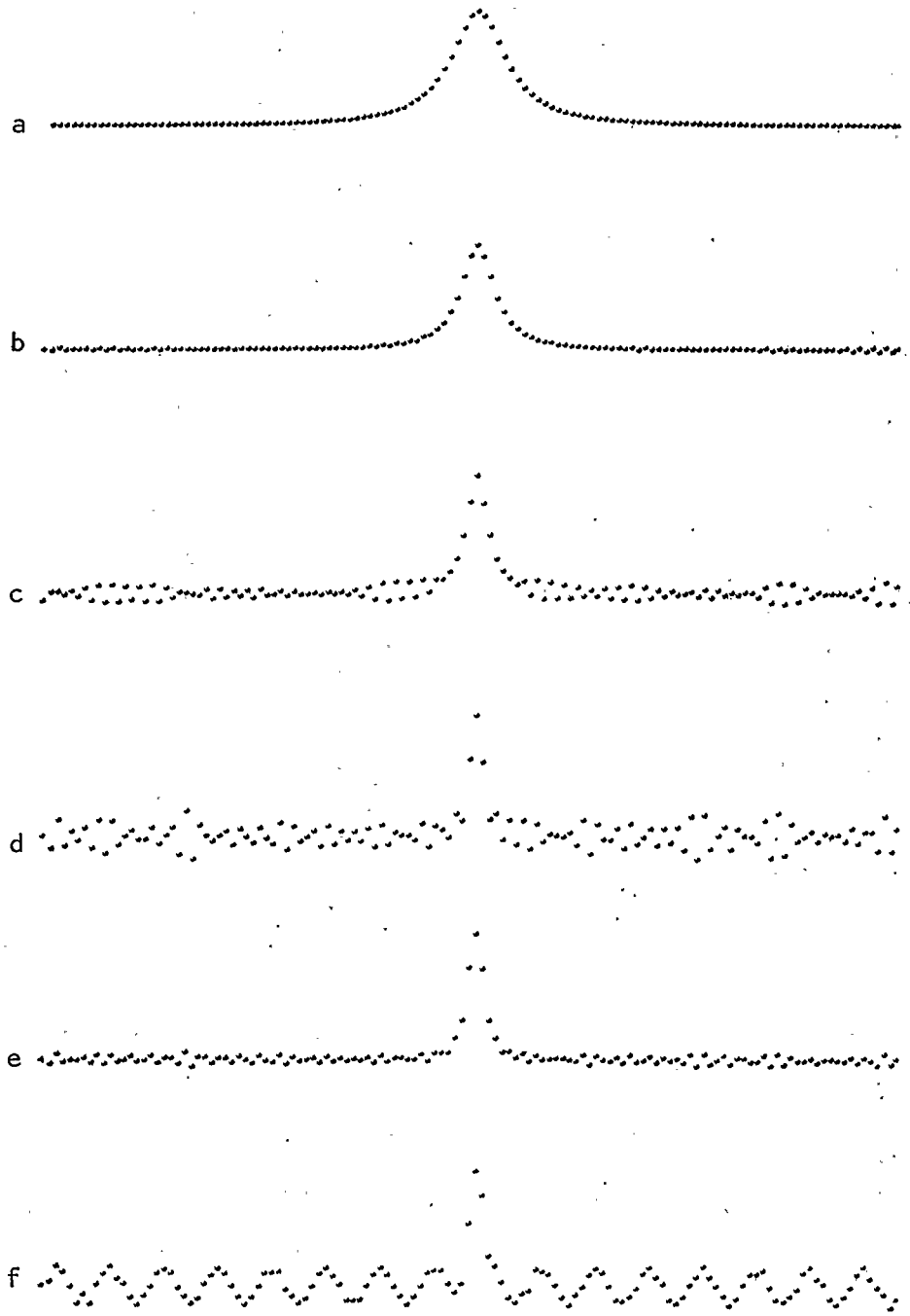

FIGURE 9.4a Illustrations of deconvolution processing on HP5450 with N=128: (a) Lorentzian line with $w_{hh}=\alpha=5$; (b) result of processing described by Eq. 6.3.9b when $\beta=2$; (c) result of same processing with $\beta=3$; (d) result of same processing when $\beta=4$; (e) output of filter given by Eq. 6.3.11 when $\beta=4$ and $\gamma=1$; (f) output of same type of filter when $\beta=4.75$ and $\gamma=1$.

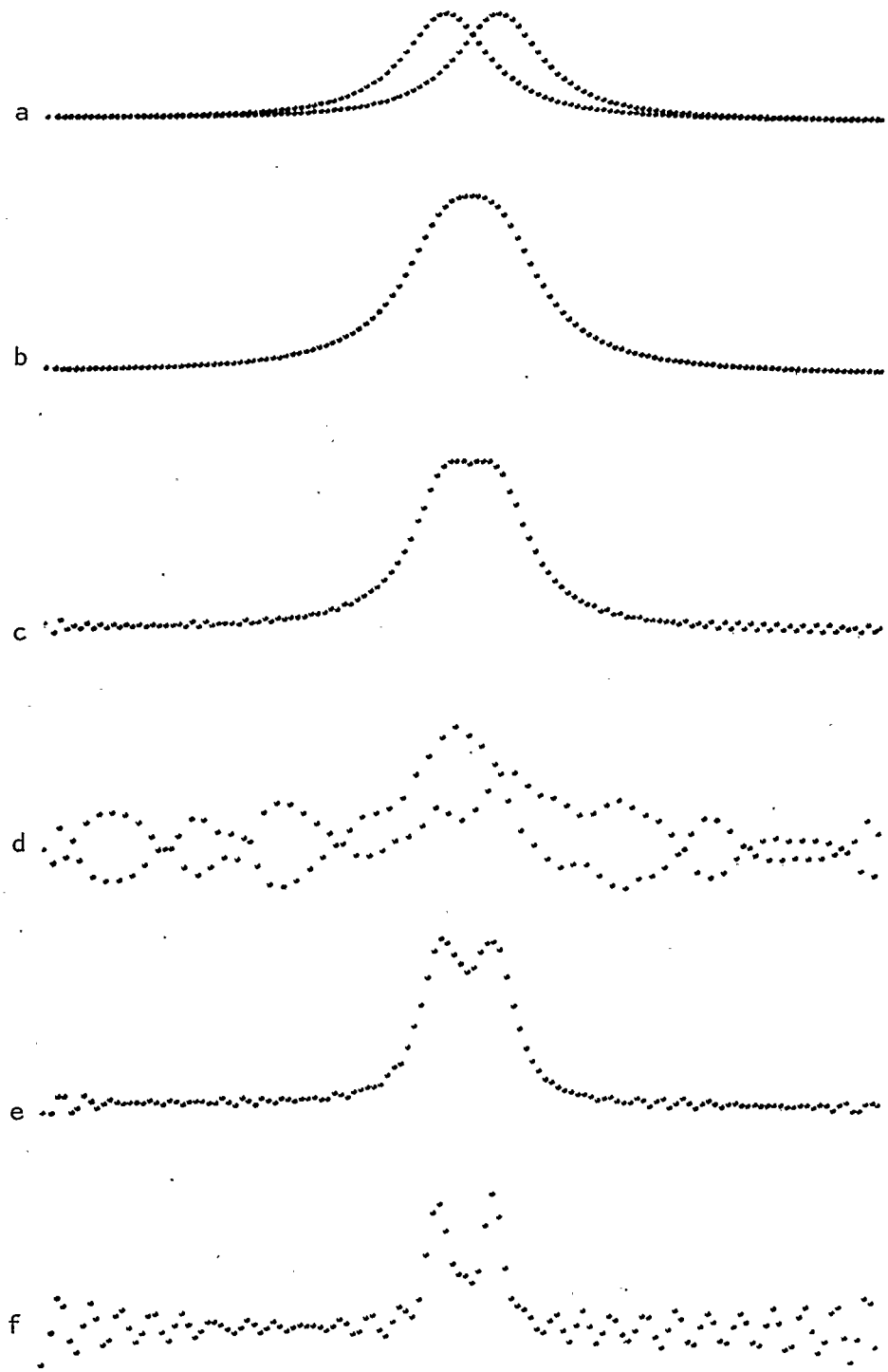

FIGURE 9.4b Illustration of resolution enhancement processing on HP5450A with N=128: (a) superposition of 2 Lorentzian lines of $w_{hh}=\alpha=8$ represented by a distance equal to $w_{hh}=8$; (b) signal formed by the summ of the two Lorentzian lines; (c) result of processing described by Eq. 6.3.9b when $\beta=2$; (d) result of same processing when $\beta=3$; (e) output of filter given by Eq. 6.3.11 when $\beta=5$ and $\gamma=2$; (f) output of same filter when $\beta=7$ and $\gamma=2$.

computational errors associated with the DFT implementation of a resolution enhancement filter. Figure 9.4 illustrates the results of using the HP5450A to enhance the resolution of Lorentzian line spectra. Unfortunately, the HP5450A Fourier analyser is not recommended for resolution enhancement processings because it operates in block-floating point arithmetic which leads to significant scaling and rounding errors. The results are even less encouraging when the resolution enhancement of noisy signals is attempted.

9.4 Special DFT Processings — Hilbert Transform

In Sec. 2.4 it was shown that the absorption and dispersion components of the magnetic susceptibility $\chi(\omega)$ are a Hilbert transform pair as are the real and imaginary parts of any frequency transfer function of a linear system.

$$H^i(f) = -(1/\pi f)*H^r(f) \tag{9.4.1a}$$

$$H^r(f) = +(1/\pi f)*H^i(f) \tag{9.4.1b}$$

where $H^r(f)$ and $H^i(f)$ are the real and imaginary parts of the transfer function.

Many EPR spectrometers can detect only one of these components, although the other may also be of interest. Some spectrometers detect a combination of the two components although accurate measurements and interpretation can be made only on "pure" components. It is then necessary to calculate the Hilbert transform of the detected signal. Ernst (1969) has analysed the use of numerical Hilbert transforms to realize an automatic phase correction system for an NMR spectrometer.

The numerical convolution of Eqs. 9.4.1 can be performed rapidly

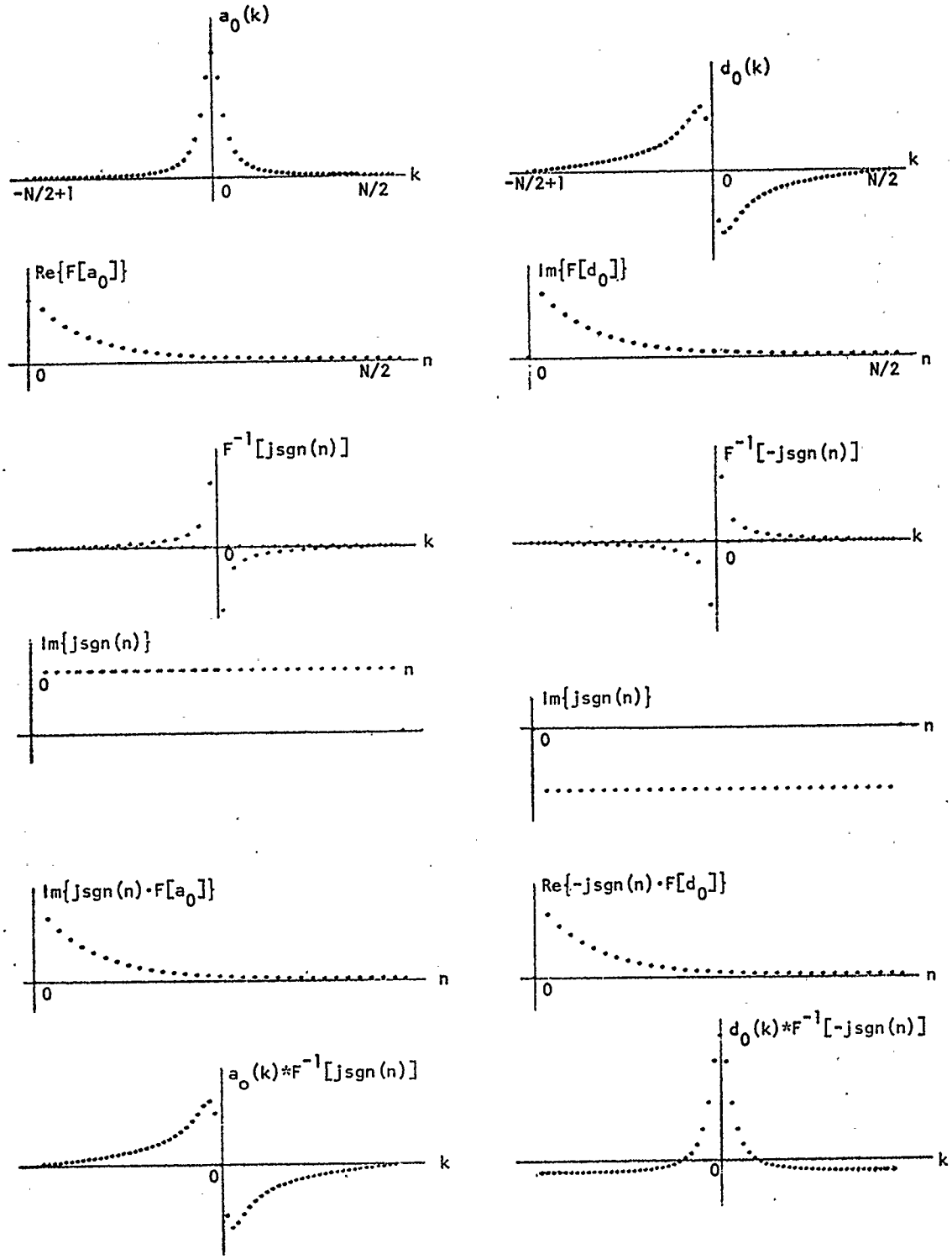

FIGURE 9.5a Illustrations of DFT realization of Hilbert transforms on HP5450A with N=64.

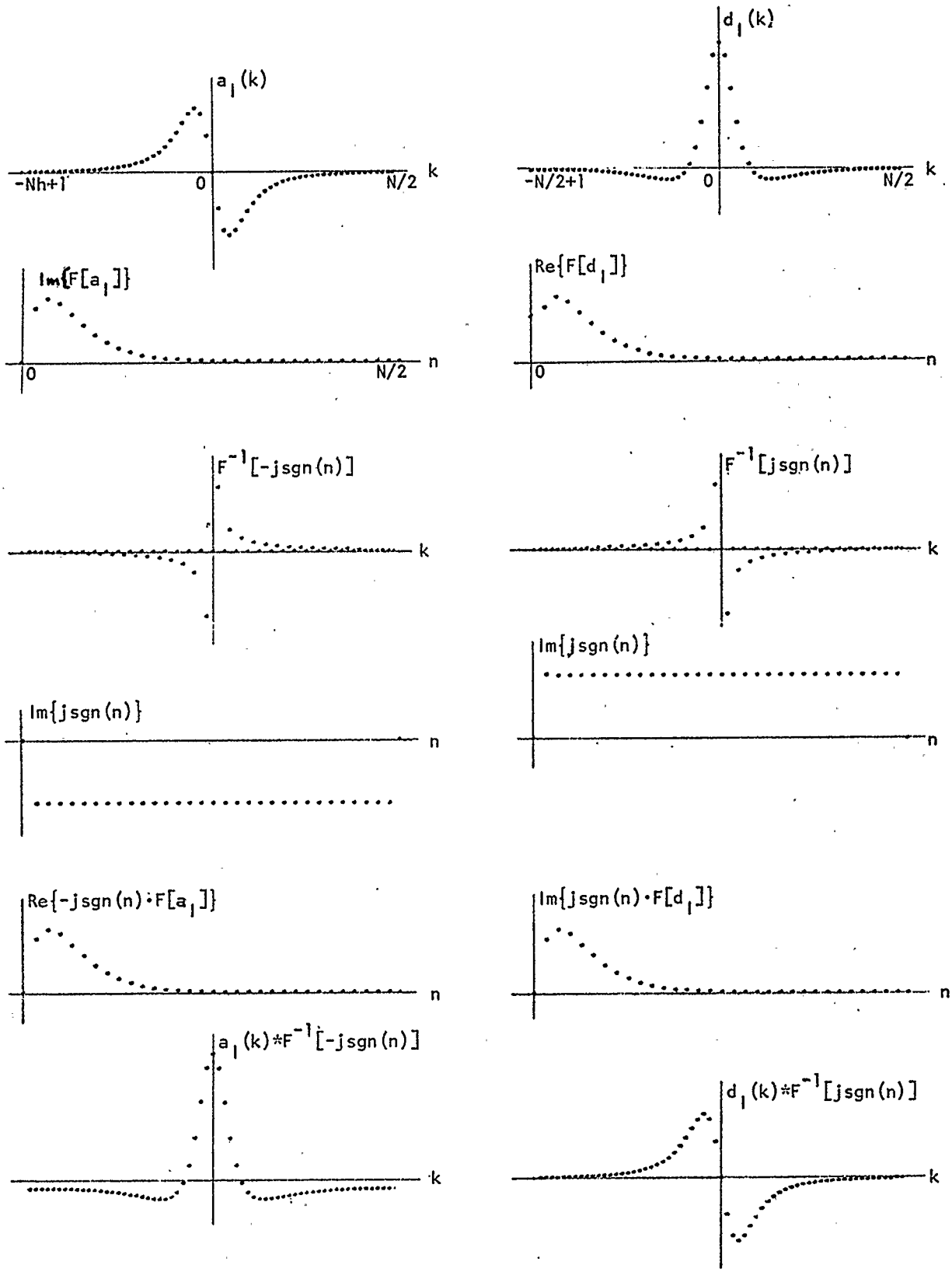

FIGURE 9.5b Illustrations of DFT realization of Hilbert transfroms on HP5450A with N=64.

using a DFT approach and the FFT algorithm. The Fourier transforms Eqs. 9.4.1 are

$$h^i(x) = j\,\mathrm{sgn}(x)\cdot h^r(x) \tag{9.4.2a}$$

$$h^r(x) = -j\,\mathrm{sgn}(x)\cdot h^i(x) \tag{9.4.2b}$$

where $h^i(x)$ and $h^r(x)$ are the Fourier transforms of $H^i(f)$ and $H^r(f)$. These operations can be implemented easily on a digital Fourier analyser. Figure 9.5 illustrates this DFT implementation on the HP5450A Fourier analyser. The processing is in principle noiseless since the Hilbert transform is equivalent to phase shifting all transform components by $\pi/2$. The computation errors associated with a DFT implementation of a convolution integral are negligible in this case. Aliasing errors do not count because Δt and N can be suitably chosen to ensure that the DFT of χ' or χ'' tends to zero at high frequencies. The scaling and rounding errors appearing in a FFT computation are not enhanced by the multiplying functions in Eqs. 9.4.2 and thus they are negligible if a sufficiently large number of word bits and a not too large value of N are used.

Signal phase shifting can be achieved by forming the appropriate linear combination of the original signal and its Hilbert transform. The effectiveness of an automatic phase correction system depends more on the determination of the necessary phase correction than on the actual implementation of the Hilbert transform. Ernst (1969) has indicated two possible criteria for determining the "phase purity" of a magnetic resonance spectrum. Nevertheless, the use of an On-Line digital computer in an automatic phase correction system seems a little bit extravagant unless the computer is already incorporated in the spectrometer as happens

for Fourier transform spectrometers or time averaging experiments. Cheaper analogue systems can be designed to achieve the same ON-LINE performance but the discrete Hilbert transform approach is indispensable for correcting the phase of spectra already recorded.

CHAPTER X

SUMMARY AND SUGGESTIONS FOR FUTURE WORK

The purpose of the study reported in this thesis was to investigate systematically the utility of a digital Fourier analyser in improving the performance of EPR spectrometers. Chapter I defined the sensitivity, the resolution and the cost as the parameters characterizing the performance of an EPR spectrometer. It was shown that the sensitivity can be improved by increasing the signal, reducing the noise and separating the signal from noise. This thesis analyses the use of a digital Fourier analyser to implement the latter two approaches as well as to process EPR signals for resolution enhancement.

The wide range of possible applications of a digital Fourier analyser in EPR spectroscopy leads to a conflict between the number of topics covered and the detail achieved in each topic. The compromise solution attempted presents investigations of large areas of interest, but they are less rigorous than initially intended. The thesis deals with topics from rather different disciplines, and consequently it was considered necessary to present the fundamentals of these disciplines, even at the expense of some lack of rigour in other areas. Chapter II is an introduction to the theory of EPR spectroscopy, Chapter III reviews the basic concepts of random data analysis while Chapter VII presents the fundamental properties of the discrete finite Fourier transform and the problems related to its implementation using the FFT algorithm. The basic EPR instrumentation is analysed systematically in Chapter IV; the principle system components were identified and their performance and influence on the signal strength is analysed with particular attention

to these elements as noise sources.

Chapter V analysed the role of these noise sources in limiting the sensitivity of EPR spectrometers. The detector noise level can be reduced by employing backward or Schottky barrier diodes or by using very low noise microwave preamplifiers. The effect of (1/f) diode noise can be reduced by shifting the signal center frequency to a frequency above the "knee" of the diode noise by employing magnetic field modulation techniques or a superheterodyne configuration. The literature describing various pseudosuperheterodyne configurations is reviewed critically and constructively. The propagation of oscillator noise in the signal arm was studied to obtain analytical expressions for the spectrometer "noise" transfer functions. These expressions were used to deal with the problem of reducing the sensitivity limiting effect of microwave oscillator noise in a comprehensive and systematic manner. Thus it was possible to appraise the importance of absolute and relative frequency stabilization. It is suggested that the resonant frequency of the sample cell be stabilized to the microwave oscillator frequency and not vice versa because the electromagnetic field frequency is more fundamental. The stabilization of phase is also discussed although phase instabilities play a secondary role in limiting the sensitivity of EPR spectrometers. Particular attention is paid to the oscillator noise rejection properties of bimodal cavities. A general transfer function describing this role was derived to permit a more realistic assesment of the usefulness of bimodal cavities. After analysing the effect of the other noise sources, it is concluded that the complexity of EPR instrumentation makes it imperative that an *in situ* assessment of the relative influence of these noise sources be made before a systematic approach to minimize these sensitivity limiting factors should be attempted.

Chapter VIII demonstrates that such an in situ noise assessment can be performed conveniently by using a digital Fourier analyser. A Hewlett-Packard HP5450A Fourier analyser was used to determine experimentally the effect of both microwave detector and oscillator noise. These are the first comprehensive measurements at sideband frequencies up to 20kHz from the microwave carrier frequency. The theoretical assertions made in Chapter V concerning the influence of resonant cavity quality factor and magnetic field modulation frequency on the role played by oscillator noise in limiting the sensitibity could be verified experimentally. The advantage of using balanced mixer detectors was demonstrated convincingly. It is proposed that the noise power spectral density be used to measure the spectrometer sensitivity since it avoids introducing factors which are under the control of experimentalists.

In addition, it is shown that a digital Fourier analyser can be successfully used to determine the performance of microwave detectors. It is suggested that a PIN diode modulator be incorporated in an EPR spectrometer so that an in situ determination of the figure-of-merit of microwave detectors can be made rapidly and accurately. Attention is drawn to the necessity of using balanced mixers to reduce the noise introduced by the microwave oscillator. The experimental performance of backward diodes was evaluated using the HP5450A Fourier analyser. This performance agrees with that obtained using conventional measurement techniques. The literature describing methods to measure microwave oscillator noise is discussed critically and constructively. It is pointed out that conventional methods are based on noise propagation equations which lack in profoundness because the elements of the measuring system are considered as being ideal.

Chapter VI analyses theoretically both methods to separate the signal from noise as well as methods to increase the resolution. For the first time, a mean square estimator is considered as a processor of EPR signals and it is proven that it may be preferable to other filters because it preserves the information carried by the lineshape. It is surprising that the S/N maximization criterion is used exclusively in EPR although it disregards lineshape information which is not very important for other types of signals but is essential in EPR spectroscopy. Consequently, it was necessary to analyse carefully the definition of S/N and its influence on the shape of the filter output signal. A clear distinction is made between energy and amplitude S/N definitions as well as between single line and line pattern S/N definitions. The matched filter which is the optimum S/N filter was discussed to show how it affects the resolution. Filters which compromise between sensitivity enhancement and resolution degradation are also described. The second part of Chapter VI analyses signal processings for resolution enhancement. The ideal filter to increase the resolution is derived and discussed after various parameters used to measure the resolution were enumerated. It is shown that the resolution filter is the inverse of the matched filter and that, again, a compromise must be achieved between resolution enhancement and sensitivity degradation. Various filters which realize this compromise are described critically. The analogue methods of improving the resolution are analysed as variants of the "derivative" approach. The third part of this chapter describes some digital methods of increasing the sensitivity or the resolution of EPR spectrometers. These methods include discrete time filters, time averaging and least square approximation techniques.

The DFT implementation of optimum filters is analysed in Chapter IX. This analysis brings into evidence the requirements for reducing aliasing errors inherent in a DFT approach as well as the limitations imposed by the computation errors related to the FFT algorithm. Examples processed on the HP5450A are introduced to illustrate the theoretical analysis of Chapter VI. It is shown that pattern filters do not preserve information unrelated to the presence of the respective pattern and it is shown that some of the claims made by Bryson (1971) are incorrect. It is shown that Lorentzian and Gaussian functions are self-convolving and hence EPR spectra described by these functions can be processed in optimum filters which conserve the nature of the spectral line. Special attention is paid to processing lineshapes which can be considered as derivatives of an original line since matched filters "double" the order of differentiation. To avoid this effect, it is suggested that filters matched for the original line be used. It is shown that DFT and FFT computation errors do not play a significant role in sensitivity improvement processings, but that they definitely limit the applicability of a DFT approach to resolution enhancement. It is concluded that such processings must be performed in floating point arithmetic. A DFT approach to implementing the Hilbert transform (Kramers-Krönig relations) and correcting the phase of EPR spectra is reviewed in the last part of Chapter IX.

In conclusion, a digital Fourier analyser proves to be a very useful tool both in the design of EPR spectrometers when it is instrumental in deciding upon the optimum configuration, and to process EPR spectra for resolution and/or sensitivity enhancement. In addition, it can be used as part of a measurement system to determine the <u>in situ</u> performance of microwave devices.

Due to the vast area investigated, it was inevitable that this thesis would indicate many interesting subjects for future work. It would be interesting to study experimentally the use of bimodal cavities in rejecting oscillator noise as well as the role played by the resonance phenomenon in transmitting this noise to the detector system. Bimodal cavities appear very promising for use in EPR pulse spectrometers since they represent an elegant solution to the problem of isolating the detector from the generator during the high power microwave pulse. The idea of stabilizing the resonant frequency of the sample cell to that of the microwave oscillator needs a more thorough theoretical and experimental analysis.

Measurements of microwave detector performance should be extended to various other types of detectors as well as to higher frequencies, now that faster A/D converters are available. It is suggested that the methods of measuring microwave oscillator noise be studied in depth and measurements be performed using a digital Fourier analyser.

The implementation of deconvolutions using the DFT should be studied further to provide a more quantitative analysis of the limitations set by the computation errors. It would be also interesting to study the applicability of the Walsh transform to EPR spectra processing.

The use of random or Fourier transform spectroscopy in EPR was not possible because of technical limitations in the instrumentation available, namely microwave a.m. pulse modulators and A/D converters are not sufficiently fast to be used in EPR. It is proposed that these techniques be studied and analysed with emphasis on possible application in EPR.

REFERENCES

Abragam, A. and Bleaney, B., 1970, Electron Paramagnetic Resonance of Transition Ions, (Clarendon Press, Oxford).

Alger, R.S., 1968, Electron Paramagnetic Resonance, (Interscience, N.Y.).

Allen, L.C., Gladney, H.C., and Glarum, S.H., 1964, J. Chem. Phys. 40, 3134.

Ashley, J.R., Searles, C.B. and Palka, F.M., 1968, IEEE Trans. Microwave Theory Tech. MTT-16, 753.

Bendat, J.S. and Piersol, A.G., 1971, Random Data Analysis and Measurement Procedures, (Wiley Interscience, N.Y.).

Bergland, G.D., 1969, IEEE Spectrum 6, 7, 41.

Bloch, F., 1946, Phys. Rev. 70, 460.

Bonnet, G., 1965, Nucl. Instr. Meth. 37, 217.

Bosch, B.G. and Gambling, W.A., 1961, J. Brit. Inst. Radio Engrs. 21, 503.

_____, 1962, J. Brit. Inst. Radio Engrs. 24, 389.

Bremermann, H., 1965, Distributions, Complex Variables and Fourier Transforms, (Addison-Wesley, Reading, Mass.).

Bryson III, C.E., 1971, Rev. Sci. Instrum. 42, 1504.

Buckmaster, H.A., 1971, J. Appl. Phys. 42, 1225.

Buckmaster, H.A. and Dering, J.C., 1965, Can. J. Phys. 43, 1088.

_____, 1966, Proc. XIV Colloque AMPERE, 1017, Ed. J.Blinc, (North Holland, Amsterdam).

_____, 1966, J. Sci. Instrum. 43, 554.

_____, 1967, IEEE Trans. Instrum. Measurement IM-16, 13.

_____, 1967, Can. J. Phys. 45, 107.

_____, 1968, J. Appl. Phys. 39, 4486.

Buckmaster, H.A. and Gray, A.L., 1971, J. Phys. E. 4, 1041.

Buckmaster, H.A. and Rathie, R.S., 1971-I, Can. J. Phys. 49, 849.

_____, 1971-II, Can. J. Phys. 49, 853.

Buckmaster, H.A. and Skirrow, J.D., 1972, Can. J. Phys. 50, 1092.

Buckmaster, H.A. and Cohn-Sfetcu, S., 1972-I, Proc. XVII Congress AMPERE, Ed. V. Hovi, (North Holland, Amsterdam), (in press).

_____, 1972-II, Proc. XVII Congress AMPERE, Ed. V. Hovi, (North Holland, Amsterdam), (in press).

Caprini, M., Cohn-Sfetcu, S. and Manof, A., 1970, IEEE Trans. Audio and Electroacoustics AU-18, 389.

Clerjaud, B. and Lambert, B., 1971, J. Phys. E. 4, 619.

Cohn-Sfetcu, S., Caprini, M. and Manof, A., 1970, Nucl. Instrum. Methods 85, 329.

_____, 1971, Proc. XVI Congress AMPERE, 822, Ed. I. Ursu, (Publishing House Academy RSR, Bucharest).

Cooley, J.W. and Tukey, J.W., 1965, Math. Comput. 19, 297.

Cooley, J.W., Lewis, P.A. and Welch, P.D., 1967, IBM Res. Paper RC-1743.

_____, 1967, IEEE Trans. Audio and Electroacoustics AU-15, 79.

Dering, J.C., 1967, Ph.D. Thesis, The University of Calgary, Canada

Ernst, R.R., 1965, Rev. Sci. Instrum. 36, 1689.

_____, 1966, Advances in Magnetic Resonance 2, 1, Ed. J.S. Waugh, (Academic Press, N.Y.).

_____, 1969, J. Mag. Res. 1, 7.

_____, 1970, J. Mag. Res. 3, 10.

Ernst, R.R. and Anderson, W.A., 1966, Rev. Sci. Instrum. 37, 93.

Ernst, R.R. and Benz, H., 1970, IEEE Trans. Audio and Electroacoustics AU-18, 380.

Faulkner, E.A. and Whippey, P.W., 1966, Proc. IEEE 113, 1159.

Fickart, J.L., Nigrin, J. and Goud, P.A., 1972, IEEE Trans. Microwave Theory Tech. MTT-20, 702.

Franconi, C., 1969, Proc. Intl. Conf. on Mag. Res., Cagliari, 397.

_____, 1970, Rev. Sci. Instrum. 41, 148.

Franks, L.E., 1969, Signal Theory, (Prentice Hall, Englewood Cliffs, N.J.).

Glarum, J.H., 1965, Rev. Sci. Instrum. 36, 771.

Gold, B. and Rader, C.M., 1969, Digital Processing of Signals, (McGraw-Hill, N.Y.).

Gray, A.L., 1971, Ph.D. Thesis, The University of Calgary, Canada.

Guillemin, E.A., 1963, Theory of Linear Physical Systems, (John Wiley and Sons, N.Y.).

Halpern, T. and Phillips, W.D., 1970, Rev. Sci. Instrum. 41, 1038.

Hardin, J. and Uebersfeld, J., 1971, Rev. Phys. Appl. 6, 169.

Harvey, A.F., 1963, Microwave Engineering, (Academic Press, London).

Hazlett, J.W., Denis, L.P., Trofimenkoff, F.N. and Streets Jr., R.B., 1970, Proc. IEEE 58, 1874.

Helms, H.D., 1967, IEEE Trans. Audio and Electroacoustics AU-15, 85.

Helstrom, C.W., 1968, Statistical Theory of Signal Detection, (Pergamon Press, Oxford).

Hyde, J.S. and Freed, J.H., 1968, J. Chem. Phys. 48, 4211.

Koepp, S., 1969, Hoch. U. Elek. 78, 57.

Kurokawa, K., 1968, IEEE Trans. Microwave Theory Tech. MTT-16, 234.

Liu, S.H., Nishina, Y. and Good, R.H., 1961, Rev. Sci. Instrum. 32, 784.

Mollier, J.C., 1972, Thèse de Doctorat, L'Université de Besançon, France

Nishina, Y. and Danielson, G.C., 1961, Rev. Sci. Instrum. 32, 790.

Ohtomo, M., 1972, IEEE Trans. Microwave Theory Tech. MTT-20, 635.

Ondria, J.G., 1968, IEEE Trans. Microwave Theory Tech. MTT-16, 767.

Oppenheim, A.V. and Weinstein, C., 1969, IEEE Trans. Audio and Electroacoustics AU-17, 120.

Orbach, R., 1961, Proc. Roy. Soc. A264, 458.

Pake, G.E., 1962, Paramagnetic Resonance, (Benjamin, N.Y.).

Papoulis, A., 1965, Probability, Random Variables and Stochastic Processes, (McGraw-Hill, N.Y.).

Pascaru, I., 1964, Nucl. Instrum. Meth. 26, 333.

Poole Jr., C.P., 1967, Electron Spin Resonance, (Interscience, N.Y.).

Poole Jr., C.P. and Farach, H.A., 1971, Relaxation in Magnetic Resonance, (Academic Press, N.Y.).

Portis, A.M., 1953, Phys. Rev. 91, 1071.

Pound, R.V., 1946, Rev. Sci. Instrum. 17, 490.

Praddaude, H.C., 1967, Rev. Sci. Instrum. 38, 339.

Rabi, I.I., 1937, Phys. Rev. 51, 652.

Rabiner, L.R., Cooley, J.W., Helms, H.D., Jackson, L.B., Kaiser, J.F., Rader, C.M., Schaffer, R.W., Steiglitz, K. and Weinstein, C.J., 1972, IEEE Trans. Audio and Electroacoustics AU-20, 322.

Ruban, M.A., 1963, Pribory. Tech. Eksper. 4, 103.

Scmidt, J. and Solomon, I., 1966, J. Appl. Phys. 37, 3719.

Slater, J.C., 1950, Microwave Electronics,(Van Nostrand, Princeton, N.J.).

Slichter, C.P., 1963, Principles of Magnetic Resonance, (Harper and Row, N.Y.).

Strandberg, M.W.P., 1972, Rev. Sci. Instrum. 43, 307.

Teaney, D.T., Klein, M.P. and Portis, A.M., 1961, Rev. Sci. Instrum. 32, 721.

Ursu, I.,Ed., 1971, Magnetic Resonance and Related Phenomena, (Publishing House Academy RSR, Bucharest).

Van der Ziel, A., 1954, Noise, (Prentice Hall, N.Y.).

Waller, I., 1932, Z. Phys. 79, 370.

Walsh, W.M. and Rupp, L.W., 1970, Rev. Sci. Instrum. 41, 1316.

Weinstein, C.J., 1969, IEEE Trans. Audio and Electroacoustics AU-17, 209.

Welch, P.D., 1969, IEEE Trans. Audio and Electroacoustics AU-17, 151.

Welchel, J.E. and Guinn, D.E., 1968, The Fast Fourier-Hadamard Transform and its Use in Signal Representation and Classification, Tech. Rept. PRC 68-11, (Melpar Inc., Fall's Church, Va.).

Welchel, J.E. and Guinn, D.E., 1970, IEEE Trans. Audio and Electroacoustics AU-18, 159.

Wilmshurst, T.H., 1967, Electron Spin Resonance Spectrometers, (Hilger, London).

Wilmshurst, T.H., 1968, J. Phys. E. 1, 353.

Zavoiski, E., 1945, Fiz. Zh. 9, 211.